

SWIR OBJECTIVE DESIGN USING SEIDEL ABERRATION THEORY

A THESIS SUBMITTED TO  
THE GRADUATE SCHOOL OF NATURAL AND APPLIED SCIENCES  
OF  
MIDDLE EAST TECHNICAL UNIVERSITY

BY

SERHAT HASAN ASLAN

IN PARTIAL FULFILLMENT OF THE REQUIREMENTS  
FOR  
THE DEGREE OF MASTER OF SCIENCE  
IN  
PHYSICS

JUNE 2016



Approval of the thesis:

**SWIR OBJECTIVE DESIGN USING SEIDEL ABERRATION THEORY**

submitted by **SERHAT HASAN ASLAN** in partial fulfillment of the requirements for the degree of **Master of Science in Physics Department, Middle East Technical University** by,

Prof. Dr. Gülbin Dural Ünver  
Dean, Graduate School of **Natural and Applied Sciences**

\_\_\_\_\_

Prof. Dr. Mehmet Tevfik Zeyrek  
Head of Department, **Physics**

\_\_\_\_\_

Assoc. Prof. Dr. Sinan Kaan Yerli  
Supervisor, **Physics Department, METU**

\_\_\_\_\_

Assist. Prof. Dr. Onur Keskin  
Co-supervisor, **Mechanical Engineering Dept., Işık Uni.**

\_\_\_\_\_

**Examining Committee Members:**

Assist. Prof. Dr. Özlem Duyar Coşkun  
Physics Engineering Dept., Hacettepe Uni.

\_\_\_\_\_

Assoc. Prof. Dr. Sinan Kaan Yerli  
Physics Department, METU

\_\_\_\_\_

Prof. Dr. Enver Bulur  
Physics Department, METU

\_\_\_\_\_

Assoc. Prof. Dr. Hakan Altan  
Physics Department, METU

\_\_\_\_\_

Assoc. Prof. Dr. Alpan Bek  
Physics Department, METU

\_\_\_\_\_

**Date:**

\_\_\_\_\_

**I hereby declare that all information in this document has been obtained and presented in accordance with academic rules and ethical conduct. I also declare that, as required by these rules and conduct, I have fully cited and referenced all material and results that are not original to this work.**

Name, Last Name: SERHAT HASAN ASLAN

Signature :

# ABSTRACT

## SWIR OBJECTIVE DESIGN USING SEIDEL ABERRATION THEORY

Aslan, Serhat Hasan

M.S., Department of Physics

Supervisor : Assoc. Prof. Dr. Sinan Kaan Yerli

Co-Supervisor : Assist. Prof. Dr. Onur Keskin

June 2016, 77 pages

Optical systems are used for increasing the situational awareness and Intelligence, Surveillance and Reconnaissance (ISR) capabilities for military purposes. MWIR (Midwave infrared) and LWIR (Long wave infrared) waveband informations are the first two wavebands information in the atmospheric transmission window that are harnessed in military night vision optical systems. Another candidate of these operable wavebands is the SWIR (Shortwave infrared). Shortwave infrared (SWIR) imaging is an extension of Near Infrared (NIR) and visible (VIS) imaging applications and SWIR waveband is defined between 0.9-1.7  $\mu\text{m}$  for InGaAs SWIR detectors. SWIR radiation in the atmosphere is based on atmospheric night glow which is a phenomenon created by the hydroxyl ion emissions in the upper atmosphere. There are benefits of SWIR such as fog and haze penetration, cloud and smoke penetration over NIR, VIS, MWIR and LWIR bands. A SWIR objective optical design process is outlined in this thesis using Seidel aberration theory or namely third order aberration theory starting from the thin lens predesign. First, typical optical layouts are discussed with respect to certain optical specifications. Using paraxial optical relations, optical design is finalized using ideal lenses. Aberrations in an optical design are defined in terms of wavefront expansions in order to correct aberrations methodologically. Third order components of wavefront expansion are considered initially and corrected by the thin lens parameters of the paraxial design. Ideal thin lenses are realized and thickened by using the thin lens parameters which are calculated in third order analysis. After third

order components are corrected perfectly, fifth order aberrations are balanced with third order aberrations using numerical optimization routines. Finally, tolerancing procedure is discussed and as built imaging quality of the optical design is calculated by tolerancing procedure.

Keywords: Optical Design, SWIR, Aberration theory

# ÖZ

## SEİDEL BOZULUM TEORİSİ KULLANILARAK SWIR OBJEKTİF TASARIMI

Aslan, Serhat Hasan

Yüksek Lisans, Fizik Bölümü

Tez Yöneticisi : Doç. Dr. Sinan Kaan Yerli

Ortak Tez Yöneticisi : Yrd. Doç. Dr. Onur Keskin

Haziran 2016 , 77 sayfa

Optik sistemler durumsal farkındalığı ve ISR yeteneklerini arttırmak için askeri sistemlerde kullanılmaktadır. Orta dalga kızılötesi ve uzun dalga kızılötesi dalgaboyları aralığı atmosferik geçirgenliği olan, askeri gece görüş sistemlerinde kullanılan ilk dalga boylarıdır. Kısa dalga boyu kızılötesi dalga boyu aralığı gece görüş sistemlerinde kullanılan diğer dalga boyu aralığıdır. Kırsadalga boyu kızılötesi görüntüleme, yakın kızılötesi ve görünür bölge görüntüleme uygulamalarının bir uzantısıdır ve dalga aralığı InGaAs dedektörleri için  $0.9-1.7 \mu\text{m}$  olarak tanımlanır. Atmosferdeki SWIR dalga boyundaki yayılım, yukarı atmosferdeki hidroksil iyonları tarafından yayılan gece ışımından kaynaklanır. SWIR dalga boyunun sisli ve puslu havadan geçme, bulut ve dumandan geçme gibi NIR, VIS, MWIR ve LWIR dalga boylarına göre faydaları vardır. Bu tezde ince lens öntasarımıyla başlanılarak üçüncü derece aberasyon teorisi olarakta bilinen Seidel aberasyon teorisi kullanılarak SWIR dalga boyunda çalışan bir objektif tasarımı yapılacaktır. İlk olarak, belli optik parametrelere göre optik yerleşim belirlenmiştir. Linear optik bağıntılar kullanılarak, ideal lenslerle optik yerleşim yapılmıştır. Optik sistemin görüntü bozulmalarının metodolojik olarak düzeltilebilmesi için dalga klavuzu polinomsal açılımla ifade edilmiştir. Üçüncü derece bileşenler ilk olarak ele alınmış ve ideal tasarım kullanılarak ideal lens parametreleri belirlenerek düzeltilmiştir. İdeal lensler üçüncü derece bileşen analizinde hesaplanan parametreler kullanılarak kalınlaştırılmış ve gerçekleştirilmiştir. Üçüncü derece bileşenlerin düzeltilmesinden sonra, beşinci derece görüntü bozulum-

ları sayısal optimizasyon yöntemleri kullanılarak üçüncü derece görüntü bozulmalarıyla dengelenmiştir. Son olarak, tolerans prosedürü tartışılmış ve optik tasarımın üretim sonrası görüntü kalitesi toleranslandırma yöntemiyle hesaplanmıştır.

Anahtar Kelimeler: Optik Tasarım, SWIR, Aberasyon Teorisi

*To my family*

## **ACKNOWLEDGMENTS**

I would like to thank to my supervisor Assoc. Prof. Dr. Sinan Kaan Yerli and co-supervisor Assist. Prof. Dr. Onur Keskin for their advice, criticism, support and encouragements throughout this work.

I am grateful to ASELSAN Electronics Industries Inc. for its all support to my studies.

Finally, it would not have been possible to write this thesis without endless support of my family: İbrahim Aslan, Çilem Aslan, Ferhat Aslan, Ebru Ataş Aslan and Bergüzar Aslan.

# TABLE OF CONTENTS

ABSTRACT . . . . .	v
ÖZ . . . . .	vii
ACKNOWLEDGMENTS . . . . .	x
TABLE OF CONTENTS . . . . .	xi
LIST OF TABLES . . . . .	xiv
LIST OF FIGURES . . . . .	xvii
LIST OF ABBREVIATIONS . . . . .	xx
CHAPTERS	
1 INTRODUCTION . . . . .	1
1.1 ISR and Optical Systems . . . . .	1
1.2 Atmospheric Windows and SWIR . . . . .	2
1.3 Why SWIR? . . . . .	5
1.4 Summary of This Work . . . . .	6
2 OPTICAL DESIGN METHODOLOGY . . . . .	9
2.1 Aberrations . . . . .	9
2.1.1 Power Series Expansions . . . . .	11

2.1.2	Primary Aberrations . . . . .	15
2.1.2.1	Aperture and Field Dependence . . . . .	15
2.1.2.2	Calculation of Seidel Coefficients . . . . .	16
2.1.2.3	Calculation of Pupil Aberrations . . . . .	18
2.1.2.4	Stop-shift Formula . . . . .	19
2.1.2.5	Aberrations in Seidel Sums . . . . .	20
2.1.2.6	Thin Lens Aberrations . . . . .	21
2.1.3	Higher Order Aberrations . . . . .	21
2.1.3.1	Fifth-order Aberrations . . . . .	22
	Extrinsic aberrations . . . . .	24
	Intrinsic aberrations . . . . .	25
2.1.3.2	Seventh and higher-order aberrations . . . . .	27
2.2	Optical Design Procedure . . . . .	27
2.2.1	Specification . . . . .	28
2.2.2	Layout . . . . .	29
2.2.3	Thin lens predesign . . . . .	31
2.2.4	Surface model . . . . .	31
2.2.5	Optimization . . . . .	32
2.2.6	Tolerancing . . . . .	33
3	SWIR OBJECTIVE DESIGN . . . . .	37
3.1	Specification . . . . .	37

3.2	Layout . . . . .	37
3.3	Thin lens predesign . . . . .	41
3.4	Surface Model . . . . .	56
3.5	Optimization . . . . .	57
3.6	Tolerancing . . . . .	64
4	CONCLUSION, DISCUSSION AND FUTURE WORK . . . . .	71
4.1	Conclusion and Discussion . . . . .	71
4.2	Future Work . . . . .	73
	REFERENCES . . . . .	75

## LIST OF TABLES

### TABLES

Table 1.1	Infrared windows in atmosphere . . . . .	4
Table 2.1	Wavefront aberrations . . . . .	14
Table 2.2	Field and aperture dependence of wave aberrations . . . . .	16
Table 2.3	Optical specification . . . . .	29
Table 2.4	Commonly toleranced lens parameters . . . . .	34
Table 2.5	Typical manufacturing tolerance data [35] . . . . .	35
Table 3.1	SWIR objective specifications . . . . .	37
Table 3.2	Paraxial lens data . . . . .	40
Table 3.3	Paraxial raytrace data . . . . .	41
Table 3.4	Maximum Abbe separation glasses with minimum partial dispersion difference . . . . .	42
Table 3.5	Materials resulted in highest determinant . . . . .	44
Table 3.6	Power distributions with materials resulted in highest determinant . . . . .	45
Table 3.7	Final paraxial configuration surface data . . . . .	46
Table 3.8	Shape independent aberration coefficients for final paraxial config- uration . . . . .	46
Table 3.9	Parameter values in shape dependent aberration equations . . . . .	47
Table 3.10	Shape factors of lenses . . . . .	49
Table 3.11	Total third order Seidel aberration coefficients in lens units . . . . .	50
Table 3.12	Realized paraxial lens data . . . . .	51

Table 3.13 Realized lens data . . . . .	51
Table 3.14 Ray trace data for fifth order aberration coefficient calculations . . .	52
Table 3.15 Third order aberration coefficients of surfaces in waves in configuration . . . . .	53
Table 3.16 Fifth order intrinsic aberration coefficients of surfaces in configuration in waves . . . . .	54
Table 3.17 Fifth order extrinsic aberration coefficients of surfaces in configuration in waves . . . . .	54
Table 3.18 Lens data after aberration balancing . . . . .	54
Table 3.19 Total fifth order aberration coefficients in configuration in waves . .	55
Table 3.20 Third order aberration coefficients after aberration balancing . . . .	55
Table 3.21 Fifth order aberration coefficients after aberration balancing . . . .	55
Table 3.22 Surface models and principle point compensation values . . . . .	56
Table 3.23 Lens data after lens thickening . . . . .	57
Table 3.24 Third order aberration coefficients after lens thickening in waves . .	57
Table 3.25 Fifth order aberration coefficients after lens thickening . . . . .	57
Table 3.26 First solution lens data . . . . .	59
Table 3.27 Second solution lens data . . . . .	59
Table 3.28 Third order aberration coefficients after lens optimization . . . . .	59
Table 3.29 Fifth order aberration coefficients after lens optimization . . . . .	64
Table 3.30 Precision level centered tolerances . . . . .	64
Table 3.31 Precision level decentered tolerances . . . . .	65
Table 3.32 As-built wavefront errors of the design with precision level tolerances	65
Table 3.33 High precision level centered tolerances . . . . .	66
Table 3.34 High precision level decentered tolerances . . . . .	67
Table 3.35 As-built wavefront errors of the design with high precision level tolerances . . . . .	68
Table 3.36 As-built tangential MTF of the design with precision level tolerances	68

Table 3.37 As-built sagittal MTF of the design with precision level tolerances . . .	69
Table 3.38 As-built tangential MTF of the design with high precision level tolerances . . . . .	69
Table 3.39 As-built sagittal MTF of the design with high precision level tolerances	69
Table 3.40 Comparison of wavefront error of the design with high precision and precision level tolerances . . . . .	70
Table 3.41 Comparison of MTF performance with high precision and precision level tolerances . . . . .	70

## LIST OF FIGURES

### FIGURES

Figure 1.1	General purpose imaging system . . . . .	1
Figure 1.2	Total spectral transmission of atmosphere at 5 km range and 90 degree zenith angle . . . . .	3
Figure 1.3	Spectral transmission of various gases in atmosphere at 5 km range and 90 degree zenith angle . . . . .	3
Figure 1.4	SWIR illumination mechanism [5] . . . . .	4
Figure 1.5	SWIR sources [2] . . . . .	6
Figure 1.6	Imaging through haze in SWIR band [7] . . . . .	7
Figure 1.7	Imaging through smoke in SWIR band [7] . . . . .	7
Figure 1.8	SWIR image showing 0.85 and 1.55 $\mu\text{m}$ laser designators [14] . . . . .	7
Figure 1.9	Design evolution . . . . .	8
Figure 2.1	Image formation of a point source by ray intersection . . . . .	9
Figure 2.2	Aberrations of a real imaging system . . . . .	10
Figure 2.3	Ray and wavefront representation of a point source . . . . .	10
Figure 2.4	Wavefront representation of ideal imaging . . . . .	11
Figure 2.5	Wavefront aberration . . . . .	12
Figure 2.6	Field and aperture vectors and the angle $\phi$ . . . . .	12
Figure 2.7	R. Shacks' representation of 4th and 6th order wave aberrations . . . . .	15
Figure 2.8	Primary wave aberration shapes . . . . .	18
Figure 2.9	Stop shift effect and eccentricity . . . . .	20
Figure 2.10	Secondary 5th order spherical aberration . . . . .	23

Figure 2.11 Secondary 5th order coma . . . . .	23
Figure 2.12 Secondary 5th field curvature, astigmatism and distortion . . . . .	24
Figure 2.13 Optical design flow [39] . . . . .	28
Figure 2.14 Classifications of lens types [13, 15] . . . . .	30
Figure 2.15 Marginal ray height change in a thickened thin lens . . . . .	32
Figure 2.16 Tolerance procedure [12] . . . . .	36
Figure 3.1 Paraxial layout of a typical telephoto lens . . . . .	38
Figure 3.2 Paraxial relations for a typical telephoto lens . . . . .	39
Figure 3.3 F# relations of a typical telephoto lens . . . . .	39
Figure 3.4 Focal length (upper panel) and f# (lower panel) graph with respect to lens separation for 0.8 telephoto ratio . . . . .	40
Figure 3.5 Partial dispersion vs Abbe number graph according to Schott cata- log [30] . . . . .	42
Figure 3.6 Triangles formed by materials . . . . .	45
Figure 3.7 Paraxial configuration layout . . . . .	46
Figure 3.8 Realized configuration layout . . . . .	51
Figure 3.9 Spot diagram and OPD fan of configuration . . . . .	52
Figure 3.10 Configuration layout after aberration balancing . . . . .	53
Figure 3.11 Spot diagram and OPD fan after aberration balancing . . . . .	55
Figure 3.12 Configuration layout thickening lenses . . . . .	58
Figure 3.13 Spot diagram and OPD fan after lens thickening . . . . .	58
Figure 3.14 First solution layout . . . . .	60
Figure 3.15 Spot diagram,OPD fan, MTF and distortion of first solution . . . . .	60
Figure 3.16 Wavefront map at 1.4um for field 0, 7.25 and 10.25mm of first solution . . . . .	61
Figure 3.17 Second solution layout . . . . .	62
Figure 3.18 Spot diagram,OPD fan, MTF and distortion of second solution . . . . .	62

Figure 3.19 Wavefront map at 1.4um for field 0, 7.25 and 10.25mm of second solution . . . . .	63
Figure 3.20 Cumulative distribution of wavefront error with precision level tolerances . . . . .	65
Figure 3.21 Cumulative distribution of wavefront error with high precision level tolerances . . . . .	66
Figure 3.22 Cumulative distribution of tangential MTF at 33 lp/mm with precision level tolerances . . . . .	67
Figure 3.23 Cumulative distribution of sagittal MTF at 33 lp/mm with precision level tolerances . . . . .	68
Figure 3.24 Cumulative distribution of tangential MTF at 33 lp/mm with high precision level tolerances . . . . .	69
Figure 3.25 Cumulative distribution of sagittal MTF at 33 lp/mm with high precision level tolerances . . . . .	70

## LIST OF ABBREVIATIONS

ISR	Intelligence, Surveillance and Reconnaissance
MWIR	Midwave Infrared
LWIR	Longwave Infrared
SWIR	Shortwave Infrared
NIR	Near Infrared
VIS	Visible
UV	Ultra Violet
InGaAS	Indium Gallium Arsenide
UAV	Unmanned air vehicle
SWAP	Size, weight and power
DLS	Damped least squares
MTF	Modulation transfer function
AR	Anti reflective
BBAR	Broadband anti reflective
OPD	Optical path difference

# CHAPTER 1

## INTRODUCTION

### 1.1 ISR and Optical Systems

Main applications of optical systems are classified in four categories which are military, industrial, medical and scientific. The main military purpose of using optical systems is to increase situational awareness and Intelligence, Surveillance and Reconnaissance (ISR) capabilities. ISR is the acquisition, processing of accurate and relevant information and intelligence to support the military activities. Different ground, sea and air platforms such as satellites, unmanned air vehicles (UAV) are typical examples of ISR systems. The intelligence data gathered by these ISR systems can be in different forms such as optical, radar or infrared. Sensor systems operating in certain parts of electromagnetic spectrum are the mainframes of ISR systems. Electro-optical systems are examples of such sensor systems that operate in the visible and infrared regions of the electromagnetic spectrum which are used for detection, acquisition and imaging of interested objects under certain conditions in order to increase ISR and situational awareness. A general purpose optical system is depicted in Figure 1.1.

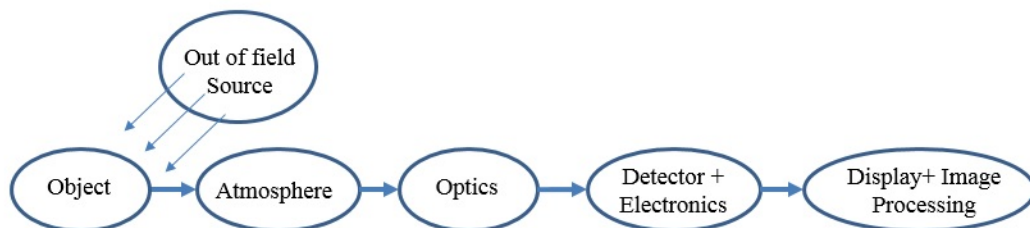


Figure 1.1: General purpose imaging system

The main components of a generic optical system include: illumination sources emitting energy, objects or targets reflecting that energy, an intervening media or atmosphere through which the energy propagates on its way to optics, optical lens or collector aperture used to collect this energy, detectors that gathers an image of the source, electronics to convert the electrons from the detector into usable signals and software and displays to interpret the results. This model can be modified or replaced with other models as necessary to be used with other optical applications such as active imaging, space-based imaging, medical imaging, airborne imaging, optical tomography, spectroscopy and underwater imaging. For a wide variety of optical detection scenarios, the object is at a remote location from the optical detection system and the intervening media is atmosphere. The main objective of this thesis is to construct a lens design methodology of a military SWIR optical imaging sensor in order to increase situational awareness and ISR capabilities.

## **1.2 Atmospheric Windows and SWIR**

Atmosphere is the intervening media for most of these imaging systems. The quality of the images taken by these systems is affected by different properties of atmosphere. Two of the main atmospheric phenomena are attenuation of the image irradiance propagating through atmosphere and blurring of image details. Before the radiation from targets to be imaged reaches the optical sensor, the radiant flux emerging from target is selectively absorbed by several gases constituting the atmosphere, scattered away by small particles suspended in the atmosphere and modulated by rapid variations of atmospheric property. In infrared portion of the electromagnetic spectrum, absorption is more dominant than scattering.

The infrared absorption by the atmosphere is due to mainly water vapour, carbon dioxide, ozone and oxygen, with a smaller contribution from gases such as  $N_2O$ ,  $CH_4$ . Total spectral transmission of atmosphere is given in Figure 1.2. Spectral transmission of water vapour, carbon dioxide, ozone and oxygen are given in Figure 1.3. Transmission is analyzed with PcModWin5 [4] for 1976 US Standard atmospheric model with Rural-VIS 23 km aerosol model. Range and zenith angle are chosen as 5 km 90 degree. Cloud and rain are not included in the model. Spectral transmit-

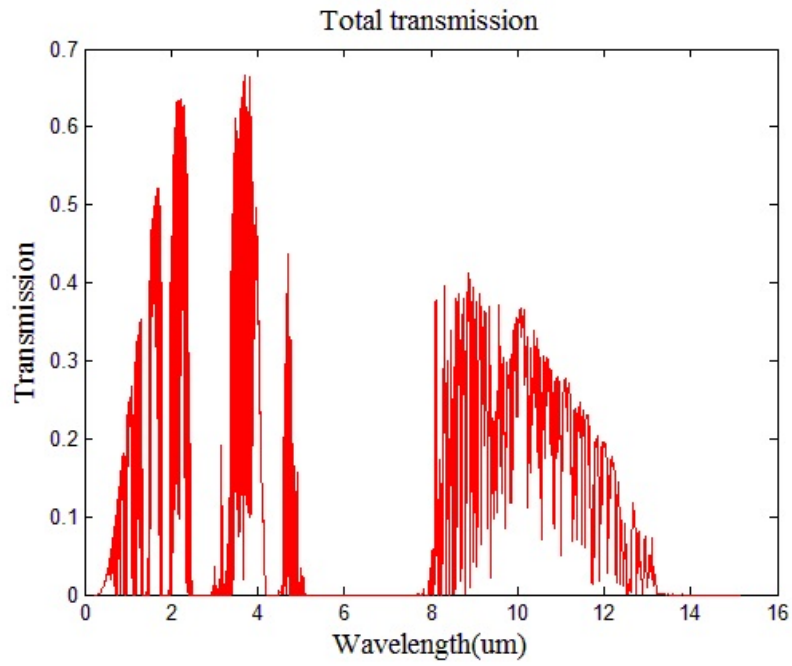


Figure 1.2: Total spectral transmission of atmosphere at 5 km range and 90 degree zenith angle

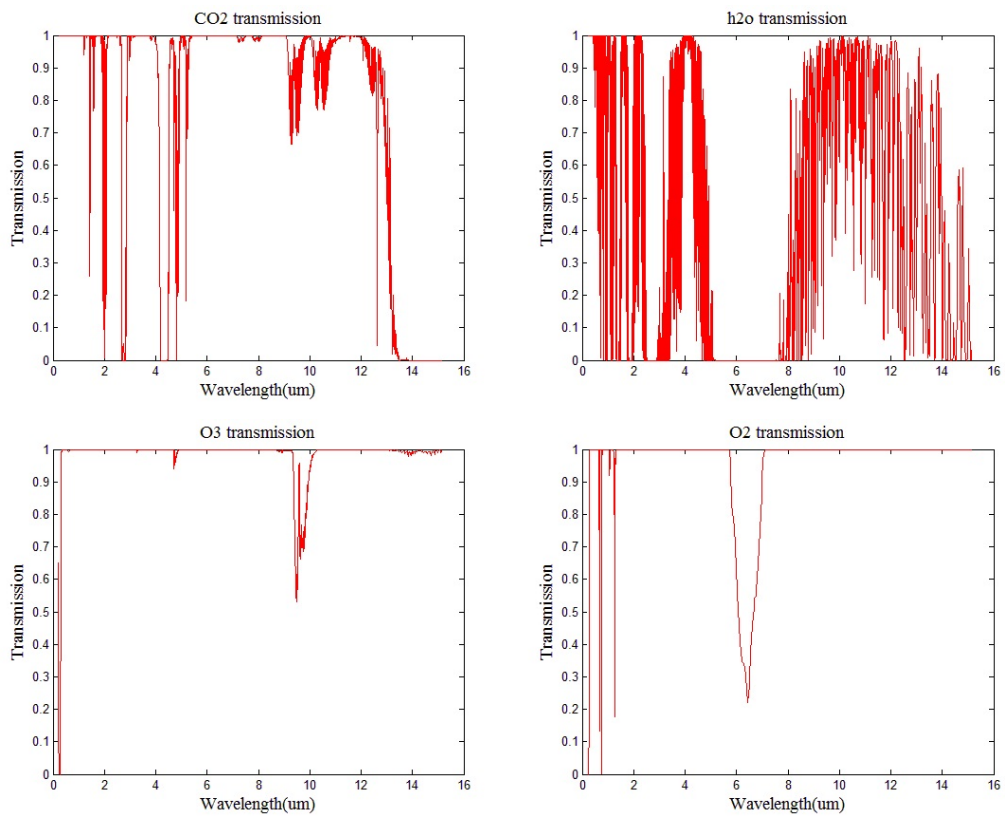


Figure 1.3: Spectral transmission of various gases in atmosphere at 5 km range and 90 degree zenith angle

Table 1.1: Infrared windows in atmosphere

Infrared region	Waveband ( $\mu\text{m}$ )
Near infrared (NIR)	0.7-1
Shortwave infrared (SWIR)	1-3
Midwave infrared (MWIR)	3-5
Longwave infrared (LWIR)	7-14
Very longwave infrared(VLWIR)	14-30

tance curve can be categorized by many different regions of high transmission called atmospheric windows which are separated by regions of high absorptions. According to the detector response, infrared portion of electromagnetic spectrum is classified as given in Table 1.1.

Wavelengths between 1.0 to 3.0  $\mu\text{m}$  are considered to be SWIR. Sensing SWIR radiation is made possible and practical recently by the development of detectors material InGaAs. The responsivity of InGaAs is highest in 0.9-1.7 $\mu\text{m}$  wavelength. Hence, SWIR waveband is generally accepted as 0.9-1.7  $\mu\text{m}$ . Upper cutoff wavelength can be extended to 2.6  $\mu\text{m}$  by adding phosphor to detector material.

As in the visible band, imaging in SWIR band is possible such that photons are reflected or absorbed by the target, providing a useful contrast. Main natural emitters in SWIR are the ambient starlight and background radiance which is also known as airglow. Airglow is defined as the irradiance from photo-chemical reactions of hydroxyl ions in the 6 to 10 km atmospheric layer around 85 km height of atmosphere. Significant part of airglow is in SWIR band between 1.0 and 1.7  $\mu\text{m}$ . The mechanism of SWIR illumination due to airglow is given in Figure 1.4 [5].

During day, UV photons collide with water molecules and produce hydrogen and

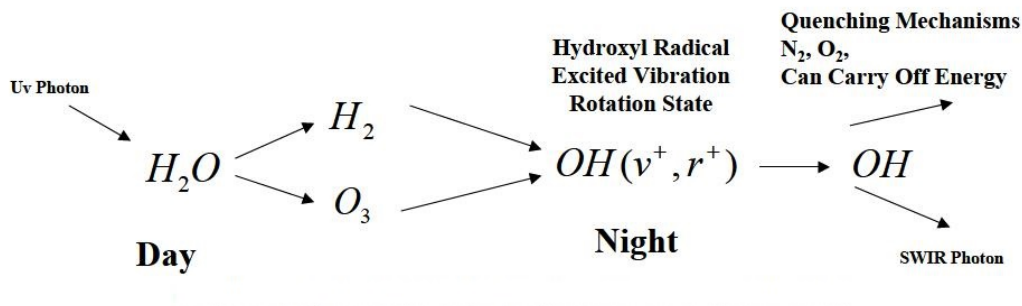


Figure 1.4: SWIR illumination mechanism [5]

ozone. At night, produced hydrogen and ozone recombine and form excited hydroxyl ions with higher vibration and rotational energy states. Then these excited states make transitions to lower energy states producing a photon which has energy corresponding to SWIR wavelength. Hence these SWIR photons illuminate the target. Comparison of different SWIR band irradiance levels from different sources are given in Figure 1.5 [2]. Airglow is the dominant illuminator in SWIR band.

### 1.3 Why SWIR?

Comparison with VIS and NIR:

- Atmospheric transmission is much larger in SWIR than VIS and NIR. As a result of increased transmission, SNR and image quality is better in SWIR with respect to Vis and NIR band. VIS band is 0.4-0.7  $\mu\text{m}$ . NIR band is 0.7-1  $\mu\text{m}$ .
- Less exposure time is required in SWIR compared to VIS and NIR. So stabilization requirements are easier compared to VIS and NIR band.
- Since SWIR wavelength is bigger than VIS and NIR wavelength, fabrication and alignment tolerances of lenses are better in SWIR optics.
- Atmospheric turbulence and dispersion are less effective in SWIR since SWIR has longer wavelength than VIS and NIR.
- Imaging through haze is much better in SWIR as shown in Figure 1.6 [7].
- Imaging through smoke is much better in SWIR as shown in Figure 1.7 [7].
- Military laser range finders and designators operate at 0.85, 1.06 and 1.55  $\mu\text{m}$ . Seeing these wavelengths in VIS and NIR sensors is difficult since these wavebands are generally beyond the cutoff wavelength of the sensor. SWIR sensor can see all of these wavelengths without any difficulty as shown in Figure 1.8 [14].

Comparison with MWIR and LWIR:

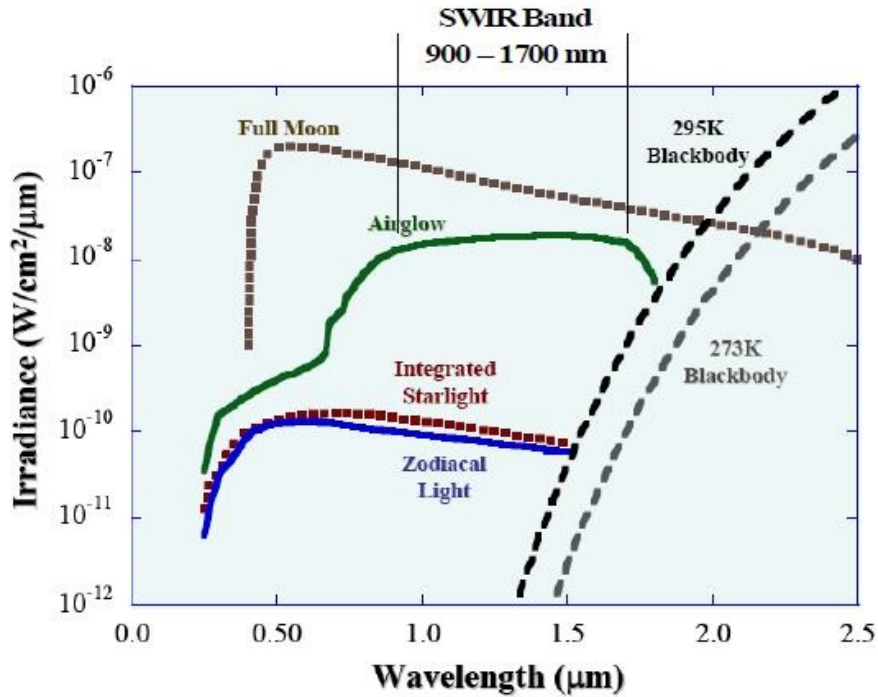


Figure 1.5: SWIR sources [2]

SWIR band is generally regarded as a complement to MWIR and LWIR bands in military applications. So a direct comparison is not suitable for these wavebands but major advantages of SWIR over MWIR and LWIR are as follows:

- No cryogenic cooler for detectors are needed. As a result SWAP requirements are much smaller than MWIR and LWIR.
- Conventional low cost visible glasses and coating materials can be used in SWIR. Expensive and exotic materials are not needed as in MWIR and LWIR.

#### 1.4 Summary of This Work

A systematic optical lens design methodology based on wavefront error polynomial expansion is proposed for SWIR band in this thesis. In Chapter 1, atmospheric transmission bands are discussed in detail and bandgap of SWIR is shown. SWIR illumination mechanism, SWIR illumination sources are given. Comparisons of SWIR with



Figure 1.6: Imaging through haze in SWIR band [7]



Figure 1.7: Imaging through smoke in SWIR band [7]

MWIR, LWIR, VIS and NIR are done. In Chapter 2, aberrations and their two representations which are namely ray based and wavefront error based representations in a typical optical design are introduced. Wavefront error representation of aberrations is used in this work. Wavefront error is expressed as a polynomial expansion in terms of the ray pupil position and ray field size. According to this expansion, fourth order

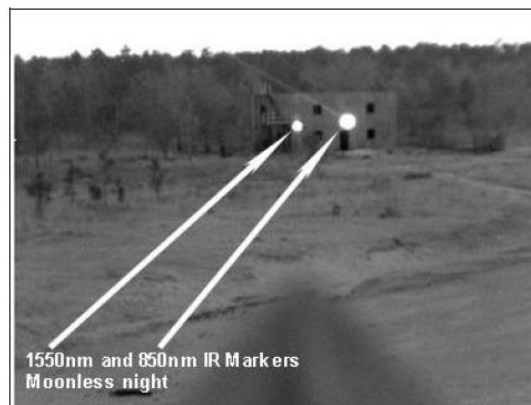


Figure 1.8: SWIR image showing 0.85 and 1.55  $\mu\text{m}$  laser designators [14]

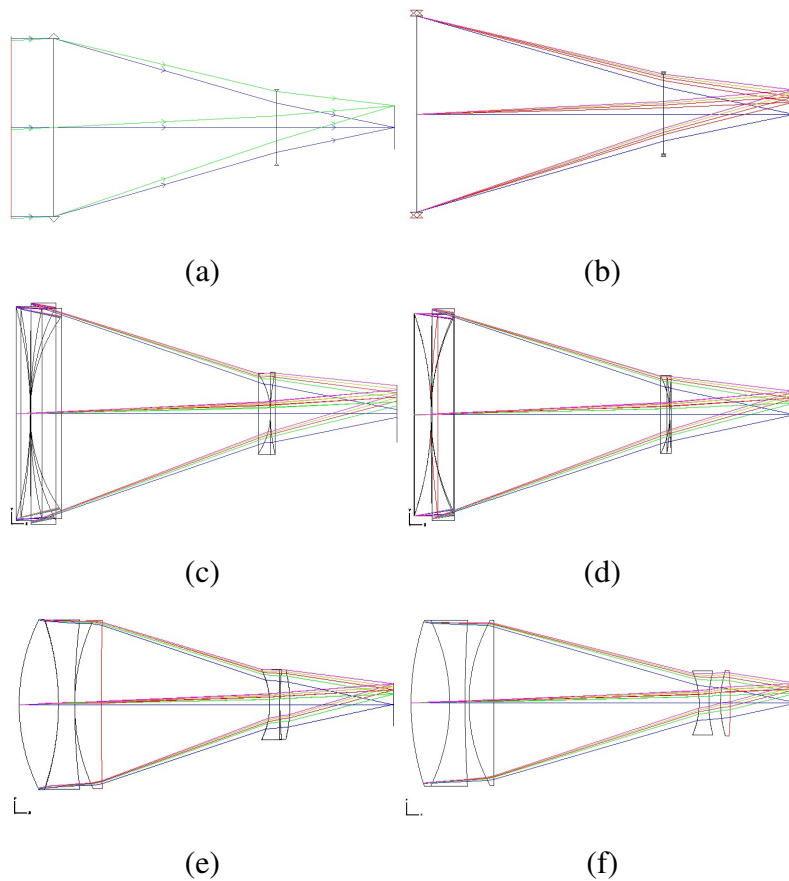


Figure 1.9: (a) Paraxial two element layout with optical powers (b) Paraxial five element layout with materials and powers (c) Layout with zero thickness real lenses (d) Layout with zero thickness real lenses in which third and fifth order aberration terms are balanced (e) Layout with thickened lenses by surface model (f) Layout after numerical optimization

and sixth order aberration terms which corresponds to third order and fifth order in ray based representation, their waveforms and calculations are discussed. Seidel coefficients which corresponds to fourth order terms in wavefront aberration polynomial expansion are given in detail for both real and ideal lenses. Fourth order and sixth order are used interchangeably with third and fifth order. A general optical design flow chart is given and each step is discussed in detail. In Chapter 3, the methodology proposed in Chapter 2 is applied to a practical case which is a typical SWIR objective. The general design evolution of a typical SWIR objective design after each step of the optical design methodology proposed in this work is shown in Figure 1.9.

## CHAPTER 2

### OPTICAL DESIGN METHODOLOGY

#### 2.1 Aberrations

Optical systems are studied in two classes which are called imaging and non-imaging optical systems. The main purpose of an imaging optical system is to form an image of an extended object which is self-luminous or which redirects the light. Extended objects are represented by a collection of point sources which light rays emerges when designing an optical system. An ideal image formation of a point source O in an ideal optical imaging system by ray intersection is shown in Figure 2.1.

Point sources are actually non-physical, idealistic representations which are useful in studying imaging optical systems. The images of this ideal point object obtained with a real optical system are not a point but a distributed point clouds which means that rays emanating from the object point do not intersect at the ideal image point due to the inherent nature of optical elements forming the imaging optical system. Distri-

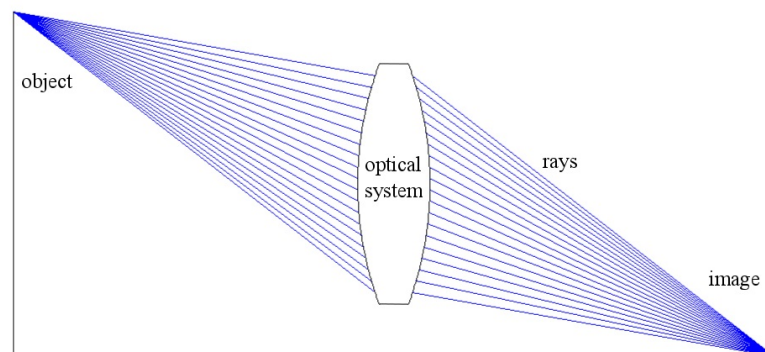


Figure 2.1: Image formation of a point source by ray intersection

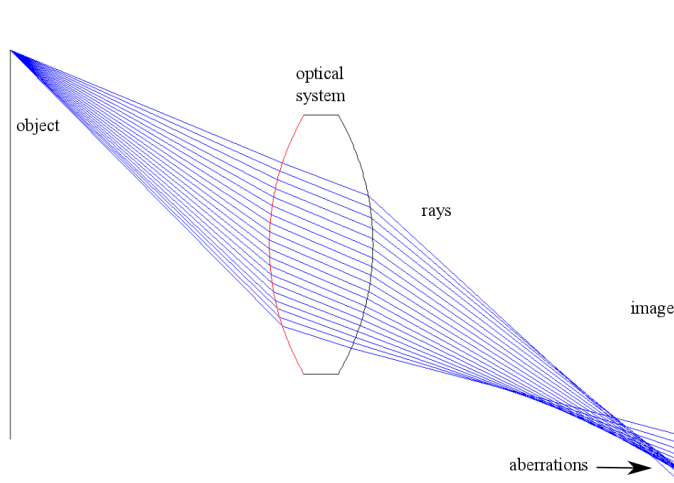


Figure 2.2: Aberrations of a real imaging system

bution of these point clouds because of the non-intersecting rays are called optical aberrations which degrade the image of extended objects obtained from a real optical system. Aberrations of a real optical imaging system when imaging a typical point source are shown in Figure 2.2. Understanding these types of aberrations in an optical system is very important in designing optical system [3, 18].

Another way of representing a point source is the wavefront which is the surface of equal optical path length (OPL). Optical path length is defined as follows:

$$OPL = \int_a^b n(s) ds \quad (2.1)$$

where  $n$  is the refractive index and  $ds$  is the arc-length. Two ways of representing a point source are shown in Figure 2.3.

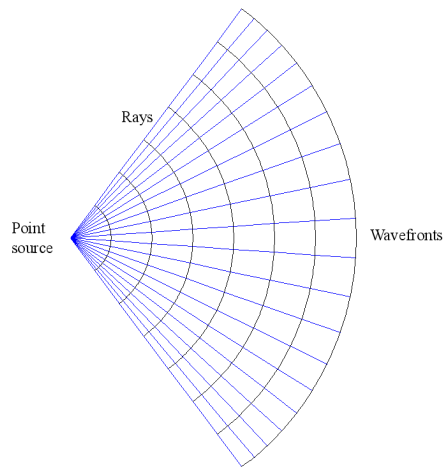


Figure 2.3: Ray and wavefront representation of a point source

In object space, wavefronts are diverging concentric spheres, with the object point as center. In ideal optical system in which perfect imaging occurs without any aberrations, the wavefronts are again concentric spheres, with the image point as center as shown in Figure 2.4.

In real optical imaging systems, as wavefront propagates through the elements constituting the optical imaging system, its geometric shape changes and deviates from the spherical form. The deviations from spherical form which is the perfect imaging wavefront are considered as wave aberrations. A typical wave aberration is given in Figure 2.5.

There are two different ways of describing aberrations. First way is the transverse and longitudinal aberrations which are the deviations of rays of point source from the ideal image point. Second way is the wavefront aberrations which are the deviations of wavefront from the reference wavefront. In this thesis, wavefront aberration description is used.

### 2.1.1 Power Series Expansions

Wave aberration of a ray from a point object depends on the position of point object in object space and also the ray position on the exit pupil. The position of object point in object space is denoted by the normalized field vector  $\vec{H}$ , position of ray in exit pupil is denoted by the normalized pupil vector  $\vec{\rho}$  and the angle between these two vectors is denoted by  $\phi$  as shown in Figure 2.6.

Since aberration function is a scalar, it is written in terms of the dot products of the

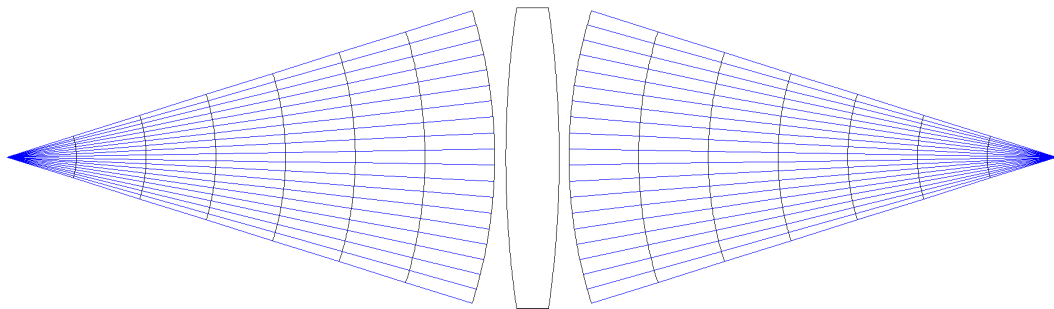


Figure 2.4: Wavefront representation of ideal imaging

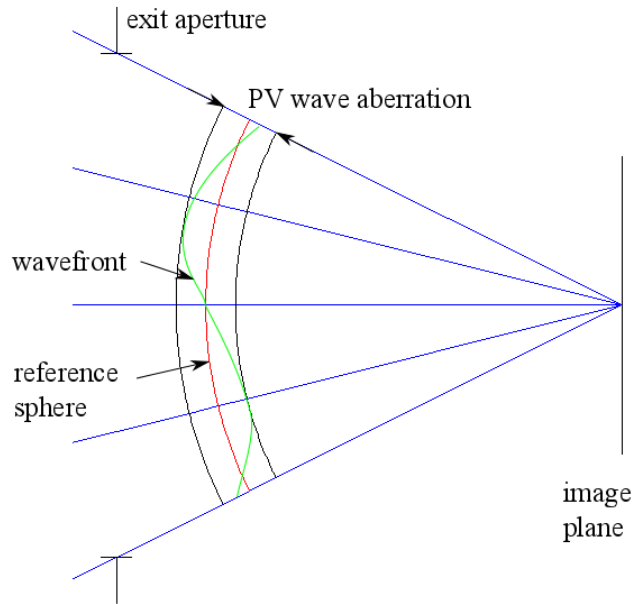


Figure 2.5: Wavefront aberration

field and pupil vector in rotationally symmetric optical imaging systems. Since there is a symmetry around the optical axis, the rotationally invariant variables are  $(\vec{H} \cdot \vec{H})$ ,  $(\vec{H} \cdot \vec{\rho})$  and  $(\vec{\rho} \cdot \vec{\rho})$ . So the aberration function is a function of these rotationally invariant variables  $W = W(\vec{H} \cdot \vec{H}, \vec{H} \cdot \vec{\rho}, \vec{\rho} \cdot \vec{\rho})$ . The aberration function as a power series expansion in terms of these rotationally invariant variables which was introduced by

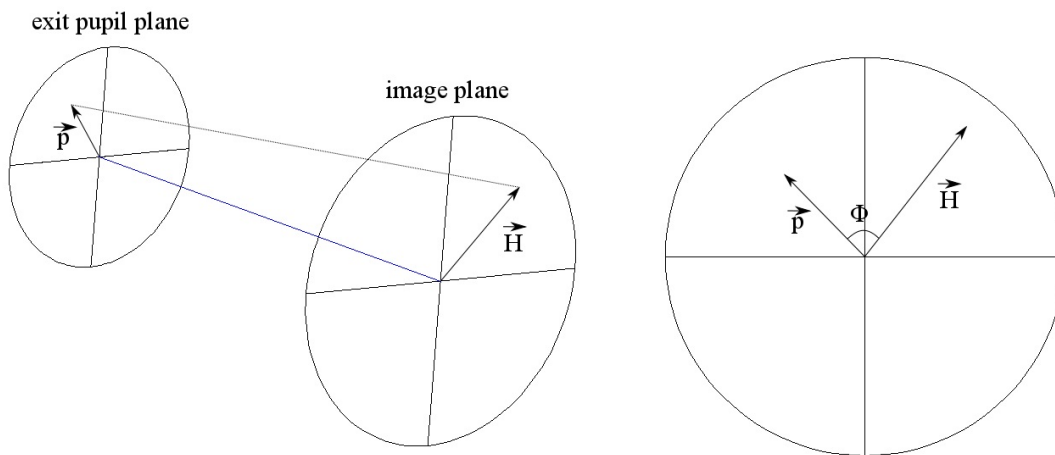


Figure 2.6: Field and aperture vectors and the angle  $\phi$

R. Shack is as follows:

$$\begin{aligned}
W(\vec{H}, \vec{\rho}) &= \sum_{j,m,n} W_{k,l,m} (\vec{H} \cdot \vec{H})^j (\vec{H} \cdot \vec{\rho})^m (\vec{\rho} \cdot \vec{\rho})^n \\
&= W_{000} + W_{200}(\vec{H} \cdot \vec{H}) + W_{111}(\vec{H} \cdot \vec{\rho}) + W_{020}(\vec{\rho} \cdot \vec{\rho}) \\
&+ W_{040}(\vec{\rho} \cdot \vec{\rho})^2 + W_{131}(\vec{H} \cdot \vec{\rho})(\vec{\rho} \cdot \vec{\rho}) + W_{222}(\vec{H} \cdot \vec{\rho})^2 \\
&+ W_{220}(\vec{H} \cdot \vec{H})(\vec{\rho} \cdot \vec{\rho}) + W_{311}(\vec{H} \cdot \vec{H})(\vec{H} \cdot \vec{\rho}) + W_{400}(\vec{H} \cdot \vec{H})^2 \\
&+ W_{240}(\vec{H} \cdot \vec{H})(\vec{\rho} \cdot \vec{\rho})^2 + W_{331}(\vec{H} \cdot \vec{H})(\vec{H} \cdot \vec{\rho})(\vec{\rho} \cdot \vec{\rho}) \\
&+ W_{422}(\vec{H} \cdot \vec{H})(\vec{H} \cdot \vec{\rho})^2 \\
&+ W_{420}(\vec{H} \cdot \vec{H})^2(\vec{\rho} \cdot \vec{\rho}) + W_{511}(\vec{H} \cdot \vec{H})^2(\vec{H} \cdot \vec{\rho}) + W_{600}(\vec{H} \cdot \vec{H})^3 \\
&+ W_{060}(\vec{\rho} \cdot \vec{\rho})^3 + W_{151}(\vec{H} \cdot \vec{\rho})(\vec{\rho} \cdot \vec{\rho})^2 + W_{242}(\vec{H} \cdot \vec{\rho})^2(\vec{\rho} \cdot \vec{\rho}) \\
&+ W_{333}(\vec{H} \cdot \vec{\rho})^3
\end{aligned} \tag{2.2}$$

where  $k, l, m$  are integers and  $k = 2j + m$ ,  $l = 2n + m$ .  $W_{k,l,m}$  represents the aberration coefficients [37]. This representation of the wavefront aberration is the starting point in this thesis. Fourth and sixth order aberration terms are summarized in both vector and algebraic notation in Table 2.1 [27].

A systematic representation of wave aberrations introduced by R. Shack is shown in Figure 2.7 [29]. Since rays are perpendicular to wavefront, once the wave aberrations are found transverse ray aberrations can be calculated with the following equations:

$$\begin{aligned}
\Delta x' &= -\frac{R}{n'} \frac{\partial W}{\partial x_p} \\
\Delta y' &= -\frac{R}{n'} \frac{\partial W}{\partial y_p}
\end{aligned} \tag{2.3}$$

where  $R$  is the radius of reference sphere and  $n'$  is the refractive index in image space which is generally air and taken as 1.

In an optical system, entrance pupil and exit pupil are optically conjugated similar to object and image conjugation. When entrance and exit pupil are considered as object and image, pupil aberrations occur. There are many optical effects of pupil aberrations [26]. In this work, pupil aberrations are used for calculating fifth order

Table 2.1: Wavefront aberrations

Aberration name	Vector form	Algebraic form	j	m	n
<b>Zero order</b>					
Uniform piston	$W_{000}$	$W_{000}$	0	0	0
<b>Second order</b>					
Quadratic piston	$W_{200}(\vec{H} \cdot \vec{H})$	$W_{200}H^2$	1	0	0
Magnification	$W_{111}(\vec{H} \cdot \vec{\rho})$	$W_{111}H\rho \cos(\phi)$	0	1	0
Focus	$W_{020}(\vec{\rho} \cdot \vec{\rho})$	$W_{020}H\rho^2$	0	0	1
<b>Fourth order</b>					
Spherical aberration	$W_{040}(\vec{\rho} \cdot \vec{\rho})^2$	$W_{040}\rho^4$	0	0	2
Coma	$W_{131}(\vec{H} \cdot \vec{\rho})(\vec{\rho} \cdot \vec{\rho})$	$W_{131}H\rho^3 \cos(\phi)$	0	1	1
Astigmatism	$W_{222}(\vec{H} \cdot \vec{\rho})^2$	$W_{222}H^2\rho^2 \cos^2(\phi)$	0	2	0
Field curvature	$W_{220}(\vec{H} \cdot \vec{H})(\vec{\rho} \cdot \vec{\rho})$	$W_{220}H^2\rho^2$	1	0	1
Distortion	$W_{311}(\vec{H} \cdot \vec{H})(\vec{H} \cdot \vec{\rho})$	$W_{311}H^3\rho \cos(\phi)$	1	1	0
Quartic piston	$W_{400}(\vec{H} \cdot \vec{H})^2$	$W_{400}H^4$	2	0	0
<b>Sixth order</b>					
Oblique spherical aber.	$W_{240}(\vec{H} \cdot \vec{H})(\vec{\rho} \cdot \vec{\rho})^2$	$W_{240}H^2\rho^4$	1	0	2
Coma	$W_{331}(\vec{H} \cdot \vec{H})(\vec{H} \cdot \vec{\rho})(\vec{\rho} \cdot \vec{\rho})$	$W_{331}H^3\rho^3 \cos(\phi)$	1	1	1
Astigmatism	$W_{422}(\vec{H} \cdot \vec{H})(\vec{H} \cdot \vec{\rho})^2$	$W_{422}H^4\rho^2 \cos^2(\phi)$	1	2	0
Field curvature	$W_{420}(\vec{H} \cdot \vec{H})^2(\vec{\rho} \cdot \vec{\rho})$	$W_{420}H^4\rho^2$	2	0	1
Distortion	$W_{511}(\vec{H} \cdot \vec{H})^2(\vec{H} \cdot \vec{\rho})$	$W_{511}H^5\rho \cos(\phi)$	2	1	0
Piston	$W_{600}(\vec{H} \cdot \vec{H})^3$	$W_{600}H^6$	3	0	0
Spherical aberration	$W_{060}(\vec{\rho} \cdot \vec{\rho})^3$	$W_{060}\rho^6$	0	0	3
Unnamed	$W_{151}(\vec{H} \cdot \vec{\rho})(\vec{\rho} \cdot \vec{\rho})^2$	$W_{151}H\rho^5 \cos(\phi)$	0	1	2
Unnamed	$W_{242}(\vec{H} \cdot \vec{\rho})^2(\vec{\rho} \cdot \vec{\rho})$	$W_{242}H^2\rho^4 \cos^2(\phi)$	0	2	1
Unnamed	$W_{333}(\vec{H} \cdot \vec{\rho})^3$	$W_{333}H^3\rho^3 \cos^3(\phi)$	0	3	0

extrinsic or induced aberrations. Pupil aberration can be expanded as a polynomial similar to wavefront error polynomial [28]. Pupil aberration polynomial is given as follows:

$$\begin{aligned}
\bar{W}(\vec{H}, \vec{\rho}) = & \bar{W}_{000} + \bar{W}_{200}(\vec{\rho} \cdot \vec{\rho}) + \bar{W}_{111}(\vec{H} \cdot \vec{\rho}) + \bar{W}_{020}(\vec{H} \cdot \vec{H}) \\
& + \bar{W}_{040}(\vec{H} \cdot \vec{H})^2 + \bar{W}_{131}(\vec{H} \cdot \vec{H})(\vec{H} \cdot \vec{\rho}) + \bar{W}_{222}(\vec{H} \cdot \vec{\rho})^2 \\
& + \bar{W}_{220}(\vec{H} \cdot \vec{H})(\vec{\rho} \cdot \vec{\rho}) + \bar{W}_{311}(\vec{\rho} \cdot \vec{\rho})(\vec{H} \cdot \vec{\rho}) + \bar{W}_{400}(\vec{\rho} \cdot \vec{\rho})^2
\end{aligned} \tag{2.4}$$

In pupil aberration calculations, marginal ray of object image system becomes chief ray and chief ray of object image system becomes marginal ray.

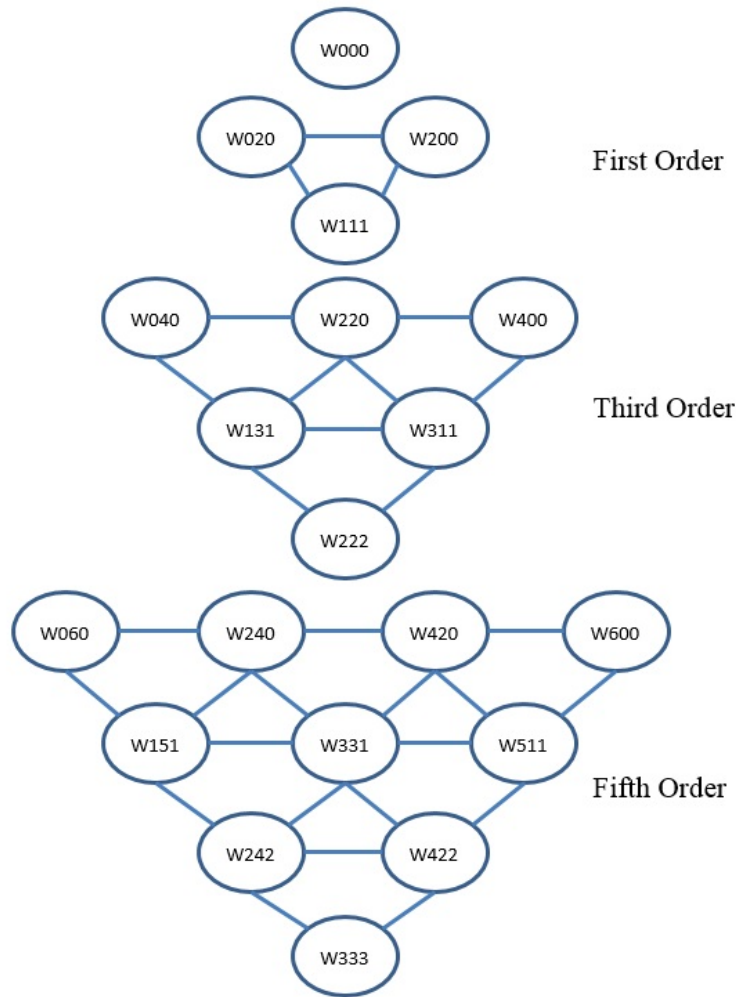


Figure 2.7: R. Shacks' representation of 4th and 6th order wave aberrations

## 2.1.2 Primary Aberrations

### 2.1.2.1 Aperture and Field Dependence

Wavefront is expanded according to the field of view and aperture position of rays. Hence, aberrations in an optical system depend on these expansion parameters. The order of magnitude of their dependence is important from design point. The dependence of wave aberrations on field and aperture is given in Table 2.2 [12].

For instance, increasing the aperture of an optical system by two increases spherical aberration by 16 while increasing field of view by two increases the distortion by 8. So the main difficulty of increasing the aperture is due to spherical aberration while increasing the field of view in an optical system is mainly due to distortion.

Table 2.2: Field and aperture dependence of wave aberrations where **C**: Coefficient,  $\sum_S$ : Seidel sum, **WA**: Wave aberration, **TA**: Transverse aberration, **LA**: Longitudinal aberration, **Ap**: Aperture, **Fld**: Field.

Aberration	C	$\sum_S$	WA		TA		LA	
			Ap.	Fld.	Ap.	Fld.	Ap.	Fld.
Spherical Aberr.	$c_1$	SI	4	0	3	0	2	0
Coma	$c_2$	SII	3	1	2	1	1	1
Astigmatism	$c_3$	SIII	2	2	1	2	0	2
Field curvature	(sagittal)	(Petzval)	2	2	1	2	0	2
	$c_4$	SIV						
Distortion	$c_5$	SV	1	3	0	3	-	-
Axial Colour	$b_1$	CI	2	0	1	0	0	0
Lateral Colour	$b_2$	CII	1	1	0	1	-	-

The three dimensional shapes of primary aberrations are given in Figure 2.8.

### 2.1.2.2 Calculation of Seidel Coefficients

The coefficients of power series expansion of wavefront are related to the parameters of optical elements constituting the imaging optical system which are radius, thickness and materials. In addition, it depends on the position of point object and on the position of aperture stop.

Seidel sums equations and quantities used in calculating them are given in Equations 2.5 and 2.6, respectively for an optical system where quantities with bar refers to chief ray while quantities without bar relates to marginal ray,  $y$  is the ray height on surface,  $u$  is the paraxial convergence angle,  $c$  is surface curvature,  $i$  is the paraxial angle of incidence,  $A$  is refraction invariant at the surface [28]. The increment is defined as  $\Delta(x) = (x - x')$ .  $\Psi$  is the Helmholtz-Lagrange invariant of the system and which corresponds to the very basic energy conservation law in optical systems.

$$\begin{aligned}
 \text{Refraction invariant marginal ray:} & \quad A = ni = nu + nyc \\
 \text{Refraction invariant chief ray:} & \quad \bar{A} = n\bar{i} = n\bar{u} + n\bar{y}c \\
 \text{Lagrange invariant:} & \quad \Psi = n\bar{u}y - nu\bar{y} = \bar{A}y - A\bar{y} \quad (2.5) \\
 \text{Surface curvature:} & \quad c = 1/r \\
 \text{Petzval sum term:} & \quad P = c \cdot \Delta(1/n)
 \end{aligned}$$

$$\begin{aligned}
W_{040} &= \frac{1}{8}S_I & S_I &= -\sum_{i=1}^j \left( A^2 y \Delta \left( \frac{u}{n} \right) \right)_i \\
W_{131} &= \frac{1}{2}S_{II} & S_{II} &= -\sum_{i=1}^j \left( A \bar{A} y \Delta \left( \frac{u}{n} \right) \right)_i \\
W_{222} &= \frac{1}{2}S_{III} & S_{III} &= -\sum_{i=1}^j \left( \bar{A}^2 y \Delta \left( \frac{u}{n} \right) \right)_i \\
W_{220} &= \frac{1}{4}(S_{IV} + S_{III}) & S_{IV} &= -\Psi^2 \sum_{i=1}^j P_i \\
W_{311} &= \frac{1}{2}S_V & S_V &= -\sum_{i=1}^j \left( \frac{\bar{A}}{A} \left[ (\Psi^2 P + \bar{A}^2 y \Delta \left( \frac{u}{n} \right)) \right] \right)_i \\
W_{311} &= \frac{1}{2}S_V & S_V &= -\sum_{i=1}^j \left( \bar{A} \left[ \bar{A}^2 \Delta \left( \frac{1}{n^2} \right) y - (\Psi + \bar{A} y) \bar{y} P \right] \right)_i \\
\delta_\lambda W_{020} &= \frac{1}{2}C_L & C_L &= \sum_{i=1}^j \left( A y \Delta \left( \frac{\delta n}{n} \right) \right)_i \\
\delta_\lambda W_{111} &= C_T & C_T &= \sum_{i=1}^j \left( \bar{A} y \Delta \left( \frac{\delta n}{n} \right) \right)_i
\end{aligned} \tag{2.6}$$

In order to calculate Seidel sums only chief ray for maximum field and marginal ray for full aperture are to be traced in an optical system. Wave aberration polynomial for primary aberrations is expressed in terms of the Seidel sums as follows:

$$\begin{aligned}
W(\rho, \phi, H) &= \frac{1}{8}S_I \rho^4 + \frac{1}{2}S_{II} H \rho^3 \cos \phi \\
&\quad + \frac{1}{2}S_{III} H^2 \rho^2 \cos^2 \phi \\
&\quad + \frac{1}{4}(S_{III} + S_{IV}) H^2 \rho^2 \\
&\quad + \frac{1}{2}S_V H^3 \rho \cos \phi
\end{aligned} \tag{2.7}$$

Primary or fourth order wave aberrations in an optical system are expressed in terms of the optical parameters such as radius, thickness, refractive index, Abbe number of elements composing the optical system. Seidel sums are the mainframe in optical design methodology discussed in this thesis.

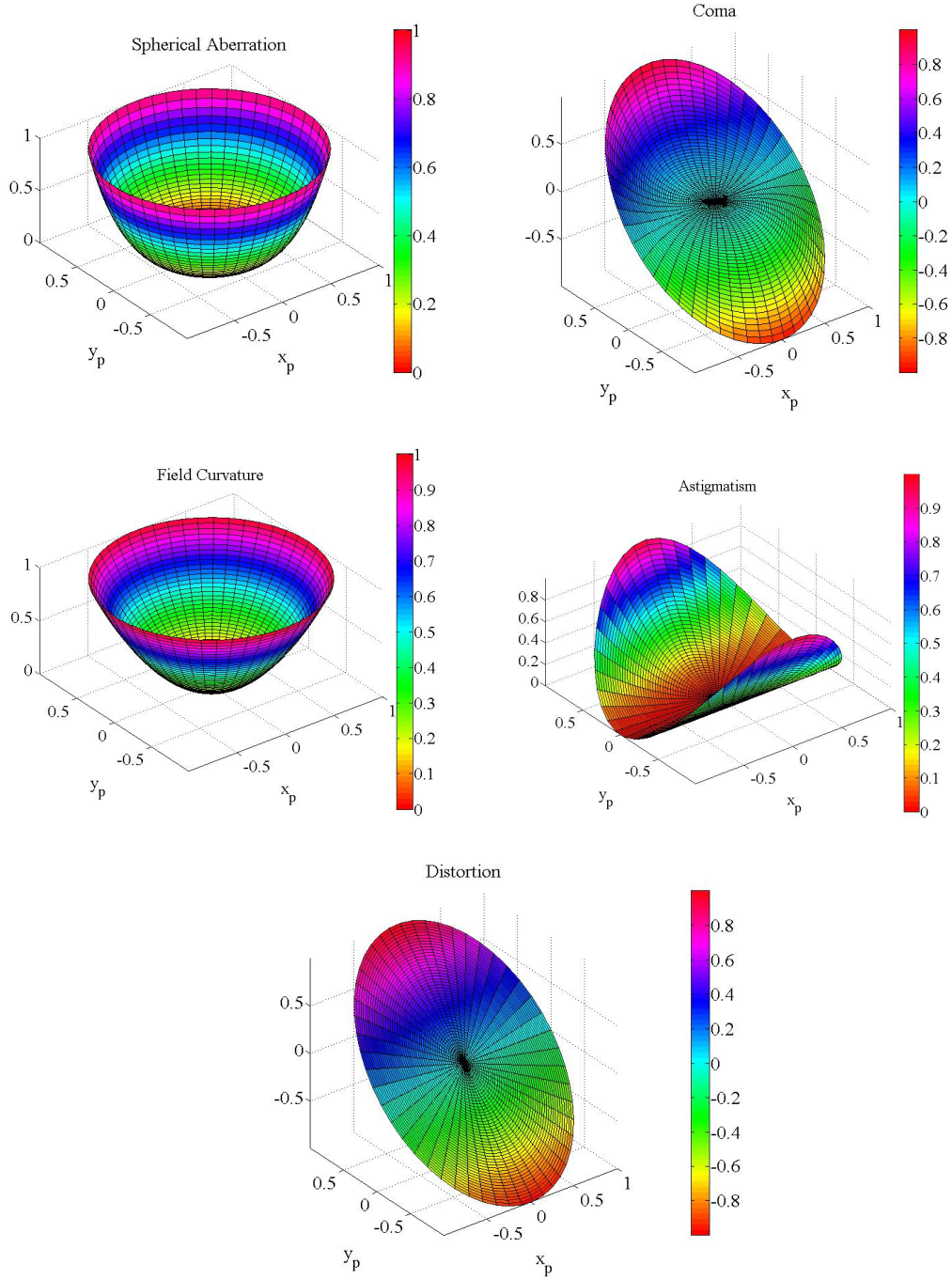


Figure 2.8: Primary wave aberration shapes

### 2.1.2.3 Calculation of Pupil Aberrations

In pupil aberrations, since marginal ray and chief ray exchange their behaviour,  $y$  and  $\bar{y}$  changes role as  $A$  and  $\bar{A}$  changes role similarly. As a result of this change, Lagrange invariant of the system,  $\Psi$ , changes sign,  $\bar{\Psi} = -\Psi$ . Pupil aberrations can be calculated with the given changes by Equations 2.6. Once primary aberrations of

object image system are calculated, pupil aberrations can also be found[28]:

$$\begin{aligned}
\bar{W}_{040} &= W_{400} \\
\bar{W}_{131} &= W_{311} + (1/2)\Psi\Delta(\bar{u}^2) \\
\bar{W}_{222} &= W_{222} + (1/2)\Psi\Delta(u\bar{u}) \\
\bar{W}_{220} &= W_{220} + (1/4)\Psi\Delta(u\bar{u}) \\
\bar{W}_{311} &= W_{131} + (1/2)\Psi\Delta(u^2) \\
\bar{W}_{400} &= W_{040}
\end{aligned} \tag{2.8}$$

#### 2.1.2.4 Stop-shift Formula

When Seidel sums equations are examined in detail,  $S_{II}$ ,  $S_{III}$  and  $S_V$  depends on the chief ray height at the surfaces. Since the chief ray height depends on the stop position,  $S_{II}$ ,  $S_{III}$  and  $S_V$  change when the stop position changes or shifts in an optical system. This is the reason why stop position is an important parameter in optimization of an optical system. In order to calculate the effect of stop shift on Seidel sum, a parameter called Seidel eccentricity is defined which indicates the shift of oblique rays with respect to axial ray. Seidel eccentricity is defined as:

$$E = \frac{\bar{h}}{h} \tag{2.9}$$

where  $h$  is marginal ray height and  $\bar{h}$  is the chief ray height. When stop is shifted, the change in eccentricity is given as:

$$\delta E = \frac{\bar{h}_{new} - \bar{h}_{old}}{h} \tag{2.10}$$

Stop shift effect is shown in Figure 2.9. Stop-shift transformations of Seidel sum equations are given in Equation 2.11 [12].

$$\begin{aligned}
S_I^* &= S_I \\
S_{II}^* &= S_{II} + \delta E \cdot S_I \\
S_{III}^* &= S_{III} + \delta E \cdot S_{II} + \delta E^2 \cdot S_I \\
S_{IV}^* &= S_{IV} \\
S_V^* &= S_V + \delta E \cdot (3S_{III} + S_{IV}) + 3\delta E^2 \cdot S_{II} + \delta E^3 \cdot S_I \\
C_I^* &= C_I \\
C_{II}^* &= C_{II} + \delta E \cdot C_I
\end{aligned} \tag{2.11}$$

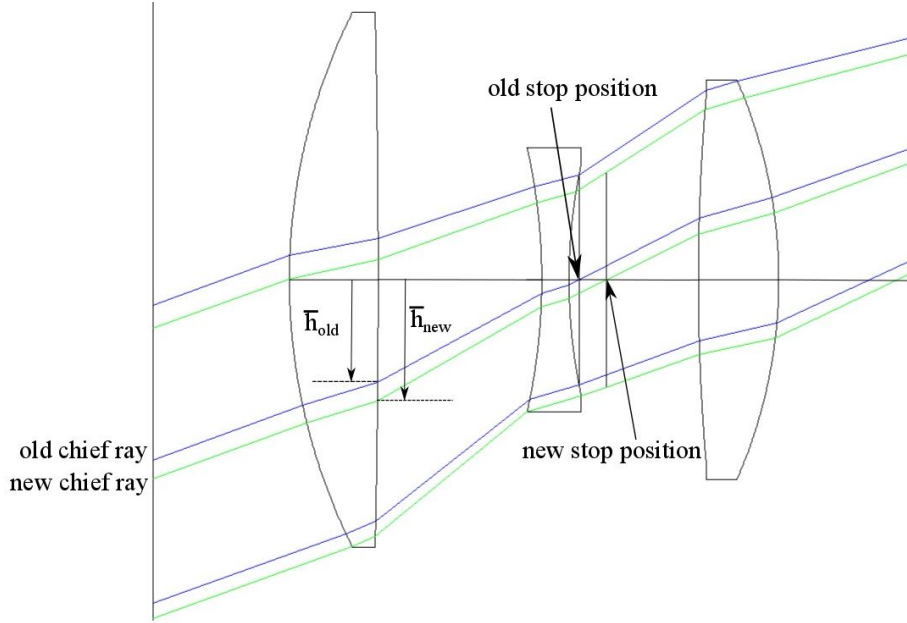


Figure 2.9: Stop shift effect and eccentricity

### 2.1.2.5 Aberrations in Seidel Sums

Primary aberrations which are also called fourth order wave aberrations in terms of Seidel sums are given below [12]:

Spherical aberration	$W_{spherical} = \frac{S_I}{8} \rho^4$	
Coma	$W_{coma} = \frac{S_{II}}{2} H \rho^3 \cos \phi$	
Astigmatism	$W_{astigmatism} = \frac{S_{III}}{2} H^2 \rho^2 \cos^2 \phi$	
Petzval field	$W_{petzval} = \frac{S_{IV}}{4} H^2 \rho^2$	
Sagittal field	$W_{sag} = \frac{S_{III} + S_{IV}}{4} H^2 \rho^2$	(2.12)
Tangential field	$W_{tan} = \frac{3S_{III} + S_{IV}}{4} H^2 \rho^2$	
Distortion	$W_{dist} = \frac{S_V}{2} H^3 \rho \cos \phi$	
Axial colour	$W_{ac} = \frac{C_I}{2} \rho^2$	
Lateral colour	$W_{lc} = C_{II} H \rho \cos \phi$	

### 2.1.2.6 Thin Lens Aberrations

Thin lenses are the idealistic representations of real lenses. Initially, designing the optical system with thin lenses relatively simplifies the design process. Even though there are no thin lenses in real case, thin lens methodology gives a good approximation in aberration analysis. A thin lens is specified with two parameters one of which is the shape factor B defined as:

$$B = \frac{c_1 + c_2}{c_1 - c_2} \quad (2.13)$$

where  $c_1$  is curvature of first surface and  $c_2$  is curvature of second surface and the other parameter is the conjugate factor and defined as:

$$G = \frac{u'_2 + u_1}{u'_2 - u_1} \quad (2.14)$$

where  $u_1$  and  $u'_2$  are paraxial marginal ray angle before and after thin lens. Primary aberrations of a thin lens in terms of conjugate parameter G and shape factor B when stop is at the thin lens are given as follows [39];

$$\begin{aligned} S_I &= \frac{K^3 h^4}{4} \left( \frac{3n+2}{n} G^2 - \frac{4n+4}{(n-1)n} BG + \frac{n+2}{(n-1)^2 n} B^2 + \frac{n^2}{(n-1)^2} \right) \\ S_{II} &= \frac{\Psi K^2 h^2}{2} \left( \frac{2n+1}{n} G - \frac{n+1}{(n-1)n} B \right) \\ S_{III} &= \Psi^2 K \\ S_{IV} &= \frac{\Psi^2 K}{n} \\ S_V &= 0 \\ C_I &= \frac{Kh^2}{V} \\ C_{II} &= 0 \end{aligned} \quad (2.15)$$

Remote stop effects are calculated easily with stop-shift effects given in Equation 2.11.

### 2.1.3 Higher Order Aberrations

Wave aberrations are expanded as power series and given in Equation 2.2. As can be seen from the expansion, it is an infinite summation over certain variables in rotationally symmetric optical systems. Primary aberrations corresponds to order 4

expansion. Expansion order is determined by the summation of the pupil parameter order and field parameter order. There are also higher orders in expansion. Next order corresponds to 6 in expansion. There are ten 6th order terms in expansion one of which is zero by definition. So effectively there are nine terms in expansion corresponding to aberrations. These nine terms are called the secondary or 6th order terms. It is generally too difficult and not feasible to correct all of these aberrations when designing an optical system. Instead, balancing of these higher terms with 4th order terms is the main approach in optical design.

### **2.1.3.1 Fifth-order Aberrations**

Fifth order aberrations' polar algebraic forms are given in Table 2.1. In higher order spherical aberrations, there is a higher order spherical aberration term with pupil order six. Besides, two new spherical aberration forms emerge. These new types of spherical aberrations are called tangential and sagittal oblique spherical aberrations. They both have second order field dependence, fourth order pupil dependence and one of them have second order azimuthal dependence. Their waveforms are given in Figure 2.10.

Similarly, there is a 6th order higher order coma term with order five in pupil parameter. Besides, there are two new coma type aberrations emerging in 6th order terms. They are called elliptical coma aberrations. Their waveforms are given in Figure 2.11. There are no new aberrations types for astigmatism, field curvature and distortion but only higher order dependence on field parameter. The waveforms of secondary astigmatism, field curvature and distortion are given in Figure 2.12.

Although sixth order aberrations conceptually seems simple, their calculations are much more involved than fourth order aberrations. The complexity stems from the fact that the sixth order aberrations of a surface depend on the aberrations of the incident waveform. As a result, sixth order aberration coefficients of a surface have an intrinsic part which is the aberration resulting from the surface itself only and extrinsic part which results from the aberrations of the incident waveform on the surface.

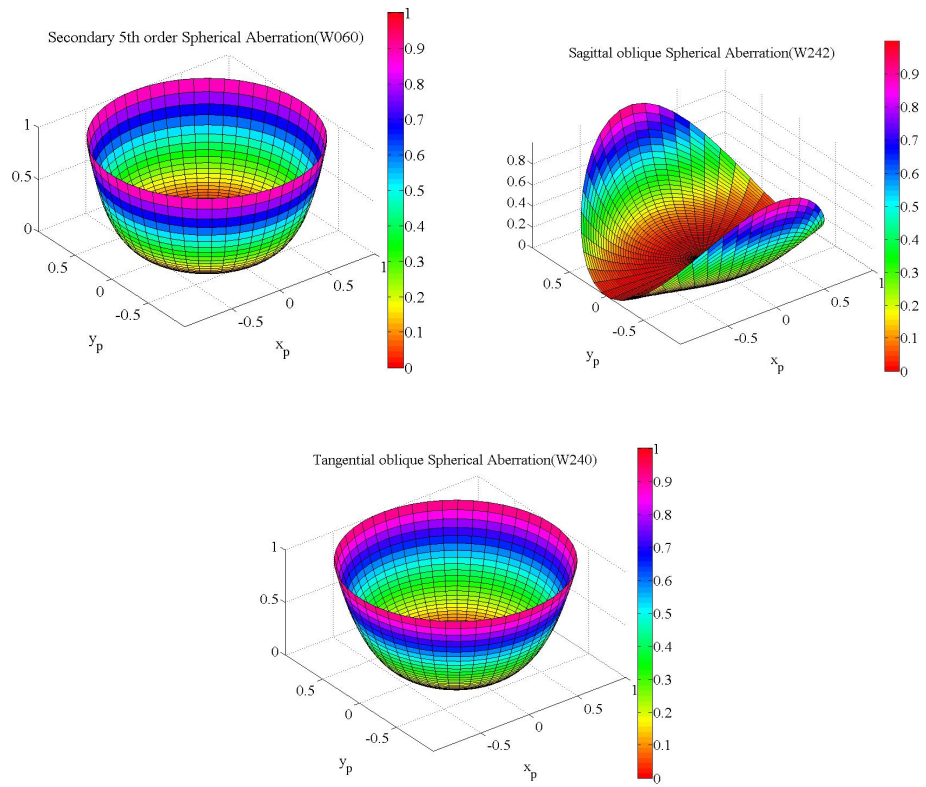


Figure 2.10: Secondary 5th order spherical aberration

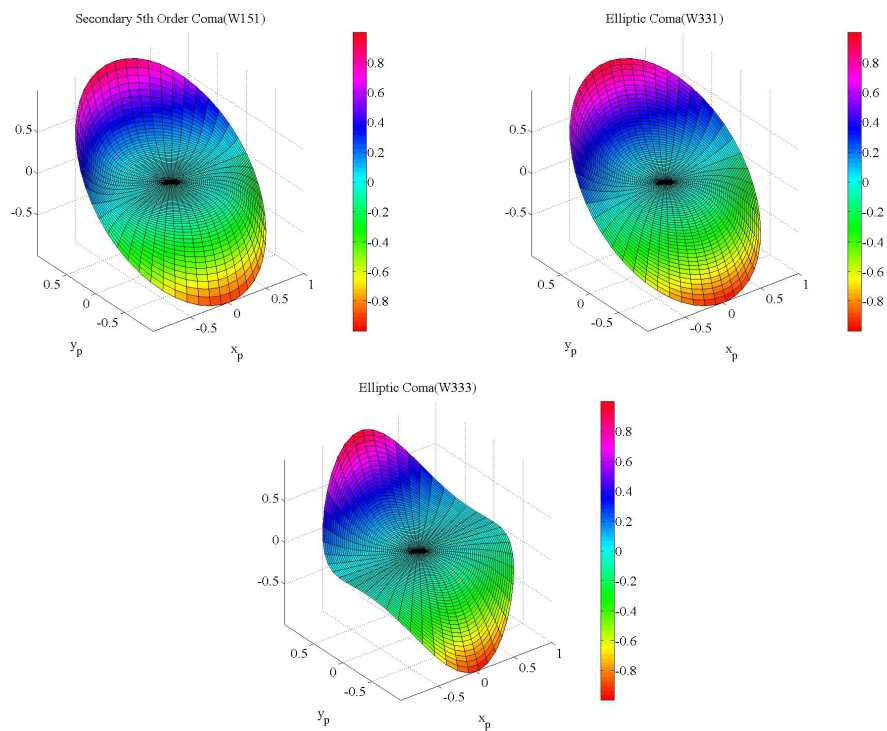


Figure 2.11: Secondary 5th order coma

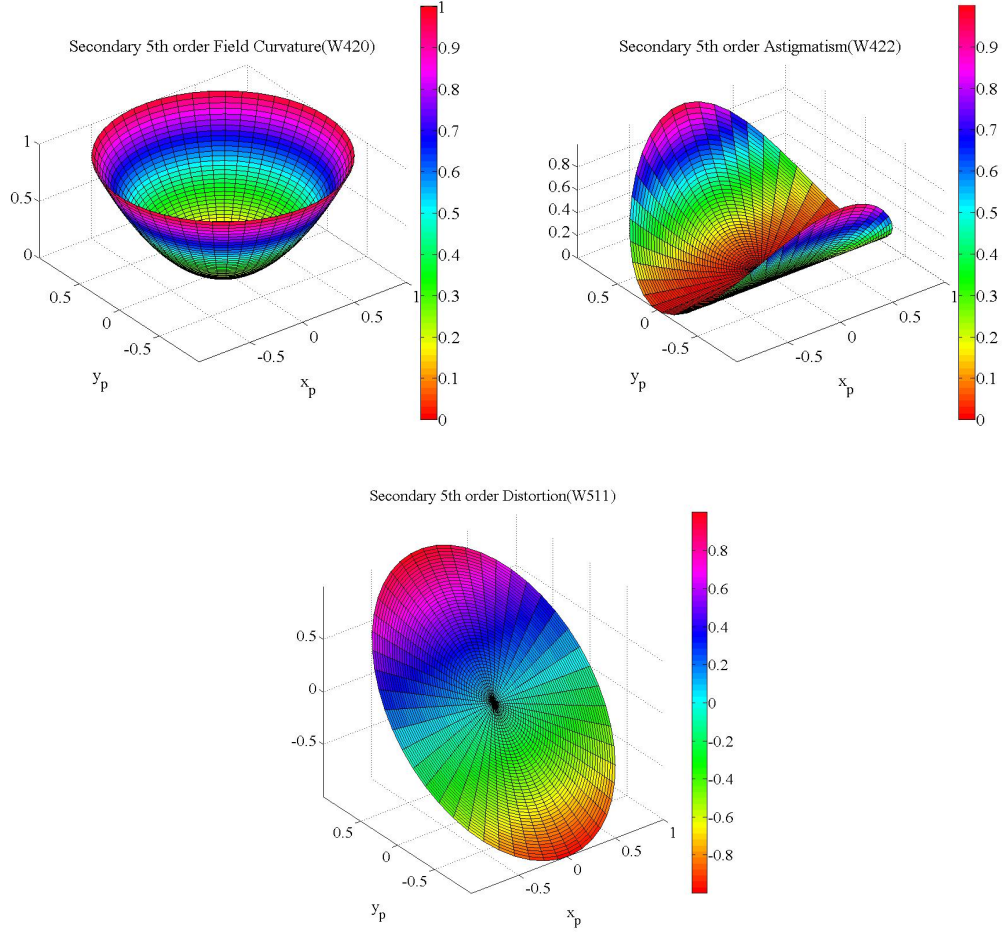


Figure 2.12: Secondary 5th field curvature, astigmatism and distortion

**Extrinsic aberrations** If two systems are denoted as A and B, then extrinsic aberrations are the sum of products of fourth order image aberrations of system A and pupil aberrations of system B. Extrinsic aberration coefficients are given in Equation 2.16 where coefficients with bar represent the pupil aberration of the surface and without bar coefficients represent the aberration of the system before that surface [28].

$$\begin{aligned}
 W_{060E} &= -\frac{1}{\Psi} (4W_{040}^A \bar{W}_{311}^B) \\
 W_{151E} &= -\frac{1}{\Psi} (3W_{131}^A \bar{W}_{311}^B + 8W_{040}^A \bar{W}_{220}^B + 8W_{040}^A \bar{W}_{222}^B) \\
 W_{242E} &= -\frac{1}{\Psi} (2W_{222}^A \bar{W}_{311}^B + 4W_{131}^A \bar{W}_{220}^B + 6W_{131}^A \bar{W}_{222}^B + 8W_{040}^A \bar{W}_{131}^B) \quad (2.16) \\
 W_{333E} &= -\frac{1}{\Psi} (4W_{131}^A \bar{W}_{131}^B + 4W_{222}^A \bar{W}_{222}^B) \\
 W_{240E} &= -\frac{1}{\Psi} (2W_{131}^A \bar{W}_{220}^B + 2W_{220}^A \bar{W}_{311}^B + 4W_{040}^A \bar{W}_{131}^B)
 \end{aligned}$$

$$\begin{aligned}
W_{331E} &= -\frac{1}{\Psi} (5W_{131}^A \bar{W}_{131}^B + 4W_{220}^A \bar{W}_{220}^B + 4W_{220}^A \bar{W}_{222}^B + 4W_{222}^A \bar{W}_{220}^B \\
&\quad + W_{311}^A \bar{W}_{311}^B + 16W_{040}^A \bar{W}_{040}^B) \\
W_{422E} &= -\frac{1}{\Psi} (2W_{311}^A \bar{W}_{222}^B + 4W_{220}^A \bar{W}_{131}^B + 6W_{222}^A \bar{W}_{131}^B + 8W_{131}^A \bar{W}_{040}^B) \\
W_{420E} &= -\frac{1}{\Psi} (2W_{220}^A \bar{W}_{131}^B + 2W_{311}^A \bar{W}_{220}^B + 4W_{131}^A \bar{W}_{040}^B) \\
W_{511E} &= -\frac{1}{\Psi} (3W_{311}^A \bar{W}_{131}^B + 8W_{220}^A \bar{W}_{040}^B + 8W_{222}^A \bar{W}_{040}^B) \\
W_{600E} &= -\frac{1}{\Psi} (4W_{311}^A \bar{W}_{040}^B)
\end{aligned} \tag{2.16}$$

**Intrinsic aberrations** Intrinsic aberrations are the extensions of primary aberration formulations. As in the primary aberration formulation, since intrinsic aberrations depend on chief ray height, they have stop-shift formulation also. Intrinsic aberration coefficients when stop is on the center of curvature are given in Equation 2.17 [28].

$$\begin{aligned}
W_{220P} &= -\frac{1}{4}\Psi^2 P \\
W_{040P} &= -\frac{1}{8}A^2 \Delta\left(\frac{u}{n}\right)y \\
W_{060CC} &= W_{040} \left[ \frac{1}{2} \frac{y^2}{r^2} - \frac{1}{2} A \left( \frac{u'}{n'} + \frac{u}{n} \right) + 2 \frac{y}{r} u' \right] \\
&\quad + \frac{8}{Ay} W_{040} W_{040} - \frac{\bar{A}}{A} \frac{8}{\Psi} W_{040} W_{040} \\
W_{240CC} &= \frac{1}{16} \frac{A}{r} \Psi^2 \Delta\left(\frac{u}{n^2}\right) + \frac{1}{8} \frac{1}{r} \Psi^2 \Delta\left(\frac{u^2}{n}\right) + \frac{1}{4} \frac{y^2}{r^2} W_{220P} \\
&\quad + \frac{y}{r} u' W_{220P} - \frac{1}{4} \frac{u}{r} \Psi^2 \Delta\left(\frac{u}{n}\right) - \frac{8}{\Psi} \left(\frac{\bar{A}}{A}\right) W_{040} W_{220P} \\
W_{420CC} &= \frac{3}{16} \frac{1}{r^3} \Psi^4 \Delta\left(\frac{1}{n}\right) \frac{1}{A^2} - \frac{2}{\Psi} \left(\frac{\bar{A}}{A}\right) W_{220P} W_{220P} \\
W_{331CC} &= -2W_{220P} u' \left( \bar{u}' - \frac{\bar{A}}{A} u' \right) \\
W_{422CC} &= -W_{220P} \left( \bar{u}' - \frac{\bar{A}}{A} u' \right)^2
\end{aligned} \tag{2.17}$$

$$\begin{aligned}
W_{151CC} &= -4W_{040}u' \left( \bar{u}' - \frac{\bar{A}}{A}u' \right) \\
W_{242CC} &= -2W_{040} \left( \bar{u}' - \frac{\bar{A}}{A}u' \right)^2
\end{aligned} \tag{2.17}$$

Total intrinsic aberration coefficients are given in Equation 2.18 [28].

$$\begin{aligned}
W_{060I} &= W_{060I} \\
W_{151I} &= 6 \left( \frac{\bar{A}}{A} \right) W_{060I} + W_{151CC} \\
W_{242I} &= 12 \left( \frac{\bar{A}}{A} \right)^2 W_{060I} + 4 \left( \frac{\bar{A}}{A} \right) W_{151CC} + W_{242CC} \\
W_{333I} &= 8 \left( \frac{\bar{A}}{A} \right)^3 W_{060I} + 4 \left( \frac{\bar{A}}{A} \right)^2 W_{151CC} + \left( \frac{\bar{A}}{A} \right) W_{242CC} \\
W_{240I} &= 3 \left( \frac{\bar{A}}{A} \right)^2 W_{060I} + 4 \left( \frac{\bar{A}}{A} \right) W_{151CC} + W_{240CC} \\
W_{331I} &= 12 \left( \frac{\bar{A}}{A} \right)^3 W_{060I} + 6 \left( \frac{\bar{A}}{A} \right)^2 W_{151CC} + 4 \left( \frac{\bar{A}}{A} \right) W_{240CC} \\
&\quad + 2 \left( \frac{\bar{A}}{A} \right) W_{242CC} + W_{331CC} \\
W_{422I} &= 12 \left( \frac{\bar{A}}{A} \right)^4 W_{060I} + 8 \left( \frac{\bar{A}}{A} \right)^3 W_{151CC} + 4 \left( \frac{\bar{A}}{A} \right)^2 W_{240CC} \\
&\quad + 5 \left( \frac{\bar{A}}{A} \right)^2 W_{242CC} + 2 \left( \frac{\bar{A}}{A} \right) W_{331CC} + W_{422CC} \\
W_{420I} &= 3 \left( \frac{\bar{A}}{A} \right)^4 W_{060I} + 2 \left( \frac{\bar{A}}{A} \right)^3 W_{151CC} + 2 \left( \frac{\bar{A}}{A} \right)^2 W_{240CC} \\
&\quad + \left( \frac{\bar{A}}{A} \right)^2 W_{242CC} + \left( \frac{\bar{A}}{A} \right) W_{331CC} + W_{420CC} \\
W_{511I} &= 6 \left( \frac{\bar{A}}{A} \right)^5 W_{060I} + 5 \left( \frac{\bar{A}}{A} \right)^4 W_{151CC} + 4 \left( \frac{\bar{A}}{A} \right)^3 W_{240CC} \\
&\quad + 4 \left( \frac{\bar{A}}{A} \right)^3 W_{242CC} + 3 \left( \frac{\bar{A}}{A} \right)^2 W_{331CC} + 2 \left( \frac{\bar{A}}{A} \right) W_{422CC} \\
&\quad + 2 \left( \frac{\bar{A}}{A} \right) W_{420CC} \\
W_{600I} &= \bar{W}_{060I}
\end{aligned} \tag{2.18}$$

### 2.1.3.2 Seventh and higher-order aberrations

In the wave aberration power series expansion, the number of aberration terms of the  $n$ 'th order,  $N$ , is given as:

$$N = \frac{(n + 3)(n + 5)}{8} - 1 \quad (2.19)$$

There are 14 terms regarded as seventh order in wavefront error aberration polynomial expansion. Since analytical representations of these seventh order aberration terms are too complicated, ray trace based numerical optimization routines will be used after third order aberration terms are corrected and balanced with fifth order aberration terms.

## 2.2 Optical Design Procedure

A fully closed form analytical solution of an optical system is too much complex to be followed since the aberration equations are too complicated and there are too many variables even in a relatively simple optical system. R. Kingslake, the father of optical design, emphasizes this point with these words: “optical design is about as nonlinear as anything in physics” [19]. Hence, an analytical solution methodology is constructed for finding a good starting point in an optical design in this thesis. In early stages of design procedure, a pre-design that is capable of satisfying the specifications and necessary optical performance is constructed. This pre-design is then taken as a starting point to optimization routines of ZEMAX [21] to get the final solution. At final stage, optimization routines of ZEMAX optical design software are used to consider the higher order aberration balancing to achieve the specified optical performance. Starting point of a design in an optimization routine is very critical in order find a solution satisfying the specified performance since the solution hyperspace topology may have different local minima and different constraint barriers depending on the number of variables [38]. According to Kidger, there are 4 different choices of starting points [17]. These starting points are given as:

1. Modification of an existing design
2. Purchase of a competing lens(reverse engineering)

3. Analytical solutions
4. Semi-analytic synthesis of new design forms

In this thesis, starting point is constructed with semi-analytic synthesis of design form. Constructing a starting point requires the first, third and fifth order aberration theory which was introduced in chapter 2.1. Using aberration theory from the beginning to the end of an optical design makes the design process much more efficient by providing a detailed classification and decompositions of aberration types. Detecting the problematic surfaces and solving them are very effective with this type of classification and decompositions of total aberrations in surface level. Optical design flow diagram is shown in Figure 2.13 [39].

### 2.2.1 Specification

In order to find a solution for an application, certain parameters of the optical system must be determined beforehand and according to these parameters the type of the optical design must be specified. In the first place, the type and the size of the source object, the spectrum and irradiance of the light that the object is imaged and the sensitivity and size of the detector which is going to be used in the optical system must be determined. Then these parameters must be converted to certain first order

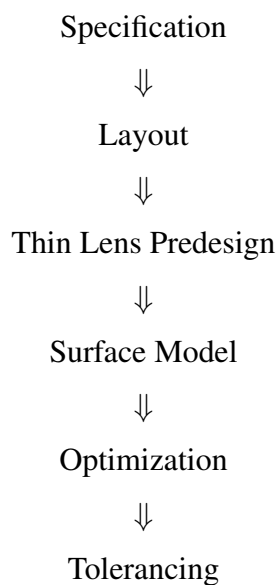


Figure 2.13: Optical design flow [39]

Table 2.3: Optical specification

Anamorphic ratio	Aspheric surfaces
Athermalization	Back focal length
Clear aperture	Cost, quantity, delivery schedule
Depth of focus	Diffractive surfaces
Distortion	Effective focal length
Environment, ambient conditions	Erect or inverted image
Ergonomics	Field angle or object size
Flat or curved field	F number
Focusing: shift part or all of system	Focus range
Front focal length	Internal image require
Lens type	Magnification
Materials	Numerical aperture
Object and image distance	Patent considerations
Performance	Plastic elements
Pupil locations and size; eyerelief	Refractive versus mirror
Sensor, spectral response	Size, weight and packaging constraints
Space for iris diaphragm	Spectral distribution and weighting
Telecentricity	Transmission
Vignetting / illumination uniformity	Visual, photographic, projection
Wavelength and bandwidth	Working distance
Zoom range: continuous or stepped	

basic optical design parameters. The most important parameters that must be specified in order to start an optical design are as follows: focal length, waveband,  $f\#$ , field of view, detector and materials of optical components. Warren Smith's optical specification and considerations checklist is given as in Table 2.3 [33].

### 2.2.2 Layout

According to first order parameters, thin lens solutions are constructed in this phase. General paraxial configurations of lens types which are mainly derived by aperture and field of view are well established. Typically categories of lenses Gross and Bentley are shown in Figure 2.14 [13, 15].

Depending on the category of the lens, the powers and air thicknesses between thin lens components are determined at this stage. Focal length of the thin lens combina-

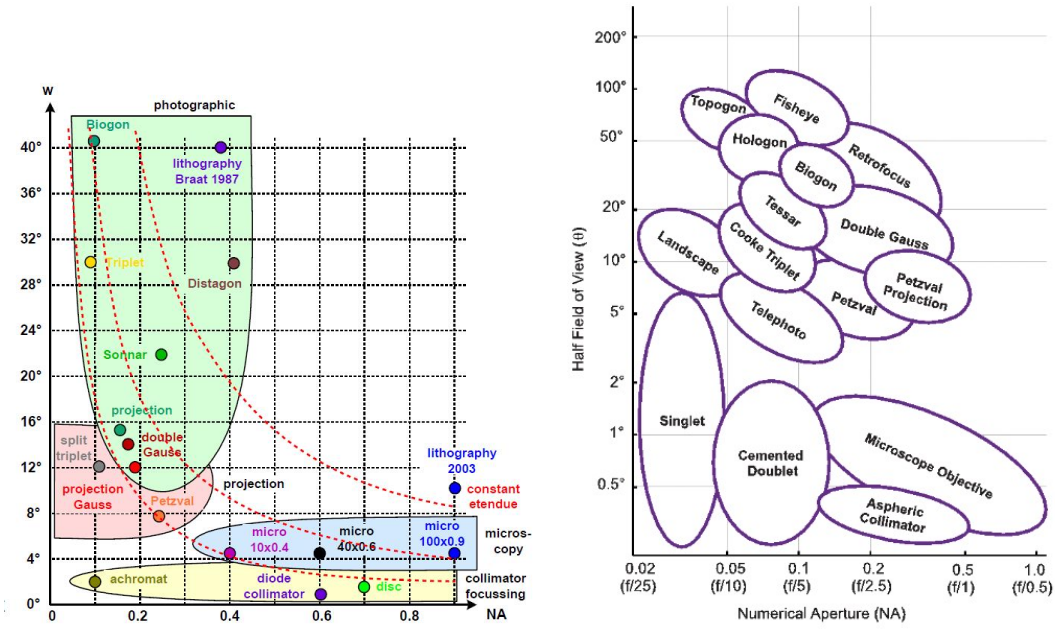


Figure 2.14: Classifications of lens types [13, 15]

tions are calculated with the scale equation given as:

$$K = \sum_{i=1}^k \frac{h_i}{h_1} K_i \quad , \quad u_1 = 0 \quad (2.20)$$

where  $K_i$ 's are the thin lens component powers,  $h_i$ 's are the marginal ray heights. Shape independent aberrations which are field curvature, axial and lateral colour aberrations are calculated and corrected in this stage also. Field curvature, axial and lateral colour aberrations are calculated and corrected with the following equations:

$$P = \sum_{i=1}^k \frac{K_i}{n_i}$$

$$C_1 = \sum_{i=1}^k \frac{h_i^2 K_i}{V_i} = \frac{h_1^2 K}{V_s} \quad (2.21)$$

$$C_2 = \sum_{i=1}^k \frac{h_i \bar{h}_i K_i}{V_i}$$

where  $n_i$ 's and  $V_i$ 's are refractive index and Abbe numbers of materials,  $h_i$  and  $\bar{h}_i$  are the marginal ray height and chief ray height correspondingly. At the end of this stage, element powers, element materials, stop position and air thickness are found with field curvature, axial and lateral colour corrected with the specified focal length.

### 2.2.3 Thin lens predesign

At thin lens predesign stage, since lens powers, materials and air thicknesses are known, conjugate parameters of thin lenses and marginal and chief ray height on each thin lens can be found, Seidel aberration formulation (Equation 2.13, Equation 2.14, Equation 2.15) and stop-shift equation sets (Equation 2.11) in terms of shape factors and conjugate factors of thin lenses can be constructed in terms of shape factors of thin lenses. Equation sets must provide enough degree of freedom to correct all Seidel aberrations paraxially. At the end of this stage, focal lengths, materials, shape factors of thin lenses are calculated with corrected Seidel aberrations paraxially.

### 2.2.4 Surface model

Up to this stage, lenses are considered as thin having zero thickness which is unphysical. In order to make lenses manufacturable, thicknesses must be assigned to each thin lens. As a rule of thumb, a positive lens thickness must be minimum 10-15% of its diameter length while its edge must be larger than 1 mm. A negative lens thickness must be minimum 6% of its diameter. Introducing thicknesses to thin lens creates many problems to be considered. First problem of introducing a thickness directly without any modification to curvatures is that the focal length distribution of lenses changes which directly disturbs the aberration correction. So the focal length change due to thickness must be compensated when introducing thicknesses to lenses. Second problem that must be considered carefully is to compensate the shift of the principle points of thin lens due to thickness introduced. Velzel's surface model methodology is used for thickening lenses [39]. First the power of the thin lens,  $K$ , is calculated with nominal curvatures taking into account the thickness.

$$K = K_1 + K_2 - \frac{dK_1K_2}{n} \quad (2.22)$$

where  $K_1$  and  $K_2$  are surface powers. Then the radius  $r_1$ ,  $r_2$  and  $d$  are scaled with  $\frac{K}{K_1+K_2}$  which compensates the focal length shift of thickness introduced. The shift of

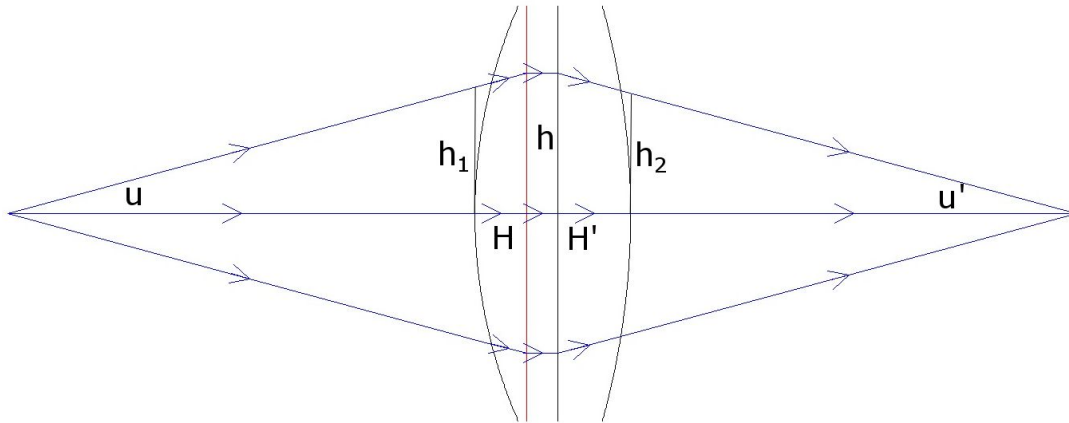


Figure 2.15: Marginal ray height change in a thickened thin lens

principle planes are given by:

$$\begin{aligned}
 V_2 H' &= -\frac{(n-1)c_1^* d^*}{n(K_1 + K_2)} \\
 V_1 H &= -\frac{(n-1)c_2^* d^*}{n(K_1 + K_2)}
 \end{aligned}
 \tag{2.23}$$

where  $c_1^*$  and  $c_2^*$  are curvatures and  $K_1 + K_2$  is the power after scale by  $\frac{K}{K_1 + K_2}$ .  $V$  represents the vertex of the thin lens. After all, thin lenses are converted to real manufacturable lenses in optical design. Last and the dominant problem of introducing thicknesses to thin lenses is the change of the marginal and chief ray height on surfaces of lenses which changes the aberration correction considerably. A typical marginal ray height change is shown in Figure 2.15. Changes in aberrations due to thicknesses will be handled in optimization phase.

### 2.2.5 Optimization

Optimization is final stage of the design before fixing the design and starting the tolerance analysis. The main purpose of all the design work up to here was to find a suitable and potential pre-design candidate of an optical system that can evolve to the final design after optimization. All of the previous stages was based on algebraic methodology based on Seidel theory and fifth order theory. Although pre-design candidate was constructed such that third order aberration coefficients are targeted to be significantly small in Seidel sum equations, these coefficients will not be significantly small because of the higher order aberrations, but balanced with higher order aber-

rations by ray trace based numerical optimization routines. Damped least squares and global optimization are two main optimization routines used in optical design. DLS optimization algorithm is discussed in detail by Meiron [22]. Global optimization is discussed in detail by Forbes [9], Kuper [20] and Thibault [36]. In numerical optimization routines, aberrations are balanced with several aperture rays with several field points at specified waveband according to the specified image quality. The quality of the design is represented by a merit function in an algorithm with different targets and constraints. In order to improve performance of the pre-design, certain optical parameters are assigned as variables in optimization routines. Typical parameters are radius of curvature, lens thickness, air gap thickness, refractive index and Abbe number of lens materials which are used in optimization. The most effective parameter in optimization is the radius of curvature. Although thickness of lenses and air gaps are not as effective as radius of curvature, they are also important parameters in optimization. Other important elements of optimization are the constraints of the system. In an optical design optimization problem, the most common constraints are the effective focal length, overall length and size, thickness of lenses, edge thickness of lenses, aspect ratio of lenses and thickness of air gaps.

### **2.2.6 Tolerancing**

Tolerancing is the final and the most time consuming step of optical design. General evolution of tolerancing in optical systems is discussed by Youngworth [40]. The steepness of nominal design solution point in design solution hyperspace is closely related to the statistical performance of the manufactured optical design. Hence tolerancing procedure is a very important step in optical design methodology. The importance of tolerancing in optical design is exposed well by Fischer [8]. In an optical design, all of the optical and optomechanical parameters, which are radius of curvature, conic constants, aspheric coefficients and center thickness of lenses, wedge of lenses, diameter of lenses, refractive index and Abbe numbers of optical materials of lenses, air thicknesses, decentering and tilting of lenses or group of lenses deviate from the nominal design values statistically according to manufacturing and optomechanical positioning techniques. Statistical nature of tolerancing is discussed by Adams [1], Forse [10] and Youngworth [41]. Since the image quality of opti-

Table 2.4: Commonly toleranced lens parameters

Item	Tolerance	Expressed as	Measured as
Radius	Length	Fringes	Fringes
Center thickness	Length	Length	Length
Edge thickness	Length	Length	Result of edging diameter
Axial spacing	Length	Length	Mount determined separation
Index of refraction	$n_d$		Melt data
Dispersion	$V_d$		Melt data
Tilt	Arc seconds	Angle	Runout
Decenter	Length	Length	Runout
Irregularity	Fringes	Surface fringes	Fringes
Asphericity	Coefficient	Surface fringes	Fringes
Wedge	Angle	Angle	Fringes
Flatness	Curvature	Fringes	Fringes

cal system depends on these optical design parameters, image quality also deviates from the design quality after manufacturing and optomechanical positioning. Manufacturing and optomechanical positioning errors are inevitable in an optical system. The main aim of the tolerancing procedure is to find a suitable set of tolerances assigned to each lens for manufacturing and optomechanical positioning which satisfy the image quality needed. Fundamental budgeting and outline of optical tolerances are discussed by Smith [34] and Ginsberg [11]. In order assign tolerances on optical parameter, the cost and capability of manufacturer must be known beforehand. Cost aspects of optical tolerancing is discussed by Nelson [6] and Kehoe [16]. Most of the time degradation of image quality in an optical system due to tolerance perturbations is compensated by chosen compensators rather than tightening the tolerances which will increase the cost considerably or even pushes the system beyond the manufacturing limits. Another aim of tolerancing step is to assign logical compensators to the optical system. Since in the majority of the optical system allows focus adjustment after alignment and assembly procedures, focal position and possibly tilt of the focal plane especially for the correction of asymmetric errors are generally used as compensators effectively in an optical system which relaxes many of the tolerances assigned and improves degraded image quality. A fast tolerancing procedure is outlined by Rimmer which enables the optimization considering the sensitivity of optical design [25]. Parameters of lenses with their units which are commonly toleranced is given in Table 2.4 [31].

Table 2.5: Typical manufacturing tolerance data [35]

Attribute	Precision	High Precision
Glass Material	$\pm 0.0005, \pm 0.5\%$	Melt data
Diameter(mm)	$+0.000 / -0.025$	$+0.000 / -0.015$
Center thickness(mm)	$\pm 0.050$	$\pm 0.025$
SAG(mm)	$\pm 0.025$	$\pm 0.015$
Clear Aperture	90%	90%
Radius(larger of two)	$\pm 0.1\%$ or 3 fr	$\pm 0.05\%$ or 1 fr
Irregularity-Interferometer(fringes)	0.5	0.2
Irregularity-Profilometer(microns)	$\pm 1$	$\pm 0.5$
Wedge Lens(ETD,mm)	0.010	0.05
Wedge Prism(TIA,arc min)	$\pm 1\%$	$\pm 0.5\%$
Bevels(face width @45,mm)	$< 0.5$	$< 0.5$
Scratch-DIG	60 – 40	20 – 10
Surface Roughness(A rms)	20	10
AR Coating( $R_{ave}$ )	BBAR $R < 0.5\%$	V-coat $R < 0.2\%$

Before starting the tolerancing procedure, allowable image degradation must be determined. Generally RMS wavefront or MTF over all of the field of view is chosen as image quality criterion. Initially, a set of tolerances of all parameters in Table 2.4 must be assigned based on an assumption. These values can be obtained from the manufacturer which will produce the optical elements. Typical tolerance values for OPTIMAX is given in Table 2.5 [35].

Once each of the tolerances are determined, individual effect of each tolerance on the image quality criterion must be calculated and sorted from the most sensitive to onwards. The most critical and sensitive part of optical system can be deduced from this step and special care must be taken at these tolerances which can sometimes be resulted in redesigning of the optical system. Since all of the assigned tolerances are effective all together in a manufactured optical system, built-in performance simulations must be done by statistical models and Monte Carlo simulations. For the prediction of production yields in Monte Carlo simulations, probabilistic distributions of tolerances must be assigned. These distributions can be obtained from manufacturer or conservative distributions like uniform or ping-pong can be assigned. After-all, performance degradation and tolerance cost estimation are done. If performance degradation is greater than allowed or cost is too high then chosen compensator can be changed or assigned tolerances can be tightened. If the degradation is still too

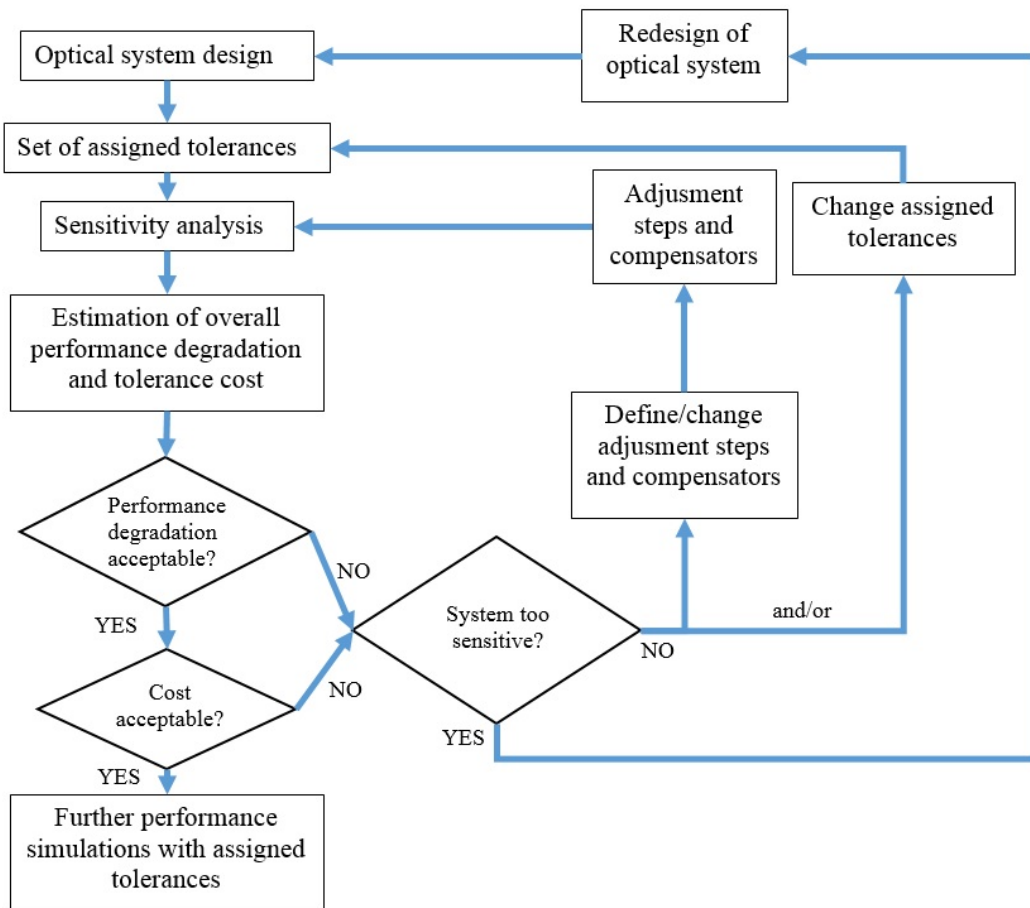


Figure 2.16: Tolerance procedure [12]

high which means that optical design is too sensitive, redesign of the optical system is needed. A general flow chart for tolerancing procedure is given in Figure 2.16 [12].

## CHAPTER 3

### SWIR OBJECTIVE DESIGN

#### 3.1 Specification

Specifications of the objective are assumed to be analysed beforehand as in Table 3.1 according to requirements considering all the detection chain elements discussed in introduction.

The category of this objective with the given specifications is a telephoto lens. In a telephoto lens, objective total length is smaller than the focal length of the objective.

#### 3.2 Layout

Typical paraxial layout of a telephoto lens is given in Figure 3.1. In its simplest paraxial representation, it consists of positive front lens and a negative lens behind so

Table 3.1: SWIR objective specifications

Focal length	200 mm
Waveband	0.9 – 1.7 $\mu\text{m}$
F- number	2.4
Field of view	5.87° (diagonal)
Detector	640×512
Detector Pitch	25 $\mu\text{m}$
Materials	Visible glasses
Resolution	MTF > 0.25 @33 lp/mm
Distortion	< 1%
Vignetting	Not allowed

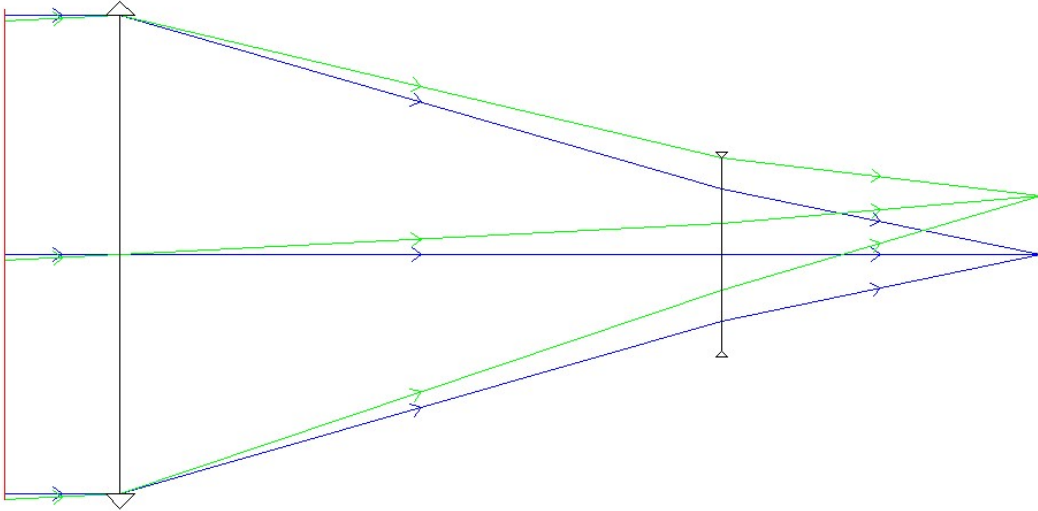


Figure 3.1: Paraxial layout of a typical telephoto lens

that the focal length of the lens is greater than the total length of the objective.

Focal lengths of two paraxial lenses,  $f_a$  and  $f_b$  must be chosen at first considering the relations between focal length ( $F$ ), total length and lens separation ( $d$ ). The ratio of total length to focal length is very useful to define lens focal lengths and is known as the telephoto ratio ( $k$ ). This ratio is generally assumed to be 0.8.

Using paraxial relations in Figure 3.2,

$$\frac{y_b}{y_a} = \frac{f_a - d}{f_a} = \frac{kF - d}{F} \quad (3.1)$$

$$f_a = \frac{Fd}{F(1 - k) + d} \quad (3.2)$$

Using lens equation for negative lens,

$$\frac{1}{f_b} = \frac{1}{kF - d} - \frac{1}{f_a - d} \quad (3.3)$$

which follows

$$f_b = \frac{(f_a - d)(kF - d)}{f_a - kF} \quad (3.4)$$

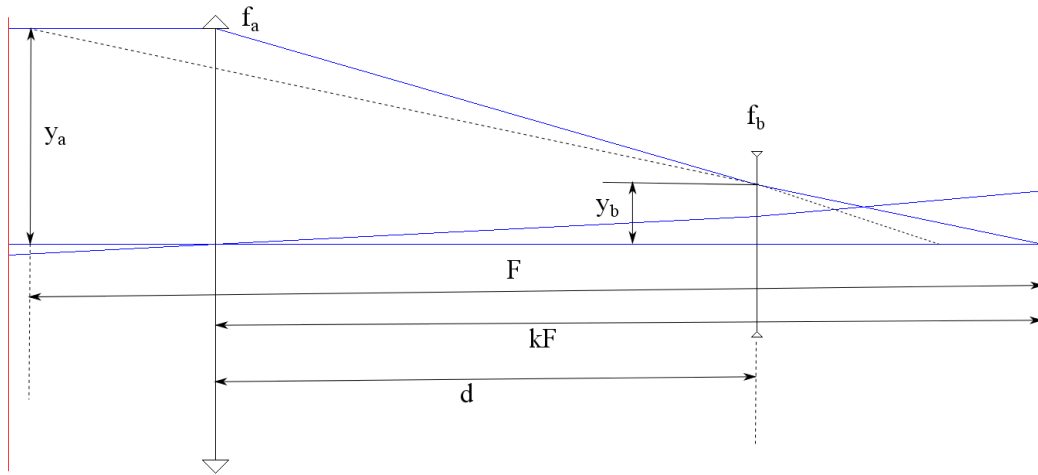


Figure 3.2: Paraxial relations for a typical telephoto lens

Focal lengths of the lenses must be chosen such that their f-numbers ( $f\#_a$  and  $f\#_b$ ) are as big as possible since higher f-number causes smaller aberrations. Using paraxial ray tracing Figure 3.3, f-number relations are as follows:

$$u' = u - \frac{y_a}{f_a} \quad (3.5)$$

$$y'_b = y_a - d \tan(u') = y_a - d \tan\left(u - \frac{y_a}{f_a}\right) \quad (3.6)$$

$$f_a\# = \frac{f_a}{y_a} \quad (3.7)$$

$$f_b\# = \frac{f_b}{y'_b} \quad (3.8)$$

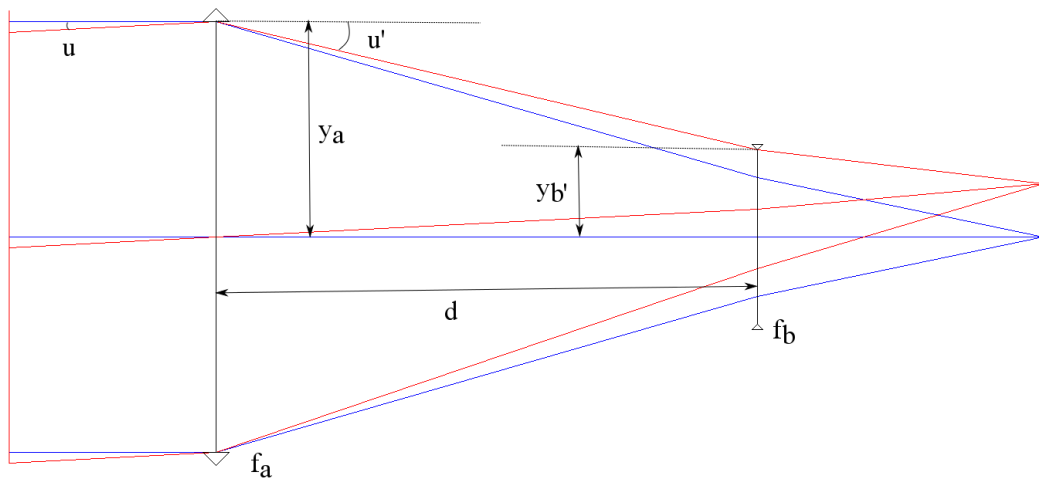


Figure 3.3: F# relations of a typical telephoto lens

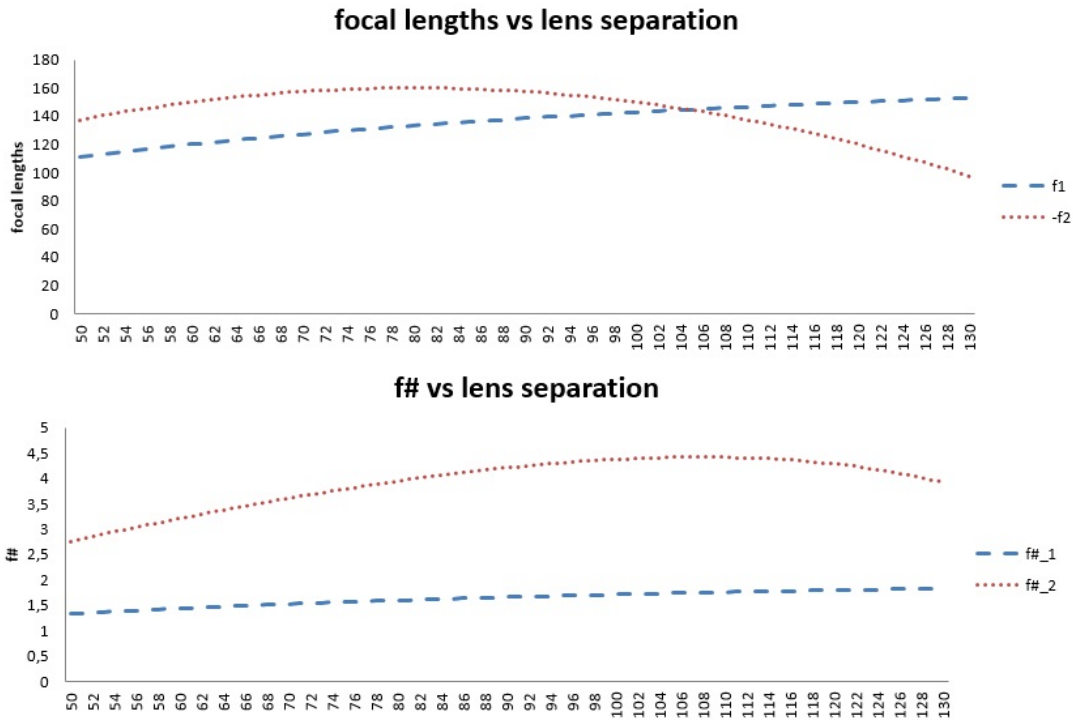


Figure 3.4: Focal length (upper panel) and  $f\#$  (lower panel) graph with respect to lens separation for 0.8 telephoto ratio

According to these equations, once the telephoto ratio and lens separation are chosen, focal lengths and  $f\#$  of positive and negative lens are defined. Focal lengths and  $f\#$  of lenses are given in for 0.8 telephoto ratio with respect to lens separation in Figure 3.4.

Equal magnitude focal length point is chosen as a starting point in this design. Equations are solved with equal magnitude focal lengths and starting paraxial design data is given in Table 3.2.

Paraxial ray trace data is given in Table 3.3.

Table 3.2: Paraxial lens data

	Focal length	Semi diameter	$F\#$
Paraxial lens 1	144.721	41.666	1.736
Paraxial lens 2	-144.721	16.883	4.286

Table 3.3: Paraxial raytrace data

	$y$	$u$	$\bar{y}$	$\bar{u}$
Paraxial lens 1	41.6667	-0.2879	0.0000	0.0513
Paraxial lens 2	11.5164	-0.2083	5.3670	0.0883
Image plane	0.0000	-0.2083	10.2500	0.0883

### 3.3 Thin lens predesign

After finding the paraxial representation of the objective, each paraxial lens is constructed with a number of lenses. Correcting each lens chromatically is a good starting point so first positive lens is constructed with an equivalent three lens combination and negative lens with an equivalent two lens combination. Material selection in SWIR is discussed by Shephard [32].

Material selection will be based on apochromatic condition for first positive lens and achromatic condition for second negative lens. Achromat and apochromat condition equations are given in Equation 3.9 and 3.10.

$$\begin{aligned}
 K_1 + K_2 &= K \\
 \frac{K_1}{V_1} + \frac{K_2}{V_2} &= 0
 \end{aligned}
 \tag{3.9}$$

$$\begin{aligned}
 K_1 + K_2 + K_3 &= K \\
 \frac{K_1}{V_1} + \frac{K_2}{V_2} + \frac{K_3}{V_3} &= 0 \\
 \frac{K_1 * Pd_1}{V_1} + \frac{K_2 * Pd_2}{V_2} + \frac{K_3 * Pd_3}{V_3} &= 0
 \end{aligned}
 \tag{3.10}$$

For achromatic condition equations, materials must be chosen according to Abbe number separation and partial dispersion similarity. Greater separation of Abbe number and smaller partial dispersion difference results in smaller lens powers. Partial dispersion (Pd) with respect to Abbe number (V) graph is given in Figure 3.5 according to Schott catalog [30]. Maximum Abbe number separation with minimum partial

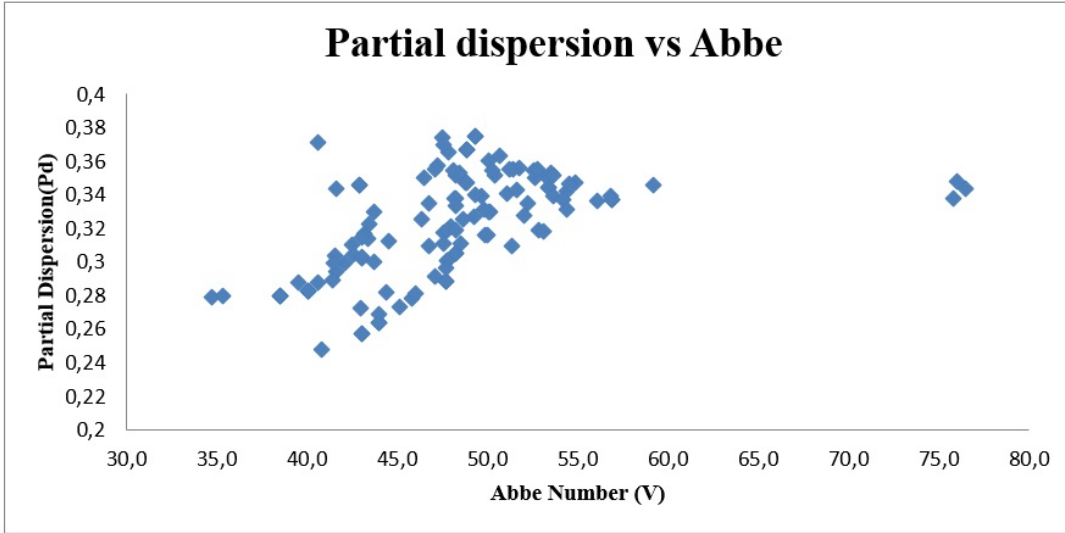


Figure 3.5: Partial dispersion vs Abbe number graph according to Schott catalog [30]

dispersion glass combinations are given in Table 3.4.

For negative lens, since N-PK52A and N-KZSF11 combination is a good combination candidate from achromatic perspective, these materials are chosen for the starting thin lens design. When apochromatic condition equations are solved, power equations 3.11 are found.

$$\begin{aligned}
 K_1 &= -T_{23} \frac{1}{E_1} V_1 K \\
 K_2 &= -T_{31} \frac{1}{E_2} V_2 K \\
 K_3 &= -T_{12} \frac{1}{E_3} V_3 K
 \end{aligned} \tag{3.11}$$

Table 3.4: Maximum Abbe separation glasses with minimum partial dispersion difference

Glass name	Refractive index	Abbe number	Partial dispersion	$\Delta V$	$\Delta Pd$
N-PK52A	1.487	76.499	0.3437	34.845	0.000124
N-KZFS11	1.614	41.653	0.3436		
N-FK51A	1.477	76.036	0.3480	29.525	0.002202
N-LAK10	1.697	46.510	0.3476		
N-PK51	1.517	75.819	0.3378	27.691	0.000378
N-BAF52	1.588	48.128	0.3382		
N-PK52A	1.487	76.499	0.3437	23.121	0.000622
N-BAK4	1.552	53.377	0.3443		

where

$$\begin{aligned}
E_1 &= -\frac{1}{V_2 - V_3} [V_1(Pd_2 - Pd_3) + V_2(Pd_3 - Pd_1) + V_3(Pd_1 - Pd_2)] \\
E_2 &= -\frac{1}{V_3 - V_1} [V_1(Pd_2 - Pd_3) + V_2(Pd_3 - Pd_1) + V_3(Pd_1 - Pd_2)] \\
E_3 &= -\frac{1}{V_1 - V_2} [V_1(Pd_2 - Pd_3) + V_2(Pd_3 - Pd_1) + V_3(Pd_1 - Pd_2)] \\
T_{12} &= \frac{P_1 - P_2}{V_1 - V_2} \\
T_{23} &= \frac{P_2 - P_3}{V_2 - V_3} \\
T_{31} &= \frac{P_3 - P_1}{V_3 - V_1}
\end{aligned} \tag{3.12}$$

T parameter stands for the slope of the line connecting two materials in partial dispersion and Abbe number graph [24]. E stands for the vertical distance of material to the line connecting the other two material in the same graph. As a result, three material must form a well separated triangle in partial dispersion vs Abbe graph so that powers of each lens are minimized which is advantageous from aberration correction perspective. In Pd-V graph, two furthest point materials are N-PK52A and N-SF66. third material will be chosen according to the correction of shape independent aberrations which are field curvature, axial colour and lateral colour. Shape independent aberration equation becomes Equation 3.13

$$\begin{aligned}
P &= \sum_{i=1}^5 \frac{K_i}{n_i} = \frac{1}{n_1} K_1 + \frac{1}{n_2} K_2 + \frac{1}{n_3} K_3 + \frac{1}{n_4} K_4 + \frac{1}{n_5} K_5 \\
C_1 &= \sum_{i=1}^5 \frac{h_i^2 K_i}{V_i} = \frac{h_1^2}{V_1} K_1 + \frac{h_2^2}{V_2} K_2 + \frac{h_3^2}{V_3} K_3 + \frac{h_4^2}{V_4} K_4 + \frac{h_5^2}{V_5} K_5 \\
C_2 &= \sum_{i=1}^5 \frac{h_i \bar{h}_i K_i}{V_i} = \frac{h_1 \bar{h}_1}{V_1} K_1 + \frac{h_2 \bar{h}_2}{V_2} K_2 + \frac{h_3 \bar{h}_3}{V_3} K_3 + \frac{h_4 \bar{h}_4}{V_4} K_4 + \frac{h_5 \bar{h}_5}{V_5} K_5 \tag{3.13} \\
\frac{1}{f_1} &= \sum_{i=1}^3 K_i = K_1 + K_2 + K_3 \\
\frac{1}{f_2} &= \sum_{i=4}^5 K_i = K_4 + K_5
\end{aligned}$$

These equations in matrix formalism are as Equation 3.14.

$$\begin{bmatrix} \frac{1}{n_1} & \frac{1}{n_2} & \frac{1}{n_3} & \frac{1}{n_4} & \frac{1}{n_4} \\ \frac{h_1^2}{V_1} & \frac{h_2^2}{V_2} & \frac{h_3^2}{V_3} & \frac{h_4^2}{V_4} & \frac{h_5^2}{V_5} \\ \frac{h_1 \overline{h_1}}{V_1} & \frac{h_2 \overline{h_2}}{V_2} & \frac{h_3 \overline{h_3}}{V_3} & \frac{h_4 \overline{h_4}}{V_4} & \frac{h_5 \overline{h_5}}{V_5} \\ 1 & 1 & 1 & 0 & 0 \\ 0 & 0 & 0 & 1 & 1 \end{bmatrix} \begin{bmatrix} K_1 \\ K_2 \\ K_3 \\ K_4 \\ K_5 \end{bmatrix} = \begin{bmatrix} 0 \\ 0 \\ 0 \\ \frac{1}{f_1} \\ \frac{1}{f_2} \end{bmatrix} \quad (3.14)$$

Hence powers of paraxial lenses are given in Equation 3.15.

$$\begin{bmatrix} K_1 \\ K_2 \\ K_3 \\ K_4 \\ K_5 \end{bmatrix} = \begin{bmatrix} \frac{1}{n_1} & \frac{1}{n_2} & \frac{1}{n_3} & \frac{1}{n_4} & \frac{1}{n_4} \\ \frac{h_1^2}{V_1} & \frac{h_2^2}{V_2} & \frac{h_3^2}{V_3} & \frac{h_4^2}{V_4} & \frac{h_5^2}{V_5} \\ \frac{h_1 \overline{h_1}}{V_1} & \frac{h_2 \overline{h_2}}{V_2} & \frac{h_3 \overline{h_3}}{V_3} & \frac{h_4 \overline{h_4}}{V_4} & \frac{h_5 \overline{h_5}}{V_5} \\ 1 & 1 & 1 & 0 & 0 \\ 0 & 0 & 0 & 1 & 1 \end{bmatrix}^{-1} \begin{bmatrix} 0 \\ 0 \\ 0 \\ \frac{1}{f_1} \\ \frac{1}{f_2} \end{bmatrix} \quad (3.15)$$

Third material is chosen so that the determinant of the square matrix is maximum which results in smaller powers of paraxial lenses. Materials giving highest determinants are given in Table 3.5. Triangles formed by these material combinations are given in Figure 3.6.

Table 3.5: Materials resulted in highest determinant

Material	Ref.index(1.4um)	Abbe number	Partial dispersion	Determinant
LASF35	1.977367	45.872289	0.278005648	1.655556
N-LASF31A	1.852499	51.341142	0.309099671	1.403879
P-SF68	1.949975	40.831249	0.247782284	1.090468
N-LASF41	1.806557	48.693564	0.325234741	0.980578
N-LASF9	1.815827	47.719068	0.288305472	0.964811
N-LASF46B	1.865436	43.779916	0.299644682	0.929596
N-LASF44	1.778128	49.795953	0.331325713	0.891307
N-LASF40	1.803027	47.618024	0.310404478	0.885771
N-LASF46A	1.865217	43.053217	0.302394816	0.866195

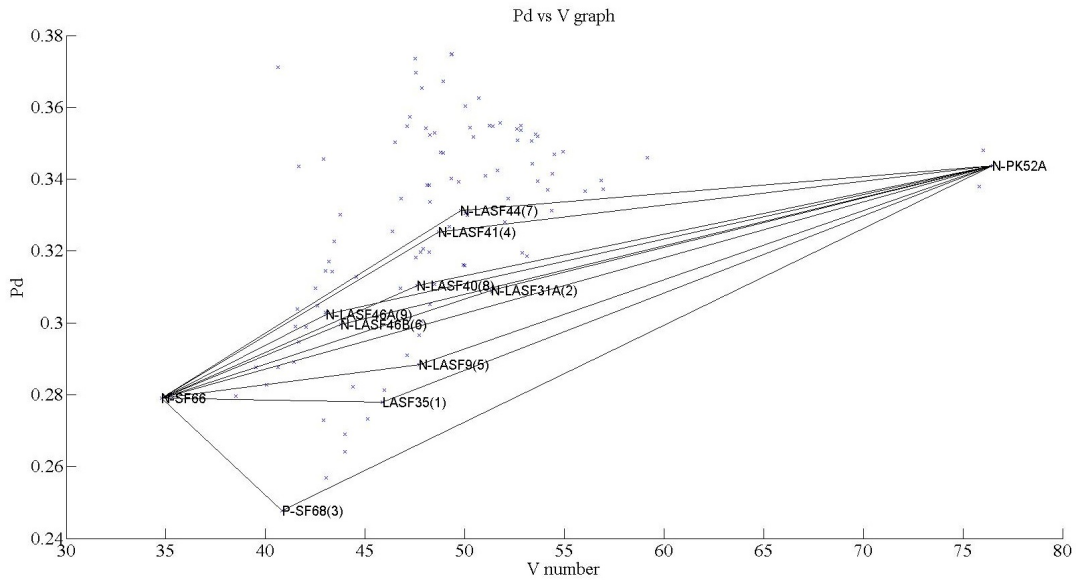


Figure 3.6: Triangles formed by materials

When power equation is solved with these material combinations, powers of each paraxial lens are given in Table 3.6. Since the lowest focal length of the first three lens in magnitude is achieved with N-LASF44, third material is chosen as N-LASF44.

Final paraxial configuration is shown in Table 3.7 and Figure 3.7.

Up to now, only first order parameters namely field of view, total length, focal length of the objective and shape independent aberrations namely the field curvature, axial colour and lateral colour are considered. Shape independent aberration coefficients are calculated and given in Table 3.8.

Table 3.6: Power distributions with materials resulted in highest determinant

	Lens1	Lens2	Lens3	Lens4	Lens5
LASF35	91.498	-125.549	253.439	-65.921	121.068
N-LASF31A	100.744	-130.389	214.911	-65.921	121.068
P-SF68	90.473	-98.682	166.933	-65.921	121.068
N-LASF41	108.823	-111.842	150.11	-65.921	121.068
N-LASF9	107.37	-109	147.697	-65.921	121.068
N-LASF46B	99.68	-98.529	142.306	-65.921	121.068
N-LASF44	115.911	-110.541	136.445	-65.921	121.068
N-LASF40	110.688	-105.27	135.597	-65.921	121.068
N-LASF46A	99.759	-93.846	132.6	-65.921	121.068

Table 3.7: Final paraxial configuration surface data

Surf number	Surface type	Thickness	Diameter	Glass	Focal length
STO	PARAXIAL	0	83.33333	N-PK52A	115.91
2	PARAXIAL	0	83.33333	N-SF66	-110.541
3	PARAXIAL	104.7208	83.33333	N-LASF44	136.445
4	PARAXIAL	0	33.7668	N-PK52A	-65.921
5	PARAXIAL	55.279	33.7668	N-KZFS11	121.068
IMA	STANDARD		20.5		

Table 3.8: Shape independent aberration coefficients for final paraxial configuration

Coefficient	Aberration	Value
SIV	Field curvature	-9.4299568E-015
CI	Axial colour	-1.1763160E-013
CII	Lateral colour	5.42968448E-015

After correcting shape independent aberrations, shape dependent aberrations namely spherical aberration, coma, astigmatism and distortion are going to be corrected by shape factors of paraxial lenses. Equation 2.11, Equation 2.14 and Equation 2.15 and will be used for solving shape factors minimizing the shape dependent parameters of paraxial lenses. Parameters in these equations are calculated for paraxial configuration in Table 3.9.

Spherical aberration equations in which stop is assumed to be on paraxial lenses are

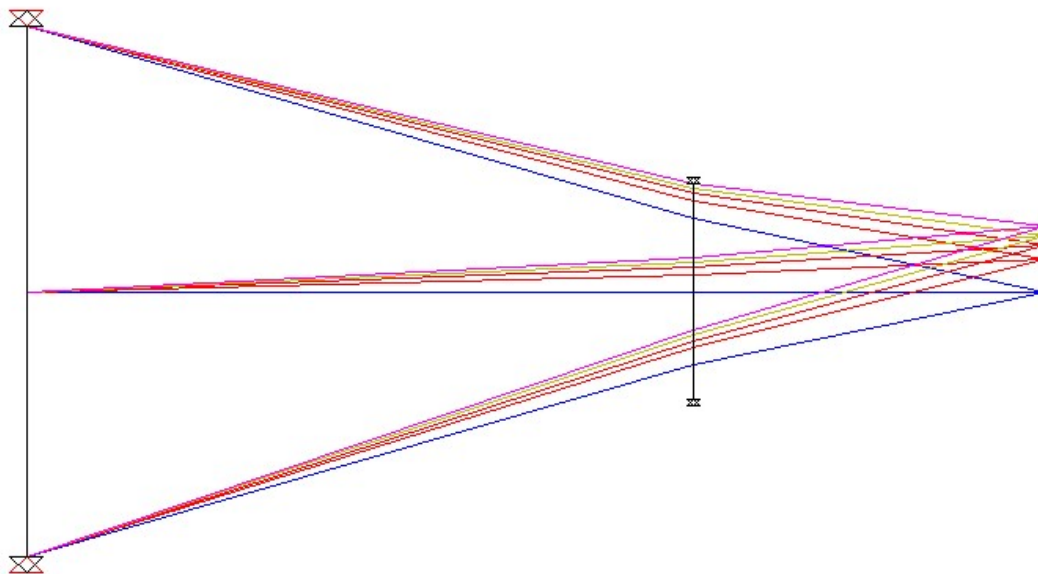


Figure 3.7: Paraxial configuration layout

Table 3.9: Parameter values in shape dependent aberration equations

	$h$	$\bar{h}$	$G$	$K$	$n$	$V$
Lens 1	41.66666	0	-1	115.911	1.487096	76.49915961
Lens 2	41.66666	0	0.9073244	-110.541	1.869611	34.79975205
Lens 3	41.66666	0	-0.885607	136.445	1.778127	49.79595333
Lens 4	11.516581	5.366899	2.2960019	-65.921	1.487096	76.49915961
Lens 5	11.516581	5.366899	-3.380186	121.068	1.614394	41.65347874

given in Equation 3.16.

$$\begin{bmatrix} S_{11} \\ S_{12} \\ S_{13} \\ S_{14} \\ S_{15} \end{bmatrix} = \begin{bmatrix} \frac{h_1^4 K_1^3}{4} \left[ \frac{n_1+2}{n_1(n_1-1)^2} B_1^2 + \frac{4(n_1+1)}{n_1(n_1-1)} G_1 B_1 + \frac{3n_1+2}{n_1} G_1^2 + \left( \frac{n_1}{n_1-1} \right)^2 \right] \\ \frac{h_2^4 K_2^3}{4} \left[ \frac{n_2+2}{n_2(n_2-1)^2} B_2^2 + \frac{4(n_2+1)}{n_2(n_2-1)} G_2 B_2 + \frac{3n_2+2}{n_2} G_2^2 + \left( \frac{n_2}{n_2-1} \right)^2 \right] \\ \frac{h_3^4 K_3^3}{4} \left[ \frac{n_3+2}{n_3(n_3-1)^2} B_3^2 + \frac{4(n_3+1)}{n_3(n_3-1)} G_3 B_3 + \frac{3n_3+2}{n_3} G_3^2 + \left( \frac{n_3}{n_3-1} \right)^2 \right] \\ \frac{h_4^4 K_4^3}{4} \left[ \frac{n_4+2}{n_4(n_4-1)^2} B_4^2 + \frac{4(n_4+1)}{n_4(n_4-1)} G_4 B_4 + \frac{3n_4+2}{n_4} G_4^2 + \left( \frac{n_4}{n_4-1} \right)^2 \right] \\ \frac{h_5^4 K_5^3}{4} \left[ \frac{n_5+2}{n_5(n_5-1)^2} B_5^2 + \frac{4(n_5+1)}{n_5(n_5-1)} G_5 B_5 + \frac{3n_5+2}{n_5} G_5^2 + \left( \frac{n_5}{n_5-1} \right)^2 \right] \end{bmatrix} \quad (3.16)$$

Coma equations in which stop is assumed to be on paraxial lenses are given in Equation 3.17:

$$\begin{bmatrix} S_{21} \\ S_{22} \\ S_{23} \\ S_{24} \\ S_{25} \end{bmatrix} = \begin{bmatrix} -\frac{h_1^2 K_1^2 \Psi}{2} \left( \frac{n_1+1}{n_1(n_1-1)} B_1 + \frac{2n_1+1}{n_1} G_1 \right) \\ -\frac{h_2^2 K_2^2 \Psi}{2} \left( \frac{n_2+1}{n_2(n_2-1)} B_2 + \frac{2n_2+1}{n_2} G_2 \right) \\ -\frac{h_3^2 K_3^2 \Psi}{2} \left( \frac{n_3+1}{n_3(n_3-1)} B_3 + \frac{2n_3+1}{n_3} G_3 \right) \\ -\frac{h_4^2 K_4^2 \Psi}{2} \left( \frac{n_4+1}{n_4(n_4-1)} B_4 + \frac{2n_4+1}{n_4} G_4 \right) \\ -\frac{h_5^2 K_5^2 \Psi}{2} \left( \frac{n_5+1}{n_5(n_5-1)} B_5 + \frac{2n_5+1}{n_5} G_5 \right) \end{bmatrix} \quad (3.17)$$

Astigmatism, field curvature and distortion equations in which stop is assumed to be on paraxial lenses are given in Equation 3.18

$$\begin{bmatrix} S_{31} \\ S_{32} \\ S_{33} \\ S_{34} \\ S_{35} \end{bmatrix} = \begin{bmatrix} \Psi^2 K_1 \\ \Psi^2 K_2 \\ \Psi^2 K_3 \\ \Psi^2 K_4 \\ \Psi^2 K_5 \end{bmatrix}, \quad \begin{bmatrix} S_{41} \\ S_{42} \\ S_{43} \\ S_{44} \\ S_{45} \end{bmatrix} = \begin{bmatrix} \frac{\Psi^2 K_1}{n_1} \\ \frac{\Psi^2 K_2}{n_2} \\ \frac{\Psi^2 K_3}{n_3} \\ \frac{\Psi^2 K_4}{n_4} \\ \frac{\Psi^2 K_5}{n_5} \end{bmatrix}, \quad \begin{bmatrix} S_{51} \\ S_{52} \\ S_{53} \\ S_{54} \\ S_{55} \end{bmatrix} = \begin{bmatrix} 0 \\ 0 \\ 0 \\ 0 \\ 0 \end{bmatrix} \quad (3.18)$$

Although field curvature is a shape independent aberration and corrected beforehand, it is going to be used in stop shift equation of distortion. Hence, field curvature

equations are included here. When parameters in Table 3.9 are used in Equation 3.16, Equation 3.17, Equation 3.18, following equations are get:

$$\begin{aligned}
 \begin{bmatrix} S_{11} \\ S_{12} \\ S_{13} \\ S_{14} \\ S_{15} \end{bmatrix} &= \begin{bmatrix} 4.782B_1^2 - 6.645B_1 + 6.612 \\ -1.527B_2^2 - 3.574B_2 - 4.448 \\ 1.041B_3^2 - 2.110B_3 + 2.509 \\ -0.152B_4^2 - 0.484B_4 - 0.495 \\ 0.015B_5^2 - 0.088B_5 + 0.137 \end{bmatrix}, & \begin{bmatrix} S_{21} \\ S_{22} \\ S_{23} \\ S_{24} \\ S_{25} \end{bmatrix} &= \begin{bmatrix} 0.474B_1 - 0.369 \\ 0.268B_2 + 0.349 \\ 0.200B_3 - 0.226 \\ 0.112B_4 + 0.200 \\ 0.025B_5 - 0.086 \end{bmatrix} \\
 \begin{bmatrix} S_{31} \\ S_{32} \\ S_{33} \\ S_{34} \\ S_{35} \end{bmatrix} &= \begin{bmatrix} 0.039 \\ -0.041 \\ 0.033 \\ -0.069 \\ 0.038 \end{bmatrix}, & \begin{bmatrix} S_{41} \\ S_{42} \\ S_{43} \\ S_{44} \\ S_{45} \end{bmatrix} &= \begin{bmatrix} 0.026 \\ -0.022 \\ 0.019 \\ -0.047 \\ 0.023 \end{bmatrix}, & \begin{bmatrix} S_{51} \\ S_{52} \\ S_{53} \\ S_{54} \\ S_{55} \end{bmatrix} &= \begin{bmatrix} 0 \\ 0 \\ 0 \\ 0 \\ 0 \end{bmatrix}
 \end{aligned} \tag{3.19}$$

Total aberration Equation 3.20 are given by using stop-shift equations which are given in Equation 2.11.

$$\begin{aligned}
 S_1^* &= \sum_{i=1}^5 S_{1i}^* = \sum_{i=1}^5 S_{1i} \\
 S_2^* &= \sum_{i=1}^5 S_{2i}^* = \sum_{i=1}^5 (S_{2i} + (\frac{\bar{h}_i}{h_i})S_{1i}) \\
 S_3^* &= \sum_{i=1}^5 S_{3i}^* = \sum_{i=1}^5 (S_{3i} + 2(\frac{\bar{h}_i}{h_i})S_{2i} + (\frac{\bar{h}_i}{h_i})^2 S_{1i}) \\
 S_5^* &= \sum_{i=1}^5 S_{5i}^* = \sum_{i=1}^5 (S_{5i} + (\frac{\bar{h}_i}{h_i})(3S_{3i} + S_{4i}) + 3(\frac{\bar{h}_i}{h_i})^2 S_{2i} + (\frac{\bar{h}_i}{h_i})^3 S_{1i})
 \end{aligned} \tag{3.20}$$

When Equations 3.19 are used in Equation 3.20, total third order shape dependent

Seidel aberration coefficients are as given in Equation 3.21:

$$\begin{aligned}
 \begin{bmatrix} S_{11}^* \\ S_{12}^* \\ S_{13}^* \\ S_{14}^* \\ S_{15}^* \end{bmatrix} &= \begin{bmatrix} 4.782B_1^2 - 6.645B_1 + 6.612 \\ -1.527B_2^2 - 3.574B_2 - 4.45 \\ 1.041B_3^2 - 2.110B_3 + 2.509 \\ -0.152B_4^2 - 0.484B_4 - 0.49 \\ 0.015B_5^2 - 0.088B_5 + 0.137 \end{bmatrix}, & \begin{bmatrix} S_{21}^* \\ S_{22}^* \\ S_{23}^* \\ S_{24}^* \\ S_{25}^* \end{bmatrix} &= \begin{bmatrix} 0.474B_1 - 0.369 \\ 0.268B_2 + 0.349 \\ 0.200B_3 - 0.226 \\ -0.071B_4^2 - 0.114B_4 - 0.03 \\ 0.007B_5^2 - 0.016B_5 - 0.02 \end{bmatrix} \\
 \begin{bmatrix} S_{31}^* \\ S_{32}^* \\ S_{33}^* \\ S_{34}^* \\ S_{35}^* \end{bmatrix} &= \begin{bmatrix} 0.039 \\ -0.041 \\ 0.033 \\ -0.033B_4^2 - 0.001B_4 + 0.01 \\ 0.003B_5^2 + 0.005B_5 - 0.012 \end{bmatrix}, & \begin{bmatrix} S_{51}^* \\ S_{52}^* \\ S_{53}^* \\ S_{54}^* \\ S_{55}^* \end{bmatrix} &= \begin{bmatrix} 0 \\ 0 \\ 0 \\ -0.015B_4^2 + 0.024B_4 - 0.04 \\ 0.001B_5^2 + 0.008B_5 + 0.022 \end{bmatrix}
 \end{aligned}
 \tag{3.21}$$

Equation 3.21 is solved with respect to shape factors of paraxial lenses ( $B_1, B_2, B_3, B_4, B_5$ ) under the zero equivalence of shape dependent aberrations  $S_1^*, S_2^*, S_3^*, S_5^*$ . Since the equations are highly complex, numerical optimization routines are used to solve these equations correcting the shape dependent aberrations. As a result, shape factors of paraxial lenses are found as given in Table 3.10.

Finally, third order Seidel aberration coefficients as a total are given in Table 3.11.

After correcting all shape dependent and shape independent third order Seidel aberration coefficients, paraxial lenses can now be realized by calculating radius of cur-

Table 3.10: Shape factors of lenses

B1	0.553593764
B2	0.083732148
B3	1.068839254
B4	1.02858805
B5	0.906766707

vatures using shape factors of paraxial lenses with Equation 3.22.

$$c_1 = \frac{1}{2} \left( \frac{K}{n-1} \right) (B+1)$$

$$c_2 = \frac{1}{2} \left( \frac{K}{n-1} \right) (B-1)$$
(3.22)

According to Equation 3.22, curvatures and radius of realized paraxial lenses are given in Table 3.12. ZEMAX layout and lens data are shown in Figure 3.8 and Table 3.13.

In this configuration, all of the third order aberrations are corrected perfectly without considering higher order aberrations. Since higher order aberrations are not considered up to this stage, the performance of this configuration is dominated by higher order aberrations. Hence the imaging quality of the lens is way behind the acceptable limits. Spot diagram and OPD fans are given in Figure 3.9.

As can be seen from the OPD fan, imaging performance is highly degraded by higher order spherical aberration. Using equations on Equation 2.16, Equation 2.17 and Equation 2.18, fifth order aberration coefficients are calculated. Ray trace data which is used in calculating the fifth order aberration coefficients is given in Table 3.14.

Third order aberration coefficients, both intrinsic and extrinsic part of total fifth order aberration coefficients and totals which are calculated by using the ray trace data in Table 3.14 are given in Table 3.15, Table 3.16, Table 3.17 and Table 3.19.

As previously guessed from the OPD fan, image performance is highly degraded by

Table 3.11: Total third order Seidel aberration coefficients in lens units

Coefficient	Aberration	Value
SI	Spherical aberration	-9.6779251E-12
SII	Coma	-3.3729963E-14
SIII	Astigmatism	1.45213182E-10
SIV	Field Curvature	-9.4299568E-15
SV	Distortion	-1.9628131E-10
CI	Axial Colour	-1.176316E-13
CII	Lateral Colour	5.42968448E-15

Table 3.12: Realized paraxial lens data

	$K$	$B$	$C_1$	$C_2$	$R_1$	$R_2$
Lens 1	115.9117	0.5536	0.013758	-0.003953	72.6833	-252.954
Lens 2	-110.5406	0.0837	-0.00564	0.0047659	-177.401	209.8238
Lens 3	136.44352	1.0688	0.009743	0.0003241	102.637	3084.583
Lens 4	-65.92100	1.0286	-0.03159	-0.000445	-31.657	-2246.39
Lens 5	121.0679	0.9068	0.012817	-0.000626	78.021	-1595.65

Table 3.13: Realized lens data

Surf	Type	Radius	Thickness	Glass	Diameter
OBJ	STANDARD	Infinity	Infinity		0
STO	STANDARD	72.68334	0	N-PK52A	84.72972
2	STANDARD	-252.954	0		91.6062
3	STANDARD	-177.401	0	N-SF66	93.3135
4	STANDARD	209.8238	0		91.86233
5	STANDARD	102.6378	0	N-LASF44	92.80552
6	STANDARD	3084.583	104.721		96.56574
7	STANDARD	-31.6574	0	N-PK52A	35.03558
8	STANDARD	-2246.39	0		35.44802
9	STANDARD	78.02056	0	N-KZFS11	35.68351
10	STANDARD	-1595.905	55.27868		35.92783
IMA	STANDARD	Infinity			24.97643

fifth order spherical aberration (W060) which has the highest value in total fifth order aberration coefficients. Although at the first stage of the design, third order aberration

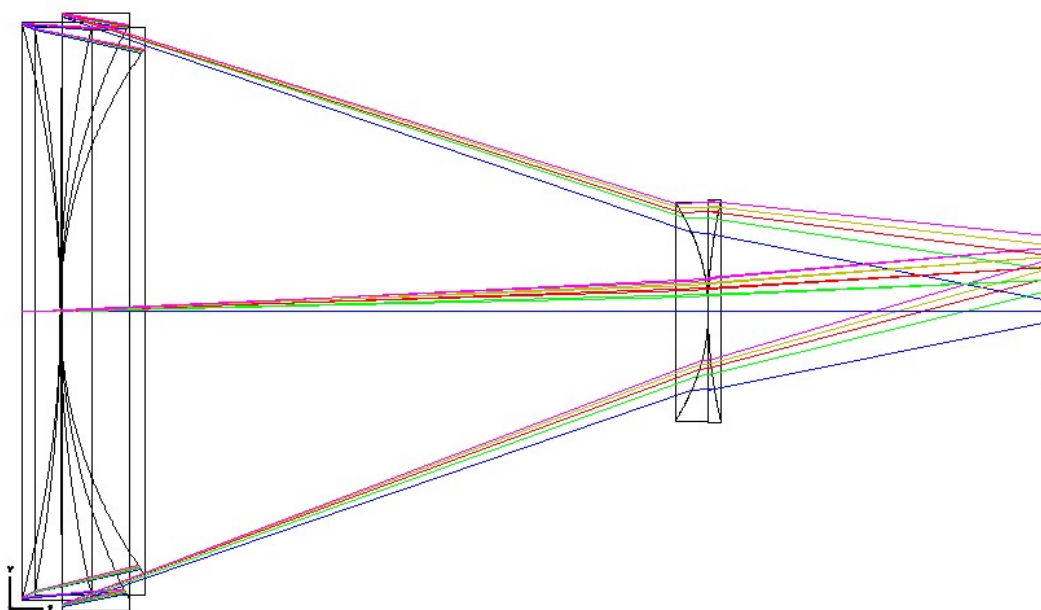


Figure 3.8: Realized configuration layout

Table 3.14: Ray trace data for fifth order aberration coefficient calculations

lens		$y$	$u$	$\bar{y}$	$\bar{u}$	$n$	$R$	$A$	$\bar{A}$
	OBJ	0	0	INF	5,1E-2	1			
1	1	41.66	-0.19	0.00	0.03	1.487	72.683	0.573	0.051
	2	41.66	-0.36	0.00	0.05	1.000	-252.954	-0.524	0.051
2	3	41.66	-0.08	0.00	0.03	1.870	-177.401	-0.594	0.051
	4	41.66	0.02	0.00	0.05	1.000	209.824	0.216	0.051
3	5	41.66	-0.17	0.000	0.03	1.778	102.638	0.423	0.051
	6	41.66	-0.29	0.00	0.05	1.000	3084.583	-0.274	0.051
4	7	11.51	-0.07	5.367	0.09	1.487	-31.657	-0.652	-0.118
	8	11.51	-0.11	5.37	0.13	1.000	-2246.391	-0.118	0.130
5	9	11.51	-0.13	5.367	0.06	1.614	78.021	0.034	0.201
	10	11.51	-0.21	5.37	0.09	1.000	-1595.645	-0.216	0.085
img.	11	0.00	-0.21	10.25	0.09	1.000	-		

coefficients are corrected perfectly without considering fifth order aberration coefficients, they are now going to be balanced with similar characteristic fifth order aberration coefficients in order to improve image quality. For instance, fifth order spherical aberration (W060) can be balanced with third order spherical aberration (W040). Third order spherical aberration (W040) can be balanced with defocus (W020). Elliptic coma (W331, W333) can be balanced with third order coma (W131). Field curvature (W220) can be balanced with sagittal oblique spherical aberration (W240). Higher order aberration balancing is done by shape factor optimization in ZEMAX in which spot size based merit function is used. Configuration layout and lens data are shown in Figure 3.10, Table 3.18 after optimization. After a few cycles of optimization, image quality is improved greatly. Spot diagram and OPD fans are shown

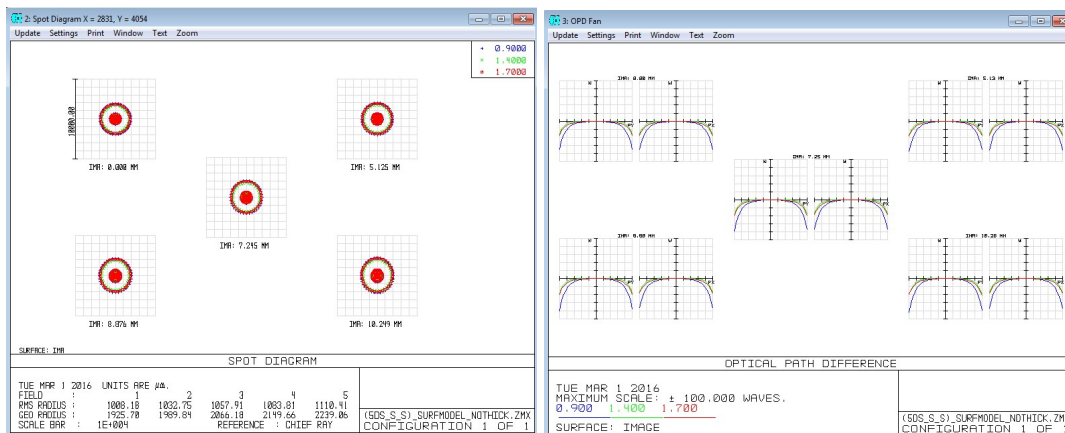


Figure 3.9: Spot diagram and OPD fan of configuration

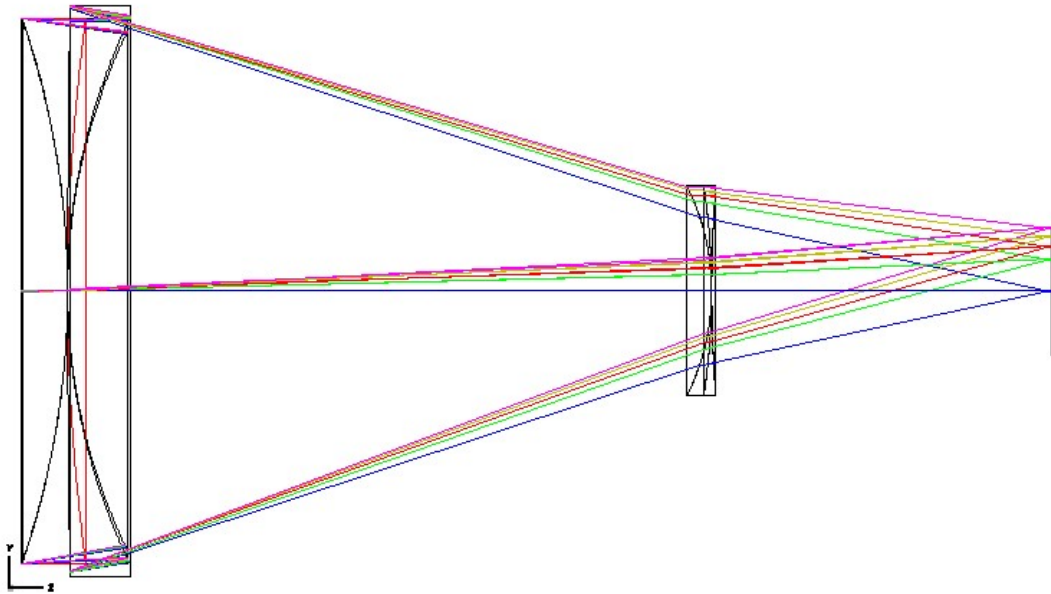


Figure 3.10: Configuration layout after aberration balancing

in Figure 3.11.

Third order aberration coefficients and total fifth order aberration coefficients are calculated again after shape optimization and compared with the values before optimization in Table 3.20 and Table 3.21.

As can be seen from the fifth order and third order aberration coefficients before and after aberration balancing, higher order aberrations are balanced with third order aberration coefficients. As a result image quality is greatly improved.

Table 3.15: Third order aberration coefficients of surfaces in waves in configuration

	$W_{040}$	$W_{131}$	$W_{222}$	$W_{220}$	$W_{311}$
1	154.37	55.20	4.94	6.14	1.10
2	238.38	-93.23	9.11	5.61	-1.10
3	-414.04	142.81	-12.31	-8.29	1.43
4	-10.74	-10.19	-2.42	-3.01	-1.43
5	74.60	36.12	4.37	5.66	1.37
6	54.21	-40.50	7.56	3.67	-1.37
7	-103.87	-75.41	-13.69	-15.27	-5.54
8	0.91	-4.00	4.41	2.32	-5.11
9	-0.04	-1.00	-5.84	1.05	12.33
10	6.22	-9.80	3.86	2.13	-1.68
$\Sigma$	0.003601	0.001591	-0.00024	-0.00012	-0.00013

Table 3.16: Fifth order intrinsic aberration coefficients of surfaces in configuration in waves

	$W_{060I}$	$W_{151I}$	$W_{242I}$	$W_{333I}$	$W_{240I}$	$W_{331I}$	$W_{422I}$	$W_{420I}$	$W_{511I}$
1	-2.281	4.719	1.095	0.032	0.114	0.061	-0.009	-0.007	-0.003
2	1.116	4.865	-2.154	0.227	-0.454	0.319	-0.047	-0.011	0.003
3	22.126	-14.23	3.274	-0.255	1.060	-0.473	0.053	0.016	-0.004
4	-0.318	-0.417	-0.133	-0.003	-0.071	-0.038	0.005	0.000	0.004
5	-2.803	0.425	0.338	0.017	-0.065	0.010	-0.007	-0.007	-0.004
6	-3.260	3.496	-1.248	0.148	-0.313	0.223	-0.040	-0.010	0.004
7	-27.43	-33.07	-10.94	-0.926	-4.310	-2.66	-0.235	-0.094	0.017
8	-0.010	0.068	-0.156	0.120	-0.039	0.181	-0.209	-0.052	0.121
9	0.001	0.017	0.056	-0.143	-0.015	-0.093	0.289	0.041	-0.069
10	-0.268	0.665	-0.550	0.151	-0.139	0.230	-0.095	-0.024	0.020

Table 3.17: Fifth order extrinsic aberration coefficients of surfaces in configuration in waves

	$W_{060E}$	$W_{151E}$	$W_{242E}$	$W_{333E}$	$W_{240E}$	$W_{331E}$	$W_{422E}$	$W_{420E}$	$W_{511E}$
1	0.000	0.000	0.000	0.000	0.000	0.000	0.000	0.000	0.000
2	8.732	1.488	-0.013	0.000	0.097	-0.015	0.000	-0.002	0.000
3	-51.0	8.102	-1.125	0.000	-0.869	0.144	0.000	0.000	0.000
4	-0.849	2.935	0.531	0.000	0.317	0.039	0.000	0.003	0.000
5	4.818	-10.09	-0.810	0.000	-0.464	0.002	0.000	0.000	0.000
6	-0.138	-0.292	0.034	0.000	0.010	0.002	0.000	0.000	0.000
7	34.114	33.867	8.240	0.546	3.511	1.333	0.125	0.032	0.007
8	0.029	-0.148	0.230	-0.095	0.067	-0.187	0.083	0.032	-0.001
9	0.023	0.110	-0.087	-0.038	-0.031	0.102	-0.104	0.009	0.039
10	0.181	-0.442	0.358	-0.097	0.090	-0.146	0.059	0.015	-0.012

Table 3.18: Lens data after aberration balancing

Surf	Type	Radius	Thickness	Glass	Diameter
OBJ	STANDARD	Infinity	Infinity		
STO	STANDARD	96.12413	0	N-PK52A	84.33188
2	STANDARD	-136.8308	0		88.57954
3	STANDARD	-135.428	0	N-SF66	88.68273
4	STANDARD	331.2593	0		88.21058
5	STANDARD	101.9872	0	N-LASF44	89.38285
6	STANDARD	2588.275	104.721		92.69013
7	STANDARD	-38.0844	0	N-PK52A	34.20922
8	STANDARD	204.6804	0		34.11067
9	STANDARD	216.2377	0	N-KZFS11	34.10874
10	STANDARD	-113.3891	55.27849		34.16497
IMA	STANDARD	Infinity			20.85045

Table 3.19: Total fifth order aberration coefficients in configuration in waves

	$W_{240}$	$W_{331}$	$W_{422}$	$W_{420}$	$W_{511}$	$W_{060}$	$W_{151}$	$W_{242}$	$W_{333}$
$\Sigma$	-1.505	-0.965	-0.131	-0.058	0.122	-17.222	2.062	-3.062	-0.315

Table 3.20: Third order aberration coefficients after aberration balancing

$\Sigma$	After balancing	Before balancing
$W_{040}$	8.315	0.003601
$W_{131}$	2.753	0.001591
$W_{222}$	4.203	-0.00024
$W_{220}$	2.102	-0.00012
$W_{311}$	-3.419	-0.00013

Table 3.21: Fifth order aberration coefficients after aberration balancing

$\Sigma$	Total after balancing	Total before balancing
$W_{240}$	-0.852	-1.505
$W_{331}$	-0.109	-0.965
$W_{422}$	-0.146	-0.131
$W_{420}$	-0.055	-0.058
$W_{511}$	0.028	0.122
$W_{060}$	-3.704	-17.222
$W_{151}$	-0.626	2.062
$W_{242}$	-2.384	-3.062
$W_{333}$	0.128	-0.315

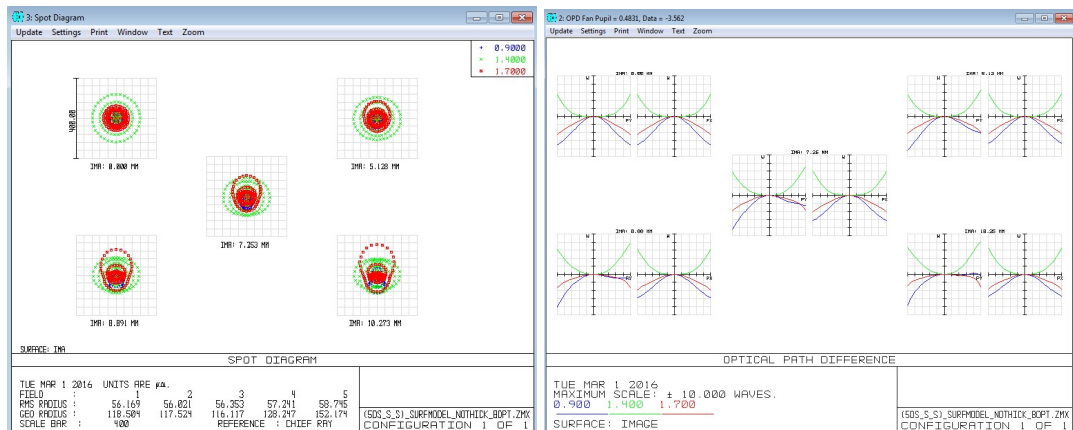


Figure 3.11: Spot diagram and OPD fan after aberration balancing

### 3.4 Surface Model

Layout is still not realistic since lenses have zero thicknesses. Applying surface model procedure described in part 2.2.4 and Equation 2.22, Equation 2.23, new radius of curvatures, thickness and principle point compensation values are found as given in Table 3.22.

Since the principle point compensation values are large because of air thickness in paraxial configuration is chosen as zero, surface model procedure is not suitable with chosen configuration. In general, surface model methodology must be used with largely air spaced lens configuration in which large negative principle compensation values can be used without disturbing the paraxial parameters of the configuration. In order to thicken the lenses, the radius of curvature and thickness values calculated by surface model methodology are used for initial values and two air thicknesses with curvatures are made variable in optimization in ZEMAX. As a rule of thumb, for positive lenses thickness is chosen as % 10-15 of its diameter, while for negative lens it is chosen as not less than %6 of its diameter. Also for positive lenses, thickness is chosen such that lens edge thickness is 1 mm at minimum. After a few cycles of optimization, a more realistic configuration without disturbing the image quality is achieved as shown in Figure 3.12, Table 3.23, Figure 3.13.

Third and fifth order aberration coefficients after thickening lenses are given in Table 3.24 and Table 3.25.

Although configuration shown in Figure 3.12 still has a poor image quality as given in Figure 3.13, it is a good candidate for a starting point for optimization routines. At this stage, configurations with improved performance will be searched by optimization routines in ZEMAX initiated from the starting point given in Figure 3.12.

Table 3.22: Surface models and principle point compensation values

$R_1$	$R_2$	$d$	$V_1H$	$V_2H'$
93.421	-132.982	19.438	5.393	-7.677
-136.507	333.898	8.064	1.252	-3.061
102.220	2594.187	13.030	-0.301	-7.628
-38.341	206.062	5.034	0.531	-2.854
214.988	-112.734	4.971	2.020	-1.059

Table 3.23: Lens data after lens thickening

Surf	Type	Radius	Thickness	Glass	Diameter
OBJ	STANDARD	Infinity	Infinity		
STO	STANDARD	95.28626	19.43757	N-PK52A	84.34192
2	STANDARD	-129.3067	0		83.68541
3	STANDARD	-133.5309	8.063787	N-SF66	83.47325
4	STANDARD	352.8246	0		82.37957
5	STANDARD	98.61558	13.02975	N-LASF44	82.98611
6	STANDARD	1305.704	83.51895		81.40488
7	STANDARD	-39.76262	5.033731	N-PK52A	34.79056
8	STANDARD	173.7546	0		34.4325
9	STANDARD	-6035.97	4.971136	N-KZFS11	34.39481
10	STANDARD	-73.50163	51.53324		34.47958
IMA	STANDARD	Infinity			20.89722

Table 3.24: Third order aberration coefficients after lens thickening in waves

$\Sigma$	$W_{040}$	$W_{131}$	$W_{222}$	$W_{220}$	$W_{311}$
After thickening	8.194	8.724	6.045	3.237	-3.926
After balancing	8.315	2.753	4.203	2.102	-3.419
Before balancing	0.0036	0.0016	-0.0002	-0.0001	-0.0001

### 3.5 Optimization

Performance of the starting configuration is relatively close to the final configuration. Configurations with much better performance in which all orders of aberrations are automatically considered by ray trace based optimization routines in ZEMAX are searched. Beforehand variable parameters are introduced to the optimization algorithms, which are the radius of curvatures of lenses, air thickness of the first group

Table 3.25: Fifth order aberration coefficients after lens thickening

	Total after thickening	Total after balancing	Total before balancing
$W_{240}$	-0.756	-0.852	-1.505
$W_{331}$	-0.084	-0.109	-0.965
$W_{422}$	-0.077	-0.146	-0.131
$W_{420}$	-0.044	-0.055	-0.058
$W_{511}$	0.017	0.028	0.122
$W_{060}$	-4.028	-3.704	-17.222
$W_{151}$	-3.34	-0.626	2.062
$W_{242}$	-2.35	-2.384	-3.062
$W_{333}$	0.0614	0.128	-0.315

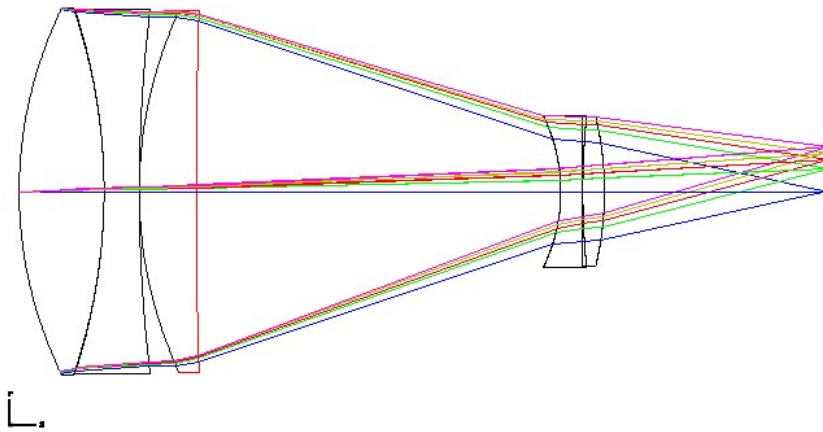


Figure 3.12: Configuration layout thickening lenses

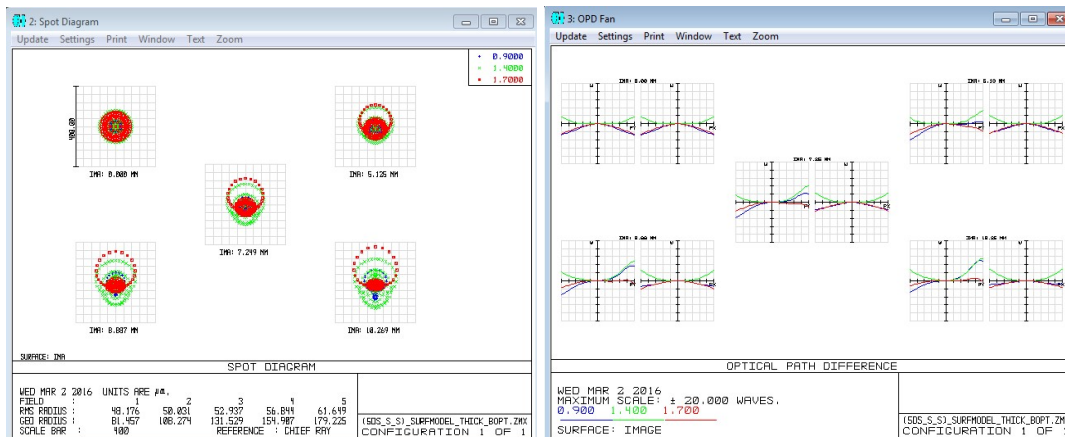


Figure 3.13: Spot diagram and OPD fan after lens thickening

and second group, air thickness of second group and image plane and finally materials. Two notable design forms are found. First solution layout and lens data are given in Figure 3.14 and Table 3.26 while optical performance is shown in Figure 3.15 and Figure 3.16.

Second solution layout and lens data are given in Figure 3.17 and Table 3.27 while optical performance is shown in Figure 3.18 and Figure 3.19.

Third and fifth order aberration coefficients of solutions are given in Table 3.28 and Table 3.29. When coefficients are studied, a much better balanced configurations are found with the help of numerical optimization algorithms.

Table 3.26: First solution lens data

Surf	Type	Radius	Thickness	Glass	Diameter
OBJ	STANDARD	Infinity	Infinity		
STO	STANDARD	137.1328	20	N-FK58	85.8
2	STANDARD	-98.61549	8	N-KZFS4HT	85.8
3	STANDARD	738.3033	2		85.2
4	STANDARD	87.73824	13	N-PK52A	85.4
5	STANDARD	Infinity	106.3		84.4
6	STANDARD	-41.09504	5	K7	33
7	STANDARD	63.9891	6.1		32.6
8	STANDARD	58.39945	5	N-LAK33B	33.8
9	STANDARD	-287.128	34.6		33.8
IMA	STANDARD	Infinity			20.49

Table 3.27: Second solution lens data

Surf	Type	Radius	Thickness	Glass	Diameter
OBJ	STANDARD	Infinity	Infinity		
STO	STANDARD	126.2677	20	N-PK52A	85.8
2	STANDARD	-92.41217	8	N-KZFS4	85.8
3	STANDARD	346.4279	2		84
4	STANDARD	76.05808	13	N-PK52A	84.2
5	STANDARD	253.8464	71.4		82.6
6	STANDARD	128.915	7	N-LAK9	52
7	STANDARD	-165.3173	12		52
8	STANDARD	-57.60586	5	P-LAK35	40.2
9	STANDARD	218.3383	61.65		38.2
IMA	STANDARD	Infinity			20.59

Table 3.28: Third order aberration coefficients after lens optimization

	$W_{040}$	$W_{131}$	$W_{222}$	$W_{220}$	$W_{311}$
Second solution	4.249	-0.228	1.272	1.266	-3.086
First solution	3.895	-3.153	1.139	0.806	1.766
Total after thickening	8.194	8.724	6.045	3.237	-3.926
Total after balancing	8.315	2.753	4.203	2.102	-3.419
Total before balancing	0.0036	0.00159	-0.0002	-0.0001	-0.0001

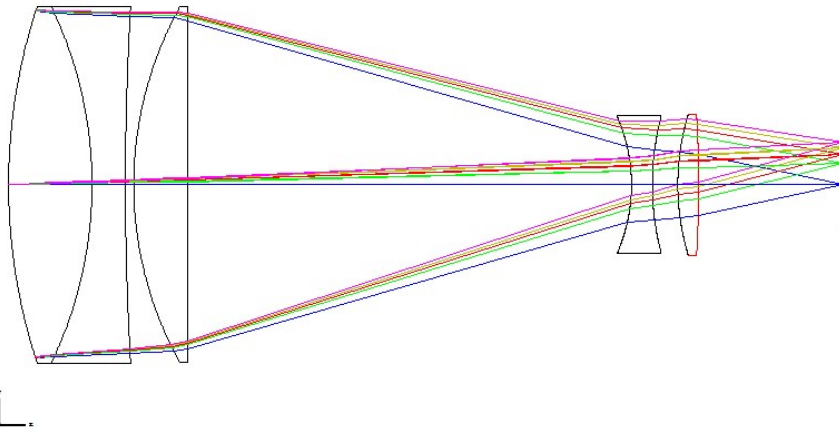


Figure 3.14: First solution layout

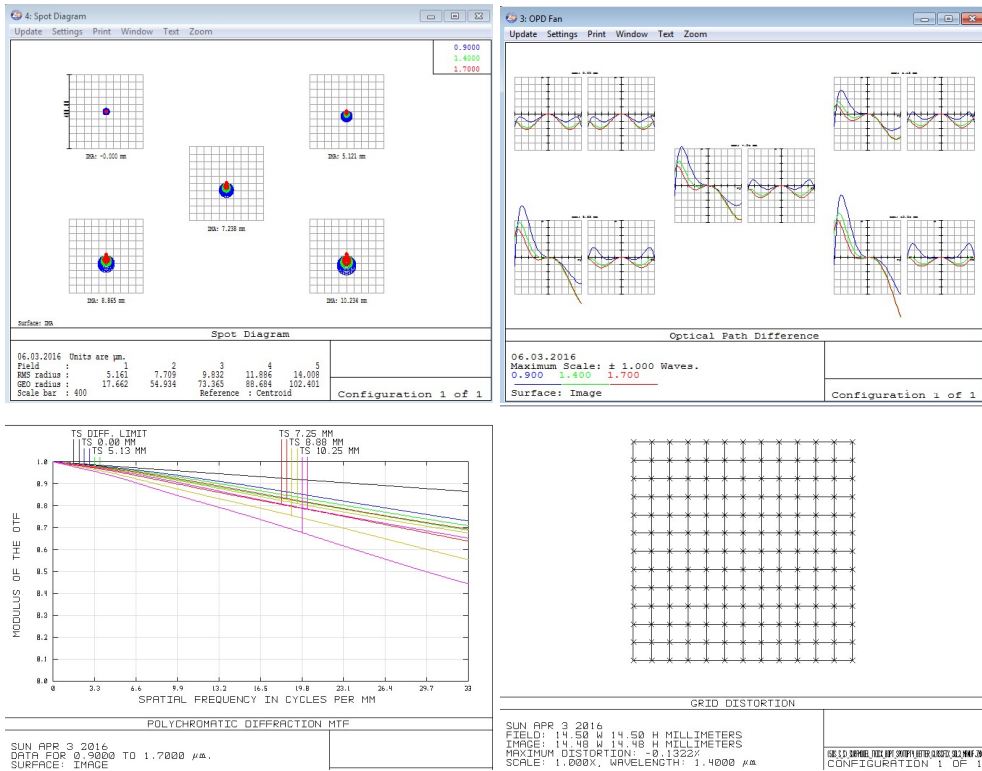


Figure 3.15: Spot diagram,OPD fan, MTF and distortion of first solution

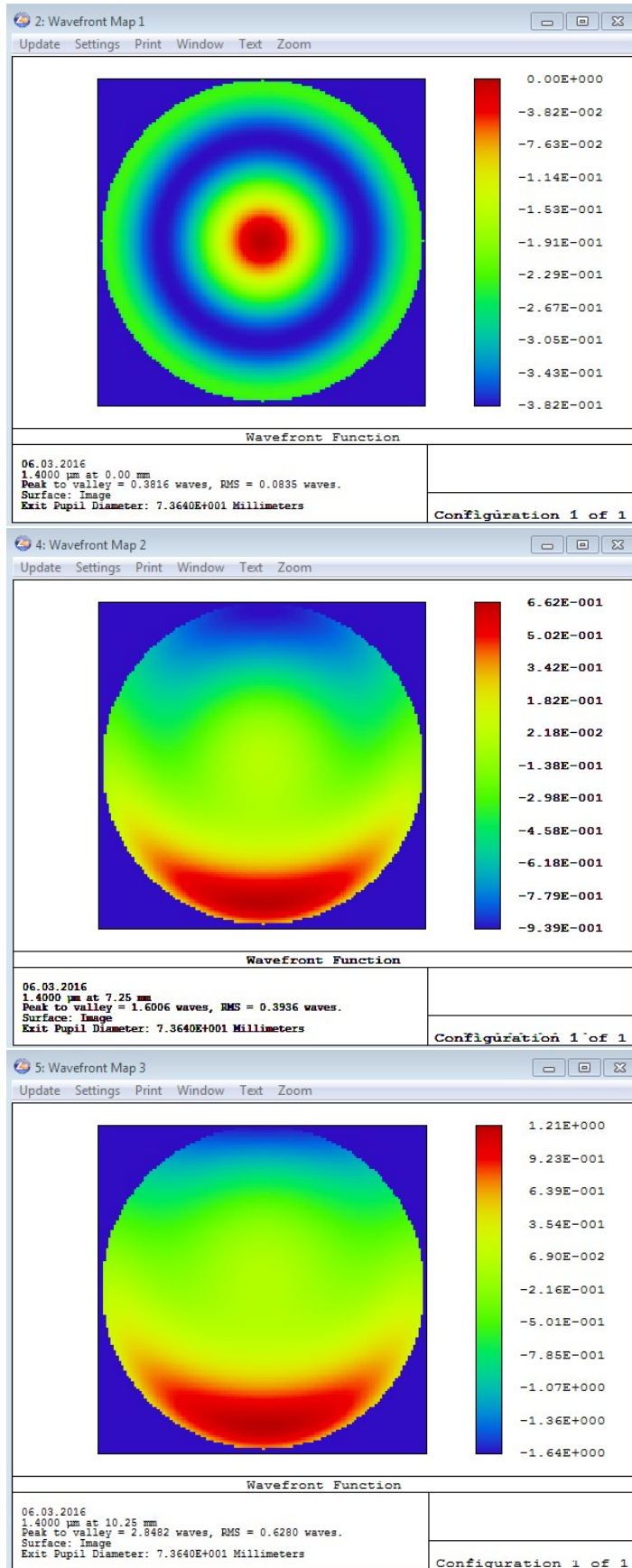


Figure 3.16: Wavefront map at 1.4 $\mu\text{m}$  for field 0, 7.25 and 10.25mm of first solution

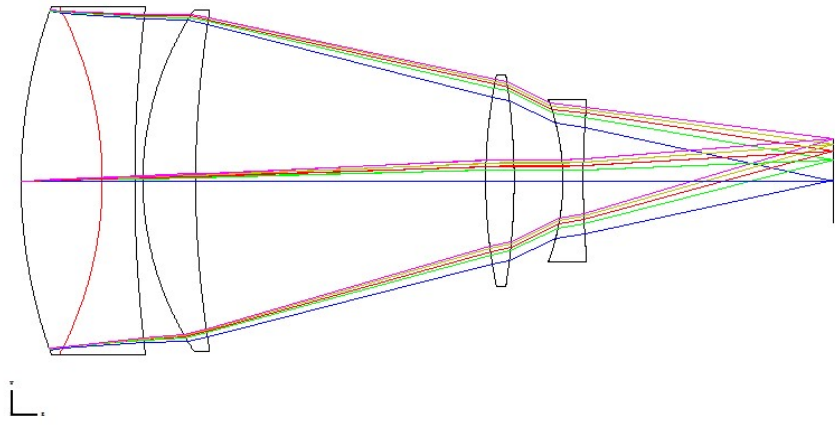


Figure 3.17: Second solution layout

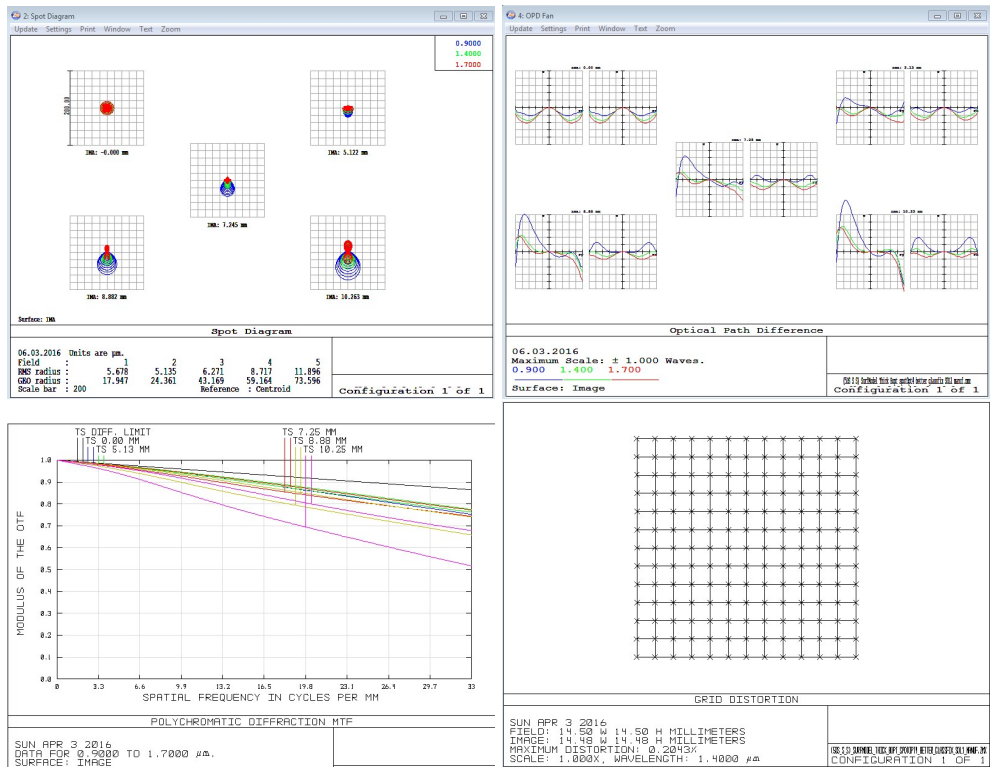


Figure 3.18: Spot diagram, OPD fan, MTF and distortion of second solution

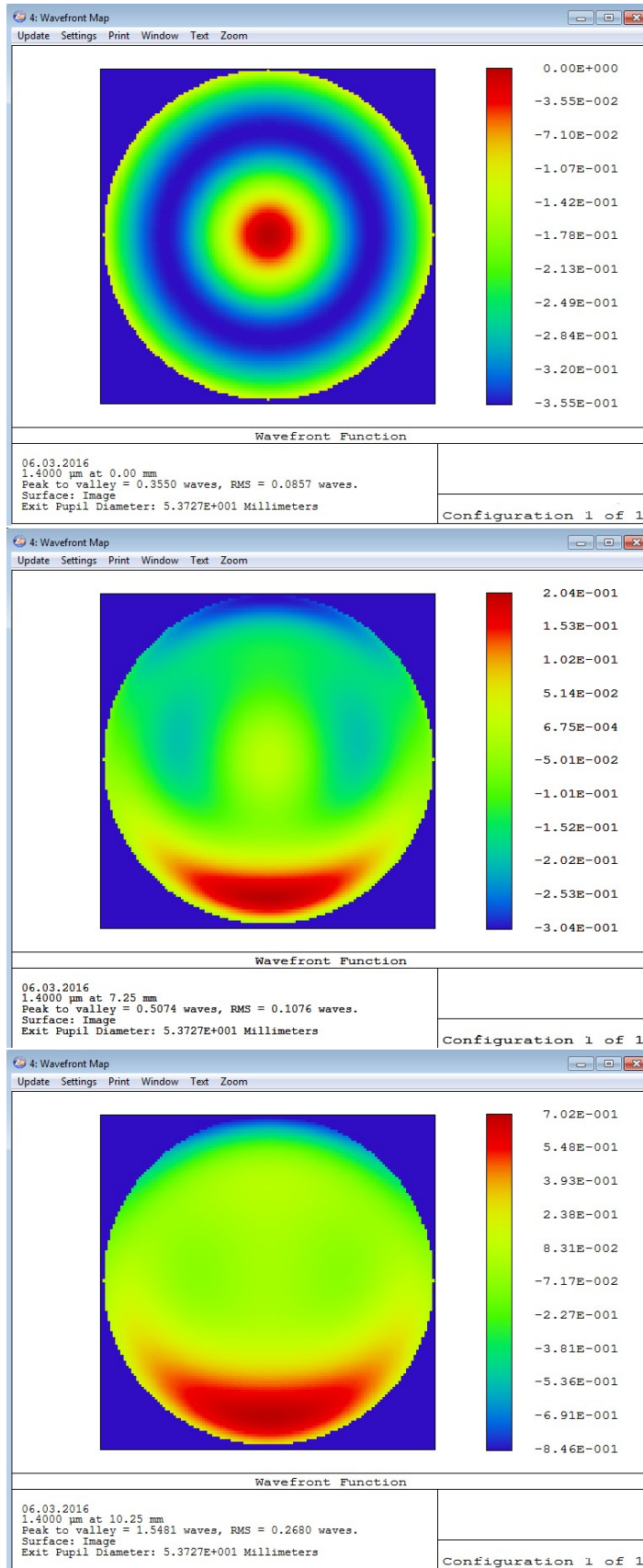


Figure 3.19: Wavefront map at 1.4μm for field 0, 7.25 and 10.25mm of second solution

Table 3.29: Fifth order aberration coefficients after lens optimization

	Second solu- tion	First solution	Total thickening	after balancing	Total before balancing
$W_{240}$	-0.8685	-0.5196	-0.756	-0.852	-1.505
$W_{331}$	-0.2502	-0.3654	-0.084	-0.109	-0.965
$W_{422}$	-0.156	-0.075	-0.077	-0.146	-0.131
$W_{420}$	-0.0596	-0.0025	-0.044	-0.055	-0.058
$W_{511}$	-0.0003	0.2325	0.017	0.028	0.122
$W_{060}$	-2.9027	-2.0025	-4.028	-3.704	-17.222
$W_{151}$	0.1164	2.0693	-3.34	-0.626	2.062
$W_{242}$	-1.212	-1.4792	-2.35	-2.384	-3.062
$W_{333}$	-0.0437	-0.1079	0.0614	0.128	-0.315

### 3.6 Tolerancing

Tolerance analysis is done with CODEV [23] fast tolerancing algorithm. Precision category tolerances given in Figure 2.5 are applied with wavefront error as optical image quality criterion initially to first solution shown in Figure 3.14 and Table 3.26. Tolerances are categorized into two groups, which are centered tolerances and decentered tolerances. Centered tolerances are given in Table 3.30 and decentered tolerances are given in Table 3.31.

Cumulative probability distribution of wavefront error of the design with the tolerances given in Table 3.30 and Table 3.31 is given in Figure 3.20 graphically and in Table 3.32 numerically.

High precision category tolerances given in Figure 2.5 are applied after applying pre-

Table 3.30: Precision level centered tolerances

Surf	Radius	Pow/irr	Thick	Thick tol	Glass	Index tol	V tol(%)
1	137.133	23/ 0.5	20	0.05	NFK58	0.0005	0.5
2	-98.616	32/ 0.5	8	0.05	NKZFS4HT	0.0005	0.5
3	738.303	4/ 0.5	2	0.05			
4	87.738	36/ 0.5	13	0.05	NPK52A	0.0005	0.5
5	INF	3/ 0.5	106.3	0.05			
6	-41.095	10/ 0.5	5	0.05	K7	0.0005	0.5
7	63.989	6/ 0.5	6.1	0.05			
8	58.399	8/ 0.5	5	0.05	NLAK33B	0.0005	0.5
9	-287.128	2/ 0.5	34.6				

Table 3.31: Precision level decentered tolerances

Lens	$R_1$	$R_2$	Element wedge		Element tilt		Element dec./Roll(R)	
			TIR	arc min	TIR	arc min	TIR	mm
1	137.133	-98.616	0.025	1			0.0133	0.01(R)
1-2	137.133	738.303			0.05	2.1	0.005	0.01
2	-98.616	738.303	0.025	1				
3	87.738	INF	0.025	1	0.05	2.1	0.0095	0.01
4	-41.095	63.989	0.01	1.1	0.05	5.6	0.0123	0.01
5	58.399	-287.128	0.01	1.1	0.05	5.5	0.0065	0.01

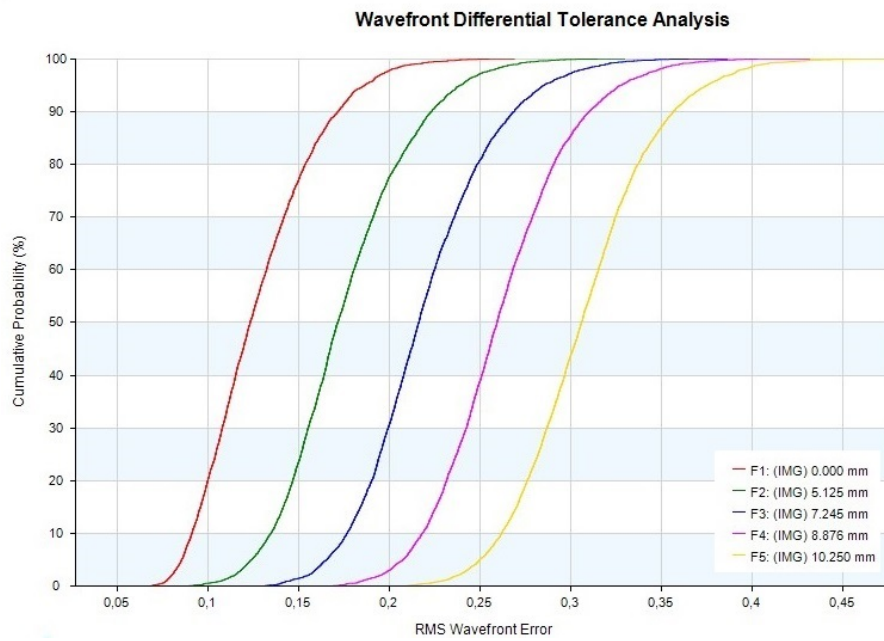


Figure 3.20: Cumulative distribution of wavefront error with precision level tolerances

precision category tolerances. Centered and decentered tolerances are given in Table 3.33 and Table 3.34.

Table 3.32: As-built wavefront errors of the design with precision level tolerances

Relative field	Weight	Design	Design + tol( $2\sigma$ )	Compensator range
0.00, 0.00	1	0.0761	0.1872	0.642
0.00, 0.50	1	0.1321	0.2411	0.642
0.00, 0.71	1	0.179	0.2888	0.642
0.00, 0.87	1	0.2238	0.3321	0.642
0.00, 1.00	1	0.2704	0.3803	0.642

Table 3.33: High precision level centered tolerances

Surf	Radius	Pow/irr	Thick	Thick tol	Glass	Index tol	V tol(%)
1	137.133	12/ 0.2	20	0.025	NFK58	0.00025	0.25
2	-98.616	16/ 0.2	8	0.025	NKZFS4HT	0.00025	0.25
3	738.303	2/ 0.2	2	0.025			
4	87.738	18/ 0.2	13	0.025	NPK52A	0.00025	0.25
5	INF	1/ 0.2	106.3	0.025			
6	-41.095	5/ 0.2	5	0.025	K7	0.00025	0.25
7	63.989	3/ 0.2	6.1	0.025			
8	58.399	4/ 0.2	5	0.025	NLAK33B	0.00025	0.25
9	-287.128	1/ 0.2	34.6				

Cumulative probability distribution of wavefront error of the design with the tolerances given in Table 3.33 and Table 3.34 are given Figure 3.21 graphically and Table 3.35 numerically.

MTF based tolerance analysis are made with the same precision and high precision tolerances after wavefront error based tolerancing. Cumulative probability distribution of tangential and sagittal MTF at 33 lp/mm with precision level tolerances are given in graphically in Figure 3.22, Figure 3.23 and Table 3.36, Table 3.37 numerically.

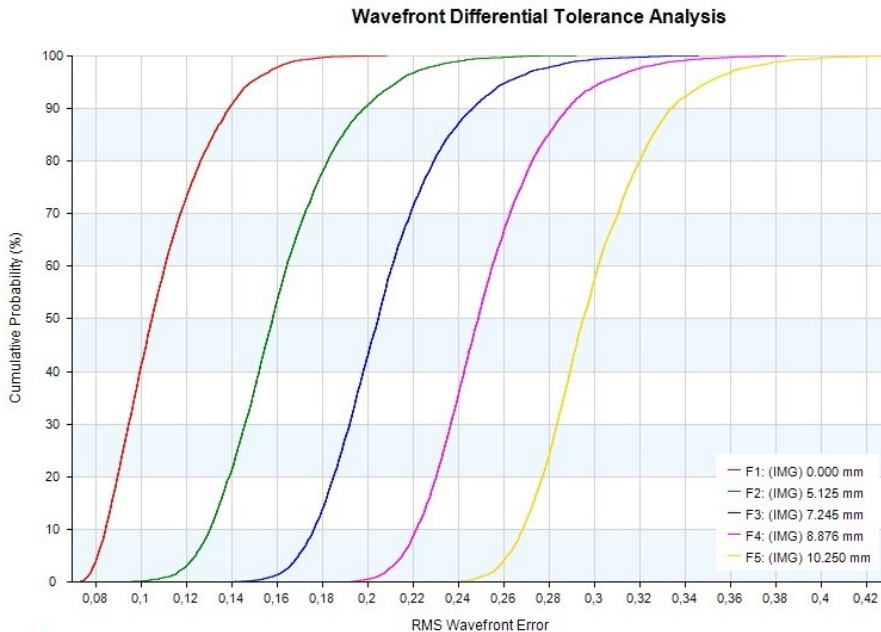


Figure 3.21: Cumulative distribution of wavefront error with high precision level tolerances

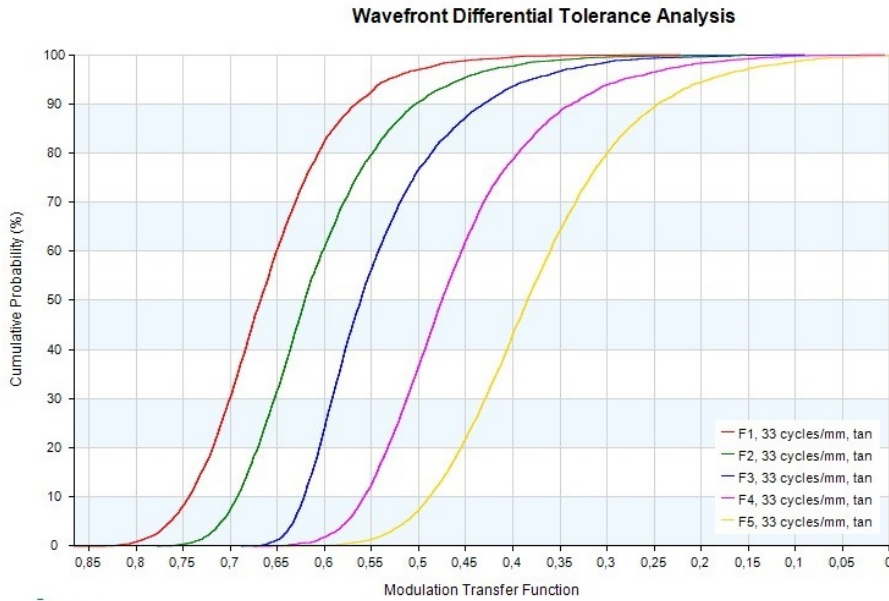


Figure 3.22: Cumulative distribution of tangential MTF at 33 lp/mm with precision level tolerances

Cumulative probability distribution of tangential and sagittal MTF at 33 lp/mm with high precision level tolerances are given in Figure 3.24, Figure 3.25 graphically and Table 3.38, Table 3.39 numerically.

Comparison of wavefront error and MTF performance of the design with high precision and precision level tolerances are given in Table 3.40 and Table 3.41.

There is a nearly %20 performance difference between a system manufactured with high precision tolerances and the one manufactured with precision tolerances. On the other hand, there will be a considerable cost and time schedule difference between

Table 3.34: High precision level decentered tolerances

Element	$R_1$	$R_2$	Element wedge		Element tilt		Element dec./Roll(R)	
			TIR	arc min	TIR	arc min	TIR	mm
1	137.133	-98.616	0.0125	0.5			0.0066	0.01(R)
1-2	137.133	738.303			0.05	2.1	0.005	0.01
2	-98.616	738.303	0.0125	0.5				
3	87.738	INF	0.0125	0.5	0.05	2.1	0.0095	0.01
4	-41.095	63.989	0.005	0.6	0.05	5.6	0.0123	0.01
5	58.399	-287.128	0.005	0.6	0.05	5.5	0.0065	0.01

Table 3.35: As-built wavefront errors of the design with high precision level tolerances

Relative field	Weight	Design	Design + tol( $2\sigma$ )	Compensator range
0.00, 0.00	1	0.0761	0.1492	0.322
0.00, 0.50	1	0.1321	0.2125	0.322
0.00, 0.71	1	0.179	0.2622	0.322
0.00, 0.87	1	0.2238	0.3052	0.322
0.00, 1.00	1	0.2704	0.3522	0.322

Table 3.36: As-built tangential MTF of the design with precision level tolerances

Relative field	freq (lp/mm)	azim deg	weight	design	design + tol( $2\sigma$ )	compensator range
0.00, 0.00	33	TAN	1	0.7285	0.5147	0.6476
0.00, 0.50	33	TAN	1	0.6893	0.4481	0.6476
0.00, 0.71	33	TAN	1	0.6353	0.3825	0.6476
0.00, 0.87	33	TAN	1	0.5514	0.2776	0.6476
0.00, 1.00	33	TAN	1	0.4443	0.176	0.6476

high precision and precision tolerances. A cost, time and performance trade off must be made according to the results of high precision and precision level tolerances with different manufacturers. Finally, solid model of the optical design can be prepared in order to start optomechanical design phase of the optical system.

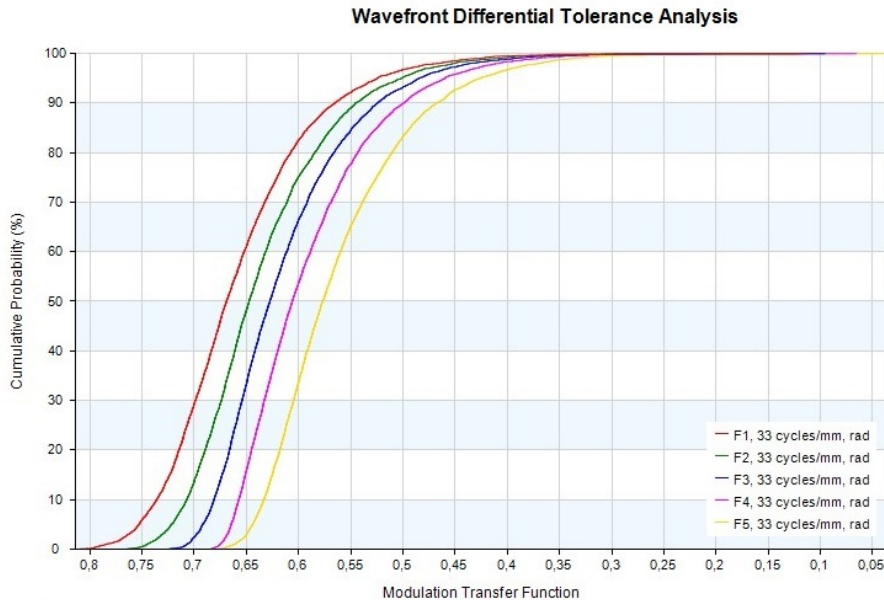


Figure 3.23: Cumulative distribution of sagittal MTF at 33 lp/mm with precision level tolerances

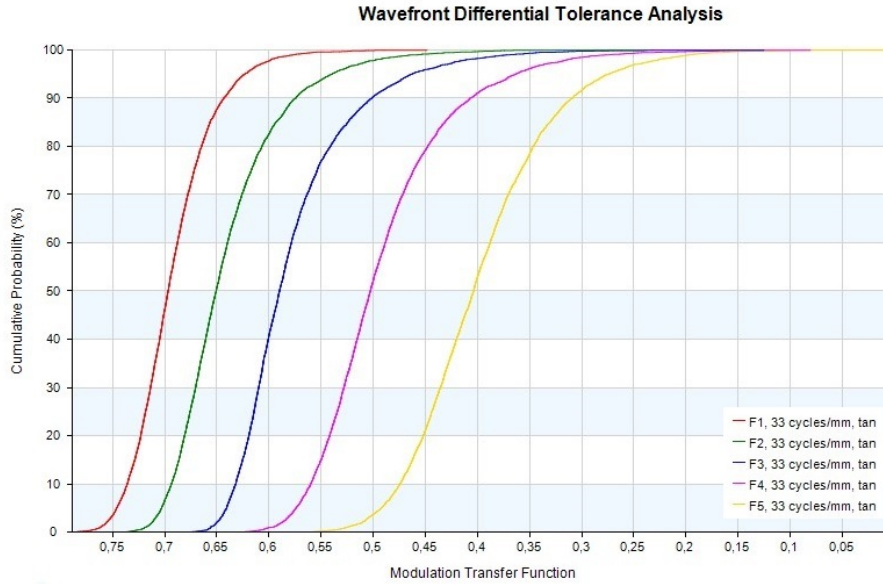


Figure 3.24: Cumulative distribution of tangential MTF at 33 lp/mm with high precision level tolerances

Table 3.37: As-built sagittal MTF of the design with precision level tolerances

Relative field	freq (lp/mm)	azim deg	weight	design	design + tol( $2\sigma$ )	compensator range
0.00, 0.00	33	RAD	1	0.7285	0.5151	0.6604
0.00, 0.50	33	RAD	1	0.7071	0.4974	0.6604
0.00, 0.71	33	RAD	1	0.6899	0.4803	0.6604
0.00, 0.87	33	RAD	1	0.672	0.4569	0.6604
0.00, 1.00	33	RAD	1	0.6473	0.4208	0.6604

Table 3.38: As-built tangential MTF of the design with high precision level tolerances

Relative field	freq (lp/mm)	azim deg	weight	design	design + tol( $2\sigma$ )	compensator range
0.00, 0.00	33	TAN	1	0.7285	0.6159	0.3245
0.00, 0.50	33	TAN	1	0.6893	0.537	0.3245
0.00, 0.71	33	TAN	1	0.6353	0.4607	0.3245
0.00, 0.87	33	TAN	1	0.5514	0.3593	0.3245
0.00, 1.00	33	TAN	1	0.4443	0.261	0.3245

Table 3.39: As-built sagittal MTF of the design with high precision level tolerances

Relative field	freq (lp/mm)	azim deg	weight	design	design + tol( $2\sigma$ )	compensator range
0.00, 0.00	33	RAD	1	0.7285	0.6191	0.3309
0.00, 0.50	33	RAD	1	0.7071	0.5934	0.3309
0.00, 0.71	33	RAD	1	0.6899	0.5719	0.3309
0.00, 0.87	33	RAD	1	0.672	0.5469	0.3309
0.00, 1.00	33	RAD	1	0.6473	0.512	0.3309

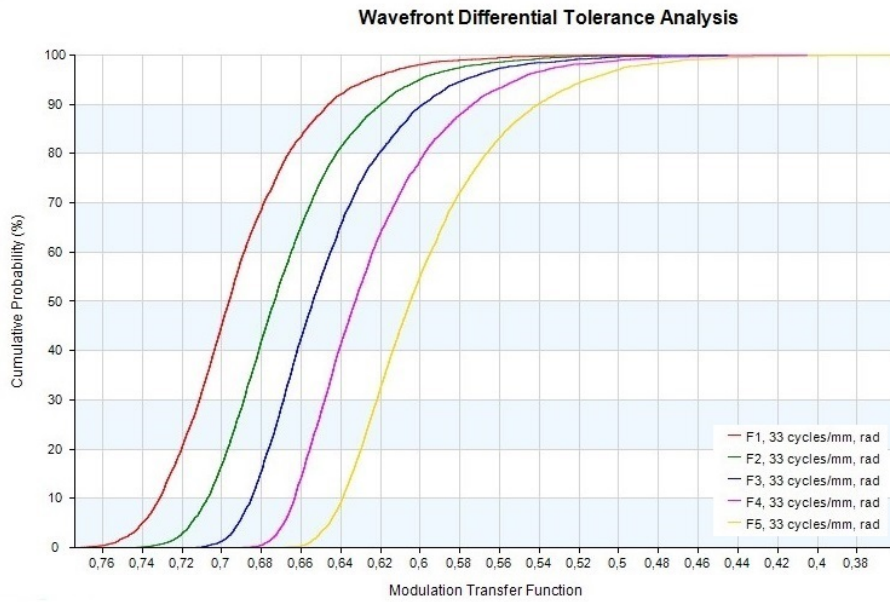


Figure 3.25: Cumulative distribution of sagittal MTF at 33 lp/mm with high precision level tolerances

Table 3.40: Comparison of wavefront error of the design with high precision and precision level tolerances

Relative field	Weight	Precision tolerance		High precision tolerance
		Design	Design + tol( $2\sigma$ )	Design + tol( $2\sigma$ )
0.00	1	0.0761	0.1872	0.1492
0.50	1	0.1321	0.2411	0.2125
0.71	1	0.179	0.2888	0.2622
0.87	1	0.2238	0.3321	0.3052
1.00	1	0.2704	0.3803	0.3522

Table 3.41: Comparison of MTF performance with high precision and precision level tolerances

Relative field	Design (TAN)	Design + tol( $2\sigma$ )		Design (RAD)	Design + tol( $2\sigma$ )	
		Precision	High precision		Precision	High precision
0.00	0.7285	0.5147	0.6159	0.7285	0.5151	0.6191
0.50	0.6893	0.4481	0.537	0.7071	0.4974	0.5934
0.71	0.6353	0.3825	0.4607	0.6899	0.4803	0.5719
0.87	0.5514	0.2776	0.3593	0.672	0.4569	0.5469
1.00	0.4443	0.176	0.261	0.6473	0.4208	0.512

## CHAPTER 4

### CONCLUSION, DISCUSSION AND FUTURE WORK

#### 4.1 Conclusion and Discussion

In this thesis, design procedure of a SWIR objective which is a subsystem in an optical detection system is discussed. Multidisciplinary nature of optical detection problem is introduced. A general purpose physical system of systems (SoS) model for the analysis of an optical system proposing a solution to an optical detection problem is defined. Transmission properties of intervening media, atmosphere, is investigated and atmospheric windows in infrared are discussed. Different atmospheric infrared windows including SWIR, MWIR and LWIR are compared from the system solution perspective. SWIR imaging system solution is studied. Definitions of specifications that have to be addressed during an objective design are given. According to these definitions, objective specifications are assumed to be given as in Table 3.1

Once the specifications are determined, different ways of finding a starting point are discussed and analytical derivation methodology is chosen as the mainframe of the design methodology. In chapter 2, optical design methodology based on aberration theory is introduced. In real imaging systems, all rays from a point in object space do not meet at a point in image space but distributed in a pattern depending on the imaging system parameters. This pattern is called the aberration of the imaging system. Different aberration types and analytical derivations of these aberrations by power series expansions are discussed. These aberrations must be corrected to some extent depending on the application in order to have better image quality. After optical aberrations are defined, systematic optical lens design methodology is discussed in a

general sense based on the aberrations defined.

Specifications are assumed to be determined from the system of systems perspective considering all the necessary building blocks of optical detection architecture. According to defined specifications, layout is chosen. Afterwards, thin lens design is studied based on Seidel aberration theory. Finally thin lenses are transformed to real thick lens with the help of surface models. In chapter 3, analytical derivation methodology discussed in chapter 2 is implemented specifically on a SWIR objective whose specifications are given in introduction. Firstly, the best suitable layout is chosen depending on the given specifications from the well-known lens categories. Main driving parameters for choosing the lens categories are field of view and numerical aperture. Given specifications is in the photographic objectives and corresponds to telephoto type lens. After lens type is chosen, first order or paraxial layout is determined, power distribution and position dependence are investigated using first order relations. Secondly, shape independent aberrations which are field curvature and colour aberrations are targeted. Primary chromatic aberrations which are axial colour and lateral colour are corrected in this layout. Field curvature is the only third order aberration considered in this stage since it is difficult to correct in later phases if it is not considered in early phases and also it is easy to calculate in this phase because of its independence of shape parameters and position of thin lenses and stop position. Also since field curvature is dependent on the assigned material parameters and powers of thin lenses, it is a must to consider field curvature with primary colour aberrations. Power distributions, positions, lens numbers and materials of thin lenses in layout are determined in this stage. Seidel aberration formula for spherical aberration, coma, astigmatism and distortion for a thin lens at the stop are given analytically with the manufacturing parameters of thin lenses assigned in first order layout. Using these formulas, stop shift equations for Seidel aberrations are discussed and used to calculate the shape and conjugate parameters for thin lenses which minimizes system Seidel coefficients. System Seidel coefficients are quadratic in shape parameters and conjugate parameters. In order to minimize system coefficients, optimization routines are used. After shape and conjugate parameters are found, thin lenses are converted to thick lens with the help of surface model procedure. Thin lens radius of curvatures are scaled so that the thickened lenses have the same power with the thin lens equiva-

lents and principles points shifts are compensated in thick lens layout. As a result of the implementation of surface model, real lenses are obtained without disturbing the third order aberration calculations and first order parameters of the thin lens layout. Using ray tracing routines in ZEMAX, system Seidel coefficients are calculated and compared with the starting point designs Seidel coefficients. Since only third order aberrations are considered up to this point in design process, real lens system has greater aberrations because of the higher order aberrations which are not taken into account in third order aberration theory. Finally, optimization procedure including merit function, aberration balancing and fifth order aberrations is discussed and applied to the starting point design which is found by using Seidel aberration theory in order to further balance higher order aberrations to get a better quality. Optimization procedure is implemented in Zemax optical design program. The last step after optimization is tolerance analysis. Since each optical parameter in the design can not be manufactured exactly the same as in the design, there is a perturbation in the optical performance of the design. Real imaging quality of the designed system is the performance after tolerance analysis which has a statistical distribution. A typical tolerance analysis flow chart is given. Two types of tolerances which are high precision and precision category are taken into account from wavefront error criterion and MTF criterion. Comparison of tolerance analysis is done and results are exposed to make a trade-off between cost, performance and time schedule.

As a conclusion, a systematic optical lens design methodology whose mainframes are third (Seidel) and fifth order aberration theory coefficients is constructed based on wavefront error polynomial expansion for SWIR waveband. The methodology can also be used for other operating wavelengths and different optical layouts. As a practical example, this methodology is applied to a typical SWIR objective used for increasing situational awareness and ISR. A ready to build SWIR lens design with commercial glasses with the given as-built image quality specification is achieved successfully at the end of the methodology proposed.

## **4.2 Future Work**

For future work, there are mainly three topics to cover:

1. Tolerancing is an important and the most time consuming step in optical design. Depending on the steepness of solution point in the design hyperspace, deviations of optical parameters from the design value will degrade the image quality so much that the design procedures must be started all over again in order to reduce the sensitivity of the parameter since there is no parameter regarding to tolerance sensitivities taken into account in early stages of optical design besides the control of angle of incidence. There are some published indirect and direct methodologies in order to solve this problem. Including sensitivity of optical parameters in early stages of optical design and optimization is open to study.
2. All of the design stages are done with an assumption that rays follow paths which are defined sequentially in order to calculate the imaging properties of the layout. But since there will be residual back reflections from lens surfaces due to imperfection of coatings, image anomalies called straylight will degrade image quality. Detailed straylight analysis and reduction methodologies are open to study.
3. Situational awareness is a very critical concept in military optical systems. A dominating parameter from situational awareness is field of view. Since telephoto lenses have smaller field of views, it is perfect for distant identification while useless in a wider field of view detection. In order to solve this problem, optical systems are designed to have multiple field of views at least three field of views which are called narrow, middle and wide or to have continuous field of views called continuous zoom lenses. SWIR continuous zoom lenses are open to study.

## REFERENCES

- [1] Geoff Adams. Some statistical aspects of tolerancing. *Proc. SPIE*, 0655:67–79, 1986.
- [2] Jeffrey Allen, David C. Dayton, John D. Gonglewski, Michael M. Myers, and Rudolph Nolasco. Seasonal hemispherical swir airglow imaging. *Proc. SPIE*, 8165:81650P–81650P–11, 2011.
- [3] Julie L. Bentley, Craig Olson, and Richard N. Youngworth. In the era of global optimization, the understanding of aberrations remains the key to designing superior optical systems. *Proc. SPIE*, 7849:78490C–78490C–13, 2010.
- [4] Ontar Corporation. Pcmowin5. <http://www.ontar.com/>, last visited on April 2016.
- [5] David Dayton, Jeff Allen, John Gonglewski, Mike Myers, Gregory Fertig, Rudy Nolasco, and Francisco Maia. Spatial and temporal variability of swir air glow measurements. *Proc. SPIE*, 7828:78280E–78280E–9, 2010.
- [6] Jessica DeGroot Nelson, Richard N. Youngworth, and David M. Aikens. The cost of tolerancing. *Proc. SPIE*, 7433:74330E–74330E–12, 2009.
- [7] Ronald G. Driggers, Van Hodgkin, and Richard Vollmerhausen. What good is swir? passive day comparison of vis, nir, and swir. *Proc. SPIE*, 8706:87060L–87060L–15, 2013.
- [8] Robert E. Fischer. Tolerances don't lie...and stories of the grand canyon! *Proc. SPIE*, 7068:706803–706803–12, 2008.
- [9] Gregory W. Forbes and Andrew E. Jones. Towards global optimization with adaptive simulated annealing. *Proc. SPIE*, 1354:144–153, 1991.
- [10] David P. Forse. Statistical tolerancing for optics. *Proc. SPIE*, 2775:18–27, 1996.
- [11] Robert H. Ginsberg. Outline of tolerancing (from performance specification to toleranced drawings). *Optical Engineering*, 20(2):202175–202175–, 1981.
- [12] Herbert Gross. *Handbook of Optical Systems, Volume 3*. Wiley-VCH, 2005.
- [13] Herbert Gross. *Handbook of Optical Systems, Volume 4*. Wiley-VCH, 2008.

- [14] Marc P. Hansen and Douglas S. Malchow. Overview of swir detectors, cameras, and applications. *Proc. SPIE*, 6939:69390I–69390I–11, 2008.
- [15] Craig Olson Julie Bentley. *Field Guide to Lens Design*. SPIE, 2012.
- [16] Michael Kehoe. Tolerance assignment for minimizing manufacturing cost. *Proc. SPIE*, 7652:76521N–76521N–10, 2010.
- [17] Michael Kidger. *Intermediate Optical Design*. SPIE, 2004.
- [18] Michael J. Kidger. Importance of aberration theory in understanding lens design. *Proc. SPIE*, 3190:26–33, 1997.
- [19] Rudolf Kingslake. *Lens Desing Fundamentals*. Academic Press, 2010.
- [20] Thomas G. Kuper and Thomas I. Harris. Global optimization for lens design: an emerging technology. *Proc. SPIE*, 1781:14–28, 1993.
- [21] ZEMAX LLC. Zemax optical design software v.13. <http://www.zemax.com/>, last visited on April 2016.
- [22] Joseph Meiron. Damped least-squares method for automatic lens design. *J. Opt. Soc. Am.*, 55(9):1105–1109, Sep 1965.
- [23] Synopsys OSG. Codev optical design software v10.8. <https://optics.synopsys.com/codev/>, last visited on April 2016.
- [24] Deqing Ren and Jeremy R. Allington-Smith. Apochromatic lenses for near-infrared astronomical instruments. *Optical Engineering*, 38(3):537–542, 1999.
- [25] M. Rimmer. Analysis of perturbed lens systems. *Appl. Opt.*, 9(3):533–537, Mar 1970.
- [26] Jose Sasian. Interpretation of pupil aberrations in imaging systems. *Proc. SPIE*, 6342:634208–634208–4, 2006.
- [27] José Sasián. Theory of sixth-order wave aberrations. *Appl. Opt.*, 49(16):D69–D95, Jun 2010.
- [28] José Sasián. *Introduction to Aberrations in Optical Imaging Systems*. Cambridge, 2013.
- [29] Roland Schack. Introduction to aberrations, opti 518. Lecture Notes, 1995.
- [30] Schott. Schott glass catalog 20150722. <http://www.schott.com/>, last visited on April 2016.
- [31] Robert Shannon. *The Art and Science of Optical Design*. Cambridge, 1997.

- [32] R. Hamilton Shepard III and Scott W. Sparrold. Material selection for color correction in the short-wave infrared. *Proc. SPIE*, 7060:70600E–70600E–10, 2008.
- [33] Warren Smith. *Modern Lens Design*. SPIE, 2005.
- [34] Warren J. Smith. Fundamentals of establishing an optical tolerance budget. *Proc. SPIE*, 0531:196–205, 1985.
- [35] Optimax Systems. Manufacturing tolerance chart. <http://www.optimaxsi.com/>, last visited on April 2016.
- [36] Simon Thibault, Christian Gagné, Julie Beaulieu, and Marc Parizeau. Evolutionary algorithms applied to lens design: case study and analysis. *Proc. SPIE*, 5962:596209–596209–11, 2005.
- [37] Kevin Thompson. Description of the third-order optical aberrations of near-circular pupil optical systems without symmetry. *J. Opt. Soc. Am. A*, 22(7):1389–1401, Jul 2005.
- [38] Eco van Driel, Florian Bociort, and Alexander Serebriakov. Topography of the merit function landscape in optical system design. *Proc. SPIE*, 5249:353–363, 2004.
- [39] Christian Velzel. *A course in Lens Design*. Springer, 2014.
- [40] Richard N. Youngworth. Twenty-first century optical tolerancing: a look at the past and improvements for the future. *Proc. SPIE*, 6342:634203–634203–15, 2006.
- [41] Richard N. Youngworth. Statistical truths of tolerance assignment in optical design. *Proc. SPIE*, 8131:81310E–81310E–15, 2011.